UNIVERSITÀ DI PISA

Scuola di Dottorato in Ingegneria "Leonardo da Vinci"

Corso di Dottorato di Ricerca in
Ingegneria dell'Informazione
SSD ING-INF/03

Tesi di Dottorato di Ricerca

Signal design and Theoretical bounds for Time-Of-Arrival estimation in GNSS applications

Autore:

Andrea Emmanuele

Relatori:
Prof. Marco Luise
Prof. Michele Morelli

Anno 2012

To my Love.

Copyright © Andrea Emmanuele, 2012

Manuscript received February 28, 2012

Accepted March 28, 2012

Sommario

La precisione del posizionamento in sistemi di navigazione satellitare dipende dalla *stima del ritardo temporale* (TDE) tra i codici trasmessi dai satelliti e le repliche locali del ricevitore. Questa tesi é incentrata sul problema di migliorare l'accuratezza della stima dei ritardi dei segnali a spettro espanso (SS), concentrandosi sul tema fondamentale della teoria della stima e sulle proprietá del segnale trasmesso. I limiti fondamentali per la stima del ritardo sono indagati a fondo, comprendendo lo studio del limite di Cramér Rao (CRB) e del limite di Ziv-Zakai (ZZB) e le loro versioni *modificate* nel caso di presenza di parametri incogniti in aggiunta al ritardo temporale. Il limite di Ziv-Zakai é investigato come riferimento per le prestazioni di stimatori durante la fase sia di acquisizione che di tracking del segnale, studiando segnali innovativi o standard quali quelli adottati dal sistema Galileo. I principali contributi di questa tesi comprendono l'analisi di applicabilitá dei segnali a spettro espanso a fase continua (SS-CPM) e filtrati multitono (SS-FMT) come segnali di ranging. Un sottoinsieme delle CPM, chiamato SiMSK e ottenuto da una particolare impostazione dei parametri, si rivela facilmente adattabile alle esigenze di emissioni, ad inviluppo intrinsecamente costante e spettralmente efficiente, consentendo buone prestazioni in fase di tracking. Inoltre, una codifica ad hoc delle SiMSK consente di ottenere un segnale ad inviluppo costante contenente due servizi indipendenti, senza approssimazioni lato trasmettitore. L'analisi del segnale multiportante ha rivelato l'elevato grado di libertá nella progettazione dello stesso, proponendo il caso particolare della modulazione filtrata multitono (FMT) come opzione per segnali di ranging. La limitatezza in banda e la massima flessibilitá spettrale possedute dal segnale vengono adoperate per adattare il sistema alle differenti condizioni di canale o emulare spettri di segnali pre-esistenti o innovativi. Per entrambi gli schemi di modulazione indagati alcuni algoritmi di stima del ritardo sono testati, confrontando le loro prestazioni con il corrispondente limite teorico.

Abstract

Positioning accuracy in satellite navigation systems depends on *time-delay estimation* (TDE) between satellite transmitted codes and local receiver replicas. This thesis is specifically focused on the problem of improving time delay estimation (TDE) accuracy of SS signals, focusing on the fundamental issue of estimation theory and on the properties of the transmitted signal. TDE fundamentals limits are deeply investigated, encompassing the Cramér Rao Bound and the Ziv-Zakai Bound, and their *modified* versions to lighten their computation in presence of unknown parameters, in addiction to the time delay. The adoption of the ZZB as benchmark for both acquisition and tracking stage performance is addressed, analyzing innovative or standard signalling waveforms such as Galileo SIS. The main contributions of this thesis are dealt with the analysis of applicability of spread spectrum continuous-phase-modulated (SS-CPM) and spread spectrum filtered multitone (SS-FMT) as ranging signals. A special subset of CPM, labeled as "Semi-integer MSK (SiMSK)" obtained by properly setting the modulation parameters, is revealed easily adaptable to the requirements on emissions, intrinsically constant envelope and spectral efficient, while still allowing good tracking performance. Besides, an ad hoc encoding of the SS-SiMSK enables the design of a constant envelope signal bearing two different rate services, without any approximation at the transmitter side. The analysis of the multicarrier (MC) signal revealed the high degree of freedom in its design, proposing the special Filtered Multitone (FMT) modulation as possible candidate for ranging signals. The strictly bandlimited property and the full spectral flexibility possessed by the FMT are exploited in some cases of study to adapt the system to channel conditions or in particular to emulate existing or innovative spectra. For both the SS-CPM and SS-FMT modulation schemes investigated, some estimation algorithms are tested and their performance are compared to the correspondent theoretical bound.

Acknowledgments

The present work has been developed during the years spent in the DSP laboratory of the *Dipartimento di Ingegneria dell'Informazione* of the University of Pisa, and there are special people I want to acknowledge because they were extremely important to me during the course of my thesis.

I would like to express my deepest gratitude to my advisor, Prof. Marco Luise for his excellent guidance and continual support during the course of my studies. He was essential for my interest in Research, thanks to his precious suggestions. I really thank him for all the opportunities he offered me since I know him. I would also like to thank the Prof. Michele Morelli, for his attentive availability. I owe my thanks to all my colleagues at the DSP lab, starting from Dr. Giacomo Bacci for his precious guidance and friendship and for his valuable daily support, to Ottavio Picchi, Vincenzo Pellegrini and Mario Di Dio for their active cooperation and friendship.

A considerable added value to my Research has been given during my stay at ESTEC, European Space Agency (ESA). I am sincerely indebted to Dr. Massimo Crisci and Dr. Francesca Zanier for giving me the opportunity of working within the Radio Navigation working group at ESTEC and for their valuable guidance. I would like to particularly thank Francesca for her moral and technical support, during all these three years and specially for the preparation of this thesis.

Thanks to the group of friends (and colleagues) with which I spent sad and happy moments in these years: Nancy, Alice and Gianfranco, thank you. A lot of thanks go to the former and new housemates of Via Tevere, for their sincere friendship and for the time spent together in all the stuffs *out of work/study*. My particular thanks are addressed to all components of my family. Without their moral support I would have

not reached this goal.

Finally I would to like to say my lovely thanks to Marzia. You daily supported me and you gave me, even from a distance, the moral strength towards this goal with your love specially in sad moments. Grazie.

Pisa, April 2012 Andrea

Contents

Sommario **i**

Abstract **iii**

Contents **vii**

List of figures **ix**

List of acronyms **xi**

List of publications **xvii**

Introduction **1**

Motivations 1

Main contributions 3

Outline 4

1 Basics of positioning systems **7**

1.1 Introduction 7

1.2 Global Positioning System (GPS) 8

1.2.1 Modernized GPS 9

1.3 Galileo 11

1.4 GLONASS 12

1.5 Compass/Beidou 13

1.6 Ranging using time of arrival (TOA) or time delay (TD) measurements 14

1.6.1 Position determination in two dimensions 14

1.6.2 Principle of Position Determination Via Satellite Ranging Signals 15

1.6.3 Position Determination Using PRN Codes 17

2 Accuracy Limits for Time-Of-Arrival (TOA) Estimation 25

2.1 Motivations 26

2.2 Estimation theory 27

2.3 Cramér-Rao bound (CRB) and Modified Cramér-Rao bound (MCRB) 29

2.3.1 The Cramér-Rao lower bound (CRB) 29

2.3.2 The Modified Cramér-Rao lower bound (MCRB) 30

2.4 Ziv-Zakai bound (ZZB) and Modified Ziv-Zakai bound (MZZB) 32

2.4.1 The Ziv-Zakai lower bound (ZZB) 32

2.4.2 The Modified Ziv-Zakai lower bound (MZZB) 34

2.5 CRB and ZZB in TOA estimation 36

2.5.1 Motivation 36

2.5.2 Signal model 37

2.5.3 Characterization of (M)CRB and (M)ZZB in TOA estimation . 38

2.5.4 Considerations on the applicability of the bounds 42

2.6 Conclusions 45

3 TOA Estimation with SS-CPM signals for GNSS 47

3.1 Introduction 47

3.2 Signal design 49

3.2.1 Signal definition 49

3.2.2 OQPSK approximation validation 53

3.2.3 Mapping to services 54

3.2.4 Signal spectral analysis 55

3.2.5 Comparison between SS-CPM and BOC formats 57

3.3 Delay tracking performance 60

3.3.1 Code Tracking loop 60

3.4 Performance results 63

3.4.1 Performance in the AWGN channel 63

3.4.2 Performance in the multipath channel 66

3.4.3 Two-rate-service (TRS) performance 68

3.4.4 Summary of performance results 70

3.5 Conclusions 71

4 TOA Estimation with SS-FMT signals for GNSS 73
4.1 Motivation . . . 73
4.2 Signal Design . . . 75
4.2.1 Signal definition . . . 75
4.2.2 Signal analysis . . . 77
4.2.3 Correlation analysis . . . 80
4.2.4 Signal spectral analysis . . . 82
4.2.5 Multicarrier flexibility exploitation . . . 84
4.2.6 Mapping to services: Time and Frequency domain ranging codes 89
4.3 Delay tracking performance . . . 89
4.3.1 Code tracking loop . . . 91
4.4 Performance results . . . 94
4.4.1 Performance in the AWGN channel . . . 94
4.4.2 Performance in a two-ray Multipath channel . . . 102
4.4.3 Summary of performance results . . . 104
4.5 Conclusions . . . 107

5 Application of the MZZB to Standard and Innovative GNSS Signals 109
5.1 Introduction . . . 109
5.2 Application of MZZB to standard SIS . . . 110
5.3 Application of (M)ZZB to Multicarrier signals . . . 116
5.3.1 True and modified ZZB convergence . . . 118
5.3.2 MZZB for innovative GNSS waveforms . . . 120
5.4 Relating the bounds for signal acquisition and tracking . . . 125
5.4.1 Case of Study - Galileo SIS Results . . . 127
5.5 Conclusions . . . 128

6 Conclusions and perspectives 131

Bibliography 135

List of Figures

1.1 User located at one of two points on shaded circle. 16
1.2 Use of replica code to determine satellite code transmission time . . . 18
1.3 User position vector representation 19

3.1 SS-CPM Signal generator. 52
3.2 Comparison of normalized correlation functions, for $h = 0.5$ and $h = 2.5$. 53
3.3 PSD of the *LREC* CPM. 56
3.4 PSD of the *LRC* CPM. 56
3.5 PSD of the *LGAU* CPM, $L = 4$. 57
3.6 PSD of the *LSQW* CPM, $L = 1$. 58
3.7 Square Wave (SQW) frequency pulse. 58
3.8 SS-CPM vs BOC 59
3.9 SS-CPM Delay Estimator. 62
3.10 Digital Delay Lock Loop code tracking loops. 65
3.11 S-curve function of the different DDLL schemes. Simulation for 4*GAU* frequency pulse. 66
3.12 RMSEE for the proposed DDLL schemes. Simulation for 4*GAU* frequency pulse for $h = 0.5$ and $h = 2.5$. 67
3.13 MPEE figures of SS-CPM for different modulation indices. 68
3.14 PSD of SS-CPM for Two-Rate-Service (TRS), $N_{rep} = 10$, for the I and Q branches and the total complex envelope. 69
3.15 MCRB of SS-CPM for Two-Rate-Service (TRS), $N_{rep} = 10$. MCRBs for slow I-branch 1st lobe, 5 and 13 lobes spectrum, fast Q-branch 1st lobe and infinite bandwidth spectrum. 69

4.1 General Spread-Spectrum Multicarrier Transmitter. 76

4.2 I/Q components of FMT with flat power distribution, N=127 and $\alpha = 0.2$. 78
4.3 Histogram of the FMT signal envelope. 79
4.4 FMT correlation composition 81
4.5 Masks of power distribution. 83
4.6 Monomodal and bimodal schemes. 84
4.7 Theoretical $BOC(6,1)$ PSD - FMT synthesis of filtered $BOC(6,1)$. . . 85
4.8 Theoretical $BOC(6,1)$ PSD - Low-pass FMT solution to minimize inter-systems interference. 86
4.9 Enhancement of the PSD synthesis. 87
4.10 FMT power spectral flexibility - no interference, high-pass and low-pass interference cases. 88
4.11 SS-FMT Receiver 92
4.12 Non coherent E-L DDLL. 93
4.13 Coherent E-L DDLL. 94
4.14 Power spectral density of the FMT schemes. 96
4.15 Correlation function of the FMT schemes. 96
4.16 S-curve function of the non coherent DDLL scheme. Simulation for Flat and Bimodal distribution on 250/1023 active subcarriers. 97
4.17 RMSE for the proposed non coherent DDLL scheme. Simulation for Flat and Bimodal distribution on 250/1023 active subcarriers. 98
4.18 Spectra of the FMT synthesis. 99
4.19 S-curve function for the proposed non coherent DDLL scheme. Simulation for the QPSK(1) SS-FMT synthesis. 100
4.20 S-curve function for the proposed non coherent DDLL scheme. Simulation for the BOC(1,1) SS-FMT synthesis. 101
4.21 RMSE for the proposed non coherent DDLL scheme. Simulation for the QPSK(1) FMT synthesis. 103
4.22 RMSE for the proposed non coherent DDLL scheme. Simulation for the BOC(1,1) FMT synthesis. 103
4.23 MPEE figures of flat and bimodal SS-FMT schemes. 105
4.24 MPEE figures of filtered QPSK(1) and filtered BOC(1,1) SS-FMT synthesis. 106

5.1 Theoretical BOC correlation functions with fixed bandwidth and ad hoc chip rates. 114
5.2 Multi-peaks effect - theoretical BOC modulations. 114
5.3 Multi-peaks effect - filtered BOC modulations. 115
5.4 (M)ZZB of MC in AWGN channel. 120
5.5 Low-Pass/Band-Pass FMT schemes Power Spectral Density 121
5.6 Low-Pass/Band-Pass FMT schemes Autocorrelation function 122
5.7 β_x-normalized RMSE vs $E_{T_{obs}}/N_0$ 124
5.8 β_x-normalized RMSE vs T_x 125
5.9 Acquisition and tracking performance of Galileo GNSS. 130

List of Acronyms

ACGN additive colored Gaussian noise

ACK acknowledge

AWGN additive white Gaussian noise

BCH Bose-Chaudhuri-Hocquenghem

BOC binary offset carrier

BPSK binary phase shift keying

C/A coarse/acquisition

CBOC composite binary offset carrier

CC central cluster

cdf cumulative distribution function

CDMA code division multiple access

CNSS Compass navigation satellite system

CPM continuous-phase-modulation

CRB Cramér-Rao lower bound

CRC cyclic redundancy check

CS control segment/commercial service

DoD Department of Defense

DS-SS direct sequence spread spectrum

EB energy-based

ESA European Space Agency

EU European Union

FDMA frequency division multiple access

FMT Filtered multitone

GB Gabor bandwidth

GEO geostationary

GIOVE Galileo In-Orbit Validation Element

GIS geographical information system

GLONASS global orbiting navigation satellite system

Gen-MSK Generalized Minimum-Shift-Keying

GNSS global navigation satellite system

GNSSs global navigation satellite systems

GPS global positioning system

HPA high power amplifier

I in-phase

i.i.d. independent, identically distributed

ICD interface control document

LOS line-of-sight

MBOC multiplexed binary offset carrier

MB-UWB multi-band UWB

MCRB Modified Cramér-Rao lower bound

MEO medium earth orbit

MF matched filter

ML maximum likelihood

MP multipath

MPEE multipath error envelope

MSE mean squared error

MSEE mean squared estimation error

MSK Minimum-Shift-Keying

MZZB Modified Ziv-Zakai lower bound

NAV navigation

NAVSTAR navigation system for timing and ranging

NRZ non-return to zero

OCS operational control segment

OFDM orthogonal frequency division multiplexing

OOB out of band

OQPSK Offset Quadrature Phase-Shift Keying

OS open service

PAM pulse amplitude modulation

pdf probability density function

PN pseudo-noise

PPS precise position service

PRN pseudo-random noise

PRS public regulated service

PSD power spectral density

PSK phase shift keying

PVT position, velocity, and time

Q quadrature-phase

RDSS radio determination satellite service

RMS root mean square

RMSE root mean square error

RMSEE root mean square error estimation

RRC root raised cosine/radio resource control

SA selective availability

SAR search and rescue

SIS signal-in-space

SoL safety-of-life

SNR signal-to-noise ratio

sps symbols per second

SPS standard position service

SRS same-rate-service

SS spread spectrum

SS-CPM spread spectrum continuous-phase-modulated

SS-GenMSK Spread-Spectrum Generalized-Minimum-Shift-Keying

SS-FMT spread spectrum filtered multitone

SS-MC spread spectrum multicarrier

TDE time delay estimation

TMBOC time-multiplexed binary offset carrier

TOA time-of-arrival

TRS two-rate-service

TWTA traveling wave tube amplifier

U.S. United States

UE user equipment

US user segment

wrt with respect to

ZZB Ziv-Zakai lower bound

List of Publications

International Journals

1. "Spread-Spectrum Continuous-Phase-Modulated Signals for Satellite Navigation", A. Emmanuele, F. Zanier, G. Boccolini, M. Luise, Accepted to Transactions on Aerospace and Electronic Systems.

International Conferences

2. "Continuous-Phase Modulated Signals for Satellite Positioning in the C-Band", F. Zanier, A. Emmanuele, G. Boccolini, M. Luise, In Proc. of the 4th ESA Workshop on Satellite Navigation User Equipment Technologies (NAVITEC), Noordwijk, The Netherlands, Dec. 2008.

3. "Constant-Envelope Signal-in-Space Design for GNSSs in the C-band", A. Emmanuele, F. Zanier, G. Boccolini, M. Luise, In Proc. of European Navigation Conference - Global Navigation Satellite Systems (ENC-GNSS) 2009, Napoli, Italy, May 2009.

4. "Fundamental issues in time-delay estimation of multicarrier signals with applications to next-generation GNSS", F. Zanier, M. Crisci, A. Emmanuele, M. Luise, In Proc. of European Workshop on GNSS Signals and Signal Processing (GNSS Signals 2009), Oberpfaffenhofen, Germany, Dec. 2009.

5. "Constant-Envelope Modulation applied to GNSS Signal-in-Space Design", A. Emmanuele, M. Luise, F. Zanier, M. Crisci, In Proc. of European Workshop on GNSS Signals and Signal Processing (GNSS Signals 2009), Oberpfaffenhofen, Germany, Dec. 2009.

6. "Fundamental limits in signal time-of-arrival estimation with application to next generation satellite positioning", A. Emmanuele, M. Luise, In Proc. of the International Symposium ELMAR-2010, Zadar, Croatia, Sept. 2010.

7. "Fundamental limits in signal time-of-arrival estimation in AWGN and multipath with application to next GNSS", A. Emmanuele, M. Luise, In Proc. of the 5th ESA Workshop on Satellite Navigation Technologies (NAVITEC), Noordwijk, The Netherlands, Dec. 2010.

8. "Evaluation of filtered multitone (FMT) technology for future satellite navigation use", A. Emmanuele, M. Luise, J.H. Won, D. Fontanella, M. Paonni, B. Eissfeller, F. Zanier, G. Lopez-Risueno, In Proc. of the ION GNSS 2011, Portland, Oregon, Sept. 2011.

9. "Filtered Multitone (FMT) modulation for GNSS applications", A. Emmanuele, M. Luise, F. Zanier, M.Crisci, In Proc. of the 5th European Workshop on GNSS Signals and Signal Processing (GNSS Signals 2011), Toulouse, France, Dec. 2011.

10. "Ziv-Zakai bound for Time-Of-Arrival Estimation of GNSS Signal-In-Space", A. Emmanuele, M. Luise, F. Zanier, M.Crisci, In Proc. of the 5th European Workshop on GNSS Signals and Signal Processing (GNSS Signals 2011), Toulouse, France, Dec. 2011.

11. "Receiver Architecture for Multicarrier OFDM-based GNSS Signals", J.H. Won, D. Fontanella, M. Paonni, B. Eissfeller, A. G. Pena, O. Julien, C. Macabiau, A. Emmanuele, M. Luise, F. Zanier, G. Lopez-Risueno, In Proc. of the 5th European Workshop on GNSS Signals and Signal Processing (GNSS Signals 2011), Toulouse, France, Dec. 2011.

Other works

12. "Ziv-Zakai bound for time-of-arrival estimation of GNSS signal-in-space", A. Emmanuele, M. Luise, F. Zanier, Annual meeting of the National Telecommunications and Information Theory Group - GTTI, Taormina, Italy, June 2011.

13. "Final ESA Consultancy Technical Notes", A. Emmanuele, ESA internal report, TEC-ETN, Dec.2011.

14. "Innovative Signal Processing Techniques for Wireless Positioning", Elsevier, Inc. Editors: D. Dardari, E. Faletti, M. Luise. The text book includes the contribution of A. Emmanuele in Chapter V "Satellite and Terrestrial Radio Positioning Techniques". To be published in 2012.

Introduction

Motivations

New global navigation satellite systems (GNSSs) [51] such as GALILEO [1,26] are now reality, exhibiting higher performance with respect to (wrt) older GNSSs systems like global positioning system (GPS) [41] [51]. Improvements have been achieved taking full advantage of the gains obtained in the last years on concepts and technologies, such as new materials and components for spacecraft or advanced digital signal processing, just to cite a few. Nevertheless, even if at the time writing GALILEO is still not fully operational, the need for more systems and signals is already pushing the researchers to prospect new solutions for future advanced GNSSs [14, 36].

As a matter of fact, *timing recovery* represents the most critical function in every radio-location systems, including those based on satellite positioning. Current GNSSs are in fact based on the capability of a receiver to estimate the propagation times of a set of spread spectrum (SS) [52] signals broadcast by multiple satellites placed at known locations. When at least four propagation times are available, the receiver can unambiguously obtain its own spatial coordinates and the time reference [51]. In this scenario, *positioning accuracy* depends on the accuracy in *TDE* between transmitted codes and local replicas and it is apparent that the more accurate the TDE is, the more precise the user position will be.

In particular, time synchronization can easily be cast into a conventional parameter *estimation problem* [46], to be tackled with the tools of estimation theory [42]. Although acquisition and tracking issues for spreading codes in the field of satellite positioning are well documented in the literature [13, 48], their fundamental limits are relatively less investigated. Current activities aim at enhancing the overall navigation performance by providing better navigation signals to those available today, i.e., by *optimizing modulation schemes*. Actual ranging signals are based on direct sequence

spread spectrum (DS-SS) linearly modulated signals and thus signal optimization can be achieved either improving the code sequences [33], or combining existing signals like multiplexed binary offset carrier (MBOC) [37], or introducing new modulation chip waveforms [4, 9, 14, 35, 37] or, at last, optimizing a *signature waveform* given by an optimal combination of code and chip waveform as in [28, 62]. As output of these studies, several DS-SS signal options have been proposed, aiming at improving tracking performance both in an additive white Gaussian noise (AWGN) channel and in a channel affected by multipath (MP), while maintaining good acquisition and multiple access properties. In particular, TDE tracking accuracy is known to be related to the second order moment of the power spectral density (PSD) of the ranging signal [28,31,42]: the higher the second order moment the better the performance. As an example, the binary offset carrier (BOC) [9] modulations used for GALILEO have been chosen, among other features, for their characteristic of shifting the power at the edge of the band (and thus ensuring PSD higher second order moment) by means of subcarriers implemented in the modulation. This feature can reveal in contrast with the necessity of ensuring tight bandlimitation of the signal spectrum on board the satellite and the real performance of GPS and GALILEO signals are degraded wrt the theoretical ones due to the tight filtering [9].

In addition, it has also emerged that guaranteing a modulation scheme with a robust constant complex envelope has become a relevant signal design constraint that cannot be relaxed anymore [14]. This is especially true when looking at future GNSSs, where it is envisioned the use of highly non-linear high power amplifier (HPA), such as the traveling wave tube amplifier (TWTA), and for which it is foreseen that ranging signals will have to coexist with services for which out of band (OOB) emission becomes an issue [36], [14].

Innovative waveforms belonging to multicarrier (MC) modulations have been recently considered as possible GNSS solutions [21, 22, 27, 57], substantiated by their spectral and temporal flexibilities with its several degrees of freedom in its design, thanks to the large set of signal constituent parameters. Special cases such as the orthogonal frequency division multiplexing (OFDM), in Digital Video Broadcasting (DVB), and in particular the strictly bandlimited Filtered multitone (FMT), in the Digital Subscriber Line (DSL), now become popular in communication, can be reformulated and re-designed for GNSS applications.

This thesis inserts in this lively environment, tackling with the fundamental issues

of TDE and concentrating on the ultimate limits in the accuracy of such function, by focusing on the properties of the transmitted signal.

Several topics on TDE are covered at theoretical levels (thus being applicable to any positioning system, either a wireless network or a GNSS), while specific considerations are made with application to satellite positioning, due to the strong motivation in this field.

Main contributions

This thesis is specifically focused on the problem of improving TDE accuracy of SS signals [52], focusing on the fundamental issue of estimation theory and on the properties of the transmitted signal. As such, in this contribution we propose some signal design criteria and modulation schemes, that can offer practical responses when envisioning new global navigation satellite system (GNSS) services aiming at improved accuracy.

The analysis proposed in this thesis is conducted from a theoretical point of view and can be thus re-applied to many fields of digital signal processing. The results can easily be readapted to wireless communication by replacing the satellite with the communication terminal.

In this context, the main contributions of this thesis are as follows:

- the results available in the literature for TDE fundamentals limits are further exploited; formulations of the Cramér Rao Bound and of the Ziv-Zakai Bound are reported, deeply investigating on *modified* versions of the bounds, well known for the first case and innovative for the latter, to lighten their computation in presence of unknown parameters. Alternative formulations of the bounds as a function of the spectral properties of a generic modulation format are also discussed;

- the adoption of the ZZB as benchmark for both acquisition and tracking stage performance is addressed, comparing the ZZB with the CRB when the latter results correct;

- the applicability of SS-CPM as ranging signals is addressed; SS-CPM demonstrated particularly expedient due to the properties of being intrinsically constant envelope and spectral efficient; it has emerged that setting the modulation

index h to $h > 1$ allows the SS-CPM signal to behave like having a subcarrier, thus improving TDE accuracy; some estimation algorithms for SS-CPM signals are proposed and tested; an ad hoc encoding of the SS-CPM allows the transmission of two different rate services on a single constant envelope waveform;

- starting from a discussion on the signal properties in time and frequency domain, we show how a multicarrier (MC) signal can be formatted to obtain maximum estimation accuracy, or minimum interference or minimum interference simply by adaptively modifying the system's parameters, proposing the special case of Filtered Multitone (FMT) as possible candidate;

- the inherent strictly bandlimited property and the full spectral flexibility possessed by the FMT is expedient to adapt the system to different channel conditions or in particular to emulate existing or innovative spectra;

- performance of a standard tracking algorithm is tested for some SS-FMT schemes.

Outline

The remainder of this thesis is structured as follows.

In Chapter 1, we recall the *basis of positioning systems*, posing the link between time delay estimation (TDE) and positioning estimation.

In Chapter 2, we introduce the concept of *signal optimization* through TDE. In particular, we start outlining the basic concepts of estimation theory. We then provide a deep insight on the *Cramér Rao bound* (CRB) and on the *Ziv-Zakai bound* (ZZB) for TDE of modulated signals, reviewing the literature on them and rewriting the bounds as a function of the signal spectral properties of a general modulated signal, proofing their matching in particular conditions. The well known *modified* CRB is reviewed and by its formulation we were inspired to similarly find an alternative version of the ZZB to lighten its computation in the presence of *nuisance* parameters.

In Chapter 3, we address the applicability of *spread spectrum continuous-phase-modulated (SS-CPM)* as ranging signals, due to the properties of SS-CPM signals of being intrinsically constant envelope and spectrally efficient. In particular, we investigate the performance of a subset of SS-CPM signals, characterized by a modulation index h greater than one, considering the architecture of a simplified all-digital

modem. We focus on the problem of spreading code synchronization (code tracking), presenting few low-complex chip timing recovery loops based on an Offset Quadrature Phase-Shift Keying (OQPSK) approximation of the signal. The relative performance of the proposed recovery loops are analyzed in terms of root mean square (RMS) tracking error and multipath (MP) robustness. Besides, an ad hoc encoding at the transmitter side is investigated, which allows the transmission of two coupled different rate services on a single constant envelope waveform by definition.

In Chapter 4, we focus on the applicability of multicarrier (MC) modulation as ranging signals, for its high degree of freedom, due to the large set of constituent parameters. In particular, we investigated the special case of the Filtered Multitone (FMT) modulation, which results very interesting also for its strictly bandlimited spectrum, with limited out of band (OOB) emission, regardless of the particular power distribution within the active subcarriers adopted. Particular cases of study are reported and assessed in terms of root mean square error (RMSE) in AWGN channel and multipath error envelope (MPEE) in a single MP ray scenario.

In Chapter 5, the adoption of the *modified* Ziv-Zakai bound (MZZB) as benchmark for both signal acquisition and tracking performance is addressed. Testing standard and innovative GNSS cases of study, negative effects of the signal correlation function ambiguities on the TDE performance are detected and quantified.

In Chapter 6, we finally draw some conclusions for this thesis and we discuss open issues and further perspectives for this research field.

Chapter 1

Basics of positioning systems

Navigation is defined as the science of getting a craft or person from one place to another. In this thesis we explore the fundamental limits of *time delay estimation* (TDE) and more properly for navigation of *time-of-arrival* (TOA) estimation. Even if the analysis can be generally applied to many fields of digital signal processing, we here conduct the study with particular application to the *satellite positioning systems*. For the description of global navigation satellite systems, we refer to the extensive bibliography [41,51] on it. In this Chapter, we only recall the fundamentals of satellite navigation to motivate the link between *positioning accuracy* and *TOA accuracy*, as explained in [41].

1.1 Introduction

Navigation is defined as the science of getting a craft or person from one place to another. Each of us conducts some form of navigation in our daily lives. Driving to work or walking to a store requires that we employ fundamental navigation skills. For most of us, these skills require utilizing our eyes, common sense, and landmarks. However, in some cases where a more accurate knowledge of our position, intended course, or transit time to a desired destination is required, navigation aids other than landmarks are used. These may be in the form of a simple clock to determine the velocity over a known distance or the odometer in our car to keep track of the distance traveled. Some other navigation aids transmit electronic signals and therefore are more complex. These are referred to as radionavigation aids. Signals from one or more radionavigation aids enable a person (herein referred to as the user) to compute their position. (Some radionavigation aids provide the capability for

velocity determination and time dissemination as well.) It is important to note that it is the users radionavigation receiver that processes these signals and computes the position fix. The receiver performs the necessary computations (e.g., range, bearing, and estimated time of arrival) for the user to navigate to a desired location. In some applications, the receiver may only partially process the received signals, with the navigation computations performed at another location. Various types of radionavigation aids exist, and they can be categorized as either ground-based or space-based. For the most part, the accuracy of ground-based radionavigation aids is proportional to their operating frequency. Highly accurate systems generally transmit at relatively short wavelengths, and the user must remain within line of sight (LOS), whereas systems broadcasting at lower frequencies (longer wavelengths) are not limited to LOS but are less accurate. Early spaced-based systems (namely, the U.S. Navy Navigation Satellite Systemreferred to as Transitand the Russian Tsikada system) provided a two-dimensional high-accuracy positioning service. However, the frequency of obtaining a position fix is dependent on the users latitude. Theoretically, a Transit user at the equator could obtain a position fix on the average of once every 110 minutes, whereas at 80 latitude the fix rate would improve to an average of once every 30 minutes. Limitations applicable to both systems are that each position fix requires approximately 10 to 15 minutes of receiver processing and an estimate of the users position. These attributes were suitable for shipboard navigation because of the low velocities, but not for aircraft and high-dynamic users. It was these shortcomings that led to the development of the U.S. Global Positioning System (GPS).

1.2 Global Positioning System (GPS)

The NAVSTAR-GPS (NAVigation System for Timing And Ranging - Global Positioning System) project was officially launched in 1973 by the U.S. Department of Defense (DoD) to give birth to a positioning service with global coverage and continuous-time availability. The GPS was originally developed for authorized (military) use only and subsequently made available to civil users in 1983. For a detailed history of the GPS project, the interested reader may refer to [49].

The GPS system is composed of three *segments*: satellite constellation (the *space segment (SS)*), ground control/monitoring network (the *operational control segment (OCS)*), and user receiver equipment (the *user segment (US)*). The OCS, that tracks

and maintains the satellite in space, monitors satellite health and signal integrity and maintains the orbital configuration of the SS. Furthermore, the OCS updates the satellite clock corrections and ephemerides, as well as other fundamental parameters. The US is typically the user receiver equipment, that processes the GPS signals to determine user's position, velocity, and time (PVT).

At the time of this writing, the current GPS constellation consists of 31 satellites, positioned on six earth-centered orbital planes with five to six satellites on each plane. The current constellation is composed of ten Block IIA satellites, launched between 1990 and 1997, during which the system was declared fully operational, twelve Block IIR (1997-2004), seven Block IIR-M (2005-2009) and only two Block IIF (2010-present). Ten prototype satellites (called Block I) have been launched to test and validate the system concepts between 1978 and 1985 whereas Block II were launched from 1989 and 1990. First two satellites of next generation Block IIF have been launched, other ten are in preparation, whereas a number of Block III satellites are planned to be employed for a post-2014 deployment. The nominal orbital period of a GPS is one-half of a sidereal day (approximately 11 h 58 min). The orbits are nearly circular and equally spaced about the equator at a 60° separation with an inclination relative to the equator of nominally 55°, whereas the orbital radius is approximately $26,600$ km. The GPS constellation provides a 24-hr global user navigation and time determination capability.

GPS provides two services: the *standard position service (SPS)* and the *precise position service (PPS)*. The SPS is designed for the civil community, whereas the PPS is slated for the United States authorized military and selected government agency users. Further details are provided in the next subsections.

1.2.1 Modernized GPS

From the launch of the first GPS satellite in 1978 through all of 2004 there have been three navigation signals on two frequencies. Since the launch of the first Block IIR-M satellite (Sept. 26th, 2005), the SPS is also available on the L2 channel. In the near future, the number of navigation signals will increase from three to seven and the number of frequencies from two to three. In addition, the new signals will have substantially better characteristics, including a pilot carrier, much longer codes, the use of forward error correction, and a more flexible message structure with much

better resolution.

New and modern civil signals will be on L2 and on the new L5 frequency. The current GPS modernization plan, however, leaves the L1 frequency with only the outdated C/A signal for civil applications. The next level of modernization will include a new signal for the L1 frequency, named L1C. With the addition of L1C, all three GPS frequencies would then provide a modernized civil signal, completing the GPS modernization process.

There is good reason to concentrate attention on L1. Today it carries C/A, the only civil GPS signal. In the future, even with new and modern L2 and L5 signals, L1 is expected to remain the most important civil frequency. This is primarily because it is less affected by ionospheric refraction error than L2 or L5. (L1 has only 61% of the L2 error and 56% of the L5 error). This inherent advantage relative to L2 and L5 helps motivate the basic goal of this modernization project.

In order to allow the interoperability between GPS and Galileo systems, the U.S. and the European Union (EU) completed negotiations about the compatibility of Galileo L1 signals with both military and civil GPS signals [1]. As part of these negotiations, the U.S. Department of State proposed that the U.S. would implement a new signal on L1 with BOC modulation (see Sect. 1.3 for further details) if Europe would do the same on Galileo.

At the time of this writing, the interface specification [5] describes the current L1C signal. The L1C signal consists of two main components; one denoted $\mathrm{L1C_P}$ to represent a pilot signal, without any data message, that is spread by a ranging code, and $\mathrm{L1C_D}$ that is spread by a ranging code and modulated by a data message. The $\mathrm{L1C_P}$ is also modulated by an SV unique overlay code, $\mathrm{L1C_O}$. The data message on $\mathrm{L1C_D}$, denoted $\mathrm{DL1C}(t)$, includes SV ephemerides, system time, system time offsets, SV clock behavior, status messages, and other data messages. The message structure and data encoding techniques will include Bose-Chaudhuri-Hocquenghem (BCH), cyclic redundancy check (CRC) and **LDPC!** (**LDPC!**) **FEC!** (**FEC!**) codes. The resulting channel encoded symbols, $D_{L1C}(t)$, representing one message frame, will be broadcast at 100 sps.

The $\mathrm{L1C_D}$ signal is modulated on the L1 RF carrier using a Binary Offset Carrier (BOC) (1, 1) modulation technique [9]. The $\mathrm{L1C_P}$ signal is modulated on the L1 RF carrier using a Time-Multiplexed BOC (TMBOC) modulation technique, which uses a combination of BOC (1, 1) and BOC (6, 1) modulation [5].

1.3 Galileo

Galileo is the European global navigation satellite system (GNSS) providing a global positioning service under civilian control. It is inter-operable with GPS and GLONASS, the American and Russian GNSSs, respectively. The first stage of the Galileo programme was agreed upon officially on May 26, 2003 by the EU and the European Space Agency (ESA).

Galileo is based on a constellation of medium earth orbit (MEO) satellites and ground stations providing information concerning the positioning of users in many sectors such as transport (e.g., vehicle location, route searching, speed control, guidance systems), social services (e.g., aid for the disabled and for the elderly), services for the justice system and customs procedures (e.g., location of suspects, border controls), public works (e.g., geographical information systems), search and rescue (SAR), and leisure (e.g., direction-finding at the sea or in the mountains).

The fully deployed Galileo system will consist of 30 satellites (27 operational and 3 spares), positioned in three circular MEO planes at a nominal average orbit semi-major axis of $29,601.297$ km, and at an inclination of the orbital planes of $56°$ with reference to the equatorial plane.

In the Galileo project validation phase, the first experimental satellite, *GIOVE-A*, was launched in 2005 and was followed by a second test satellite, *GIOVE-B*, recently launched in 2008 to provide experimental results for the GPS-Galileo common signal using the MBOC modulation [37] in accordance with the agreement [1] drawn up by the EU and the U.S. [25]. Construction of next GIOVE, GIOVE-A2 was terminated due to the successful launch and in-orbit operation of GIOVE-B.

When in operation, the Galileo system will use two ground operations centres, near Munich, Germany and in Fucino, Italy. The system was initially expected to become operational by 2012, but that date has been repeatedly moved back. As of 2011, initial service is expected around 2014 and completion by 2019.

Five different services are expected from Galileo:

- an *open service (OS)* providing all information such as positioning, navigation and timing services, free of charge, for mass market navigation applications, interoperable with other GNSSs, and competitive to the GPS standard positioning services;

- a *safety-of-life (SoL),* compliant to the needs of safety critical users such as civil aviation, maritime and rail domain. The SoL includes high integrity and authentication capability, although the activation of these possibilities will depend on the user communities. Furthermore, the SoL service includes service guarantees;

- a *control segment/commercial service (CS),* generating commercial revenue by providing added value over the OS, such as by dissemination of encrypted navigation related data, ranging and timing for professional use, with service guarantees, high integrity level, precise timing services, high data rate broadcasting, provision of ionospheric delay modes, local differential correction signals and controlled access;

- a *public regulated service (PRS),* for application devoted to European and member states, for critical applications and activities of strategic importance. It makes use of a robust signal and is controlled by member states. This service provides services guarantees, high integrity, full range of value added features and an access controlled by encryption; and

- an *search and rescue (SAR)* service, providing assistance to the COSPAS-SARSAT system by detecting emergency beacons and forwarding return link messages to the emergency beacons. It is a service for SAR applications by providing near real time reception of distress message and precise location of alert.

1.4 GLONASS

GLONASS, GLObal'naya NAvigatsionnaya Sputnikovaya Sistema (global navigation satellite system) is a navigation satellite system developed by the former Soviet Union in response to the GPS. Like GPS, GLONASS was initially targeted to the URSS Army needs: navigating and ballistic missile targeting with world coverage. The setting-up of the system started in 1976 to reach full deployment in 1995. At that time the constellation comprehended 24 satellites and transmitted on the L1 band using a frequency division multiple access (FDMA). In the following years the lack of funding, due to collapse of the Russian economy, deeply damaged the system

efficiency. However, the strategic importance of the satellite navigation was worldwide affirmed: European Union started the Galileo project and the United States the GPS modernization. Therefore, in 1999 GLONASS became officially a dual-use system,[1] by a Presidential decree [30] and, at the beginning of the new century the GLONASS reconstruction was boosted by the Russian extra-gain due to the oil and gas export. The GLONASS system has been under a deep modernization, with the civil side managed by the Russian Space Agency. Over the three decades of development, the satellite designs have gone through numerous improvements, and can be divided into three generations: the original GLONASS (since 1982), GLONASS-M (since 2003) and GLONASS-K (since 2011). A fully operational constellation with global coverage consists of 24 satellites, while 18 satellites are necessary for covering the territory of Russia. At the time of this writing, the full constellation (24 sats) with performance comparable with GPS are expected by the end of 2011. Although the format and modulation of GLONASS (CDMA) signals are not fully finalized, statements from developers indicate that the new signals are essentially GPS/Galileo/COMPASS format signals placed at the same frequencies, [55].

1.5 Compass/Beidou

Compass is the incoming Chinese GNSS. China started the development of an indigenous navigation satellite system technology since the sixties of the last century but only during the eighties the research become really effective. In 1994 China approved a new satellite system for navigation purposes based on the *radio determination satellite service (RDSS)*, a different technology in comparison to the GPS one [40].

The first Chinese system was named Beidou, from the Chinese name of the Northern Star, the brightest star of the *Ursa Minor* constellation. Beidou was born like a regional dual system, both military an civil, to provide navigation and timing to China and surrounding areas.

With only 3 geostationary (GEO) satellites, it has been offering navigation services mainly for customers in China and from neighboring regions since 2000. The evolution of the Beidou system is usually called Beidou-2 or, more usually, Compass. The first satellite of the Compass navigation satellite system (CNSS), which is a MEO satellite,

[1] i.e., a system intended for both military and civil applications.

was launched on April 2007. The second generation of the system, which will be a global satellite navigation system consisting of 35 satellites, is still under construction. It is planned to offer services to customers in Asia-Pacific region by 2012 and the global system should be finished by 2020.

1.6 Ranging using time of arrival (TOA) or time delay (TD) measurements

GPS utilizes the concept of TOA ranging to determine user position. This concept entails measuring the time it takes for a signal transmitted by an emitter (e.g., foghorn, radiobeacon, or satellite) at a known location to reach a user receiver. This time interval, referred to as the signal propagation time, is then multiplied by the speed of the signal (e.g., speed of sound or speed of light) to obtain the emitter-to- receiver distance. By measuring the propagation time of the signal broadcast from multiple emitters (i.e., navigation aids) at known locations, the receiver can determine its position. An example of two-dimensional positioning is provided next.

1.6.1 Position determination in two dimensions

Consider the case of a mariner at sea determining his or her vessels position from a foghorn. Assume that the vessel is equipped with an accurate clock and the mariner has an approximate knowledge of the vessels position. Also, assume that the foghorn whistle is sounded precisely on the minute mark and that the vessels clock is synchronized to the foghorn clock. The mariner notes the elapsed time from the minute mark until the foghorn whistle is heard. The foghorn whistle propagation time is the time it took for the foghorn whistle to leave the foghorn and travel to the mariners ear. This propagation time multiplied by the speed of sound (approximately 335 m/s) is the distance from the foghorn to the mariner. If the foghorn signal took 5 seconds to reach the mariners ear, then the distance to the foghorn is 1,675m. Let this distance be denoted as R1. Thus, with only one measurement, the mariner knows that the vessel is somewhere on a circle with radius R1 centered about the foghorn.

Hypothetically, if the mariner simultaneously measured the range from a second foghorn in the same way, the vessel would be at range R1 from Foghorn 1 and range R2 from Foghorn 2. It is assumed that the foghorn transmissions are synchronized to

a common time base and the mariner has knowledge of both foghorn whistle transmission times. Therefore, the vessel relative to the foghorns is at one of the intersections of the range circles. Since it was assumed that the mariner has approximate knowledge of the vessels position, the unlikely fix can be discarded. Resolving the ambiguity can also be achieved by making a range measurement to a third foghorn.

This development assumed that the vessels clock was precisely synchronized with the foghorn time base. However, this might not be the case. Let us presume that the vessels clock is advanced with respect to the foghorn time base by 1 second. That is, the vessels clock believes the minute mark is occurring 1 second earlier. The propagation intervals measured by the mariner will be larger by 1 second due to the offset. The timing offsets are the same for each measurement (i.e., the offsets are common) because the same incorrect time base is being used for each measurement. The timing offset equates to a range error of 335m. The separation of intersections from the true vessel position is a function of the vessels clock offset. If the offset could be removed or compensated for, the range circles would then intersect at the point of vessel position.

If this hypothetical scenario were realized, the TOA measurements would not be perfect due to errors from atmospheric effects, foghorn clock offset from the foghorn time base, and interfering sounds. Unlike the vessels clock offset condition cited earlier, these errors would be generally independent and not common to all measurements. They would affect each measurement in a unique manner and result in inaccurate distance computations. Instead of the three range circles intersecting at a single point, the vessel location is somewhere within a triangular error space.

1.6.2 Principle of Position Determination Via Satellite Ranging Signals

GNSS employs TOA ranging for user position determination. By making TOA measurements to multiple satellites, three-dimensional positioning is achieved. We will observe that this technique is analogous to the preceding foghorn example; however, satellite ranging signals travel at the speed of light, which is approximately $3 \cdot 10^8$ m/s. It is assumed that the satellite ephemerides are accurate (i.e., the satellite locations are precisely known). Assume that there is a single satellite transmitting a ranging signal. A clock onboard the satellite controls the timing of the ranging

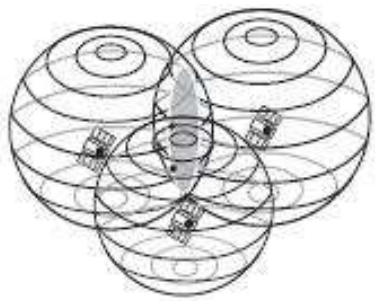

Figure 1.1: *User located at one of two points on shaded circle.*

signal broadcast. This clock and others onboard each of the satellites within the constellation are effectively synchronized to an internal system time scale denoted as GPS system time (herein referred to as system time). The users receiver also contains a clock that (for the moment) we assume to be synchronized to system time. Timing information is embedded within the satellite ranging signal that enables the receiver to calculate when the signal left the satellite based on the satellite clock time. By noting the time when the signal was received, the satellite-to-user propagation time can be computed. The product of the satellite-to-user propagation time and the speed of light yields the satellite-to-user range, R. As a result of this measurement process, the user would be located somewhere on the surface of a sphere centered about the satellite. If a measurement were simultaneously made using the ranging signal of a second satellite, the user would also be located on the surface of a second sphere that is concentric about the second satellite. Thus, the user would then be somewhere on the surface of both spheres, which could be either on the perimeter of the shaded circle in Fig.1.1, that denotes the plane of intersection of these spheres or at a single point tangent to both spheres (i.e., where the spheres just touch). This latter case could only occur if the user were collinear with the satellites, which is not the typical case. The plane of intersection is perpendicular to a line connecting the satellites. Repeating the measurement process using a third satellite, the user is at the intersection of the perimeter of the circle and the surface of the third sphere.

This third sphere intersects the shaded circle perimeter at two points; however, only one of the points is the correct user position. It can be observed that the candidate locations are mirror images of one another with respect to the plane of the satellites.

For a user on the Earths surface, it is apparent that the lower point will be the true position. However, users that are above the Earths surface may employ measurements from satellites at negative elevation angles. This complicates the determination of an unambiguous solution. Airborne/spaceborne receiver solutions may be above or below the plane containing the satellites, and it may not be clear which point to select unless the user has ancillary information.

1.6.3 Position Determination Using PRN Codes

GNSS satellite transmissions utilize direct sequence spread spectrum (DSSS) modulation. DSSS provides the structure for the transmission of ranging signals and essential navigation data, such as satellite ephemerides and satellite health. The ranging signals are PRN codes that binary phase shift key (BPSK) modulate the satellite carrier frequencies. These codes look like and have spectral properties similar to random binary sequences but are actually deterministic. These codes have a predictable pattern, which is periodic and can be replicated by a suitably equipped receiver. At the time of this writing, each GPS satellite broadcasted two types of PRN ranging codes: a short coarse/acquisition (C/A)-code and a long precision (P)-code. (Additional signals are planned to be broadcast.) The C/A code has a 1-ms period and repeats constantly, whereas the P-code satellite transmission is a 7-day sequence that repeats approximately every Saturday/Sunday midnight. Presently, the P-code is encrypted. This encrypted code is denoted as the Y-code. The Y-code is accessible only to PPS users through cryptography.

Determining Satellite-to-User Range Earlier, we examined the theoretical aspects of using satellite ranging signals and multiple spheres to solve for user position in three dimensions. That example was predicated on the assumption that the receiver clock was perfectly synchronized to system time. In actuality, this is generally not the case. Prior to solving for three-dimensional user position, we will examine the fundamental concepts involving satellite-to-user range determination with nonsynchronized clocks and PRN codes. There are a number of error sources that affect range measurement accuracy (e.g., measurement noise and propagation delays); however, these can generally be considered negligible when compared to the errors experienced from nonsynchronized clocks. Therefore, in our development of basic concepts, errors

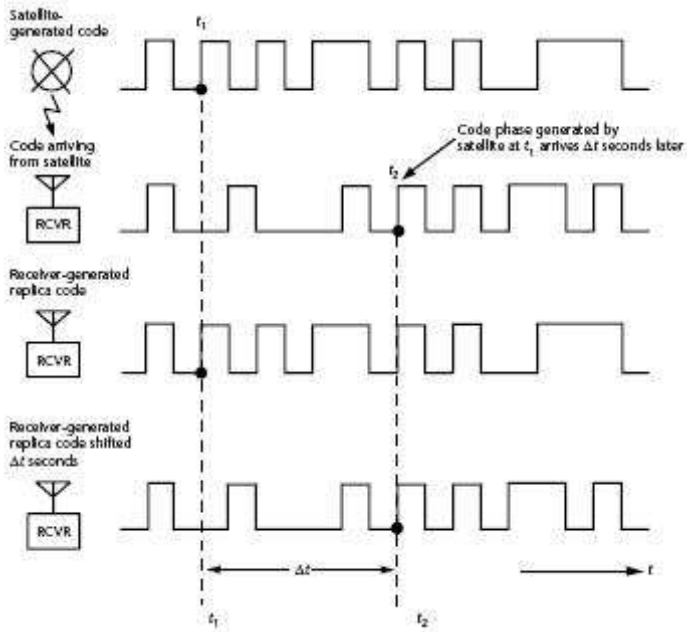

Figure 1.2: *Use of replica code to determine satellite code transmission time*

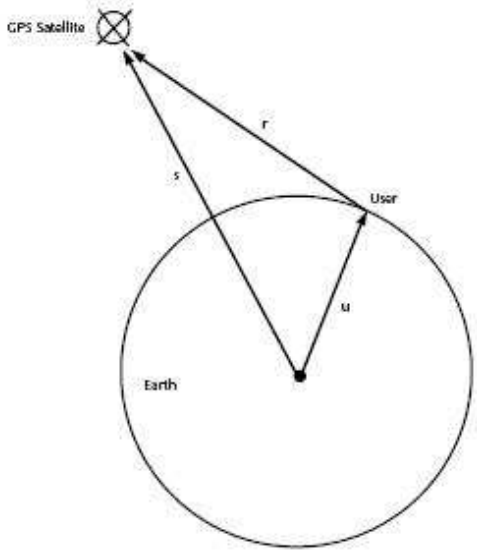

Figure 1.3: *User position vector representation*

other than clock offset are omitted.

In Fig.1.3, we wish to determine vector u, which represents a user receivers position with respect to the ECEF coordinate system origin. The users position coordinates p_x, p_y, p_z are considered unknown. Vector r represents the vector offset from the user to the satellite. The satellite is located at coordinates x_s, y_s, z_s within the ECEF Cartesian coordinate system. Vector s represents the position of the satellite relative to the coordinate origin. Vector s is computed using ephemeris data broadcast by the satellite. The satellite-to-user vector $\underrightarrow{r}$ is

$$\underrightarrow{r} = \underrightarrow{s} - \underrightarrow{u}. \tag{1.1}$$

The magnitude of vector $\underrightarrow{r}$ is

$$||\underrightarrow{r}|| = ||\underrightarrow{s} - \underrightarrow{u}||. \tag{1.2}$$

Let r represent the magnitude of $\underrightarrow{r}$,

$$r = ||\underrightarrow{s} - \underrightarrow{u}||. \tag{1.3}$$

The distance r is computed by measuring the propagation time required for a satellite-generated ranging code to transit from the satellite to the user receiver antenna. The propagation time measurement process is illustrated in Fig.1.2. As an example, a specific code phase generated by the satellite at t_1 arrives at the receiver at t_2. The propagation time is represented by t. Within the receiver, an identical coded ranging signal is generated at t, with respect to the receiver clock. This replica code is shifted in time until it achieves correlation with the received satellite-generated ranging code. If the satellite clock and the receiver clock were perfectly synchronized, the correlation process would yield the true propagation time. By multiplying this propagation time, Δt, by the speed of light, the true (i.e., geometric) satellite-to-user distance can be computed. We would then have the ideal case described in the previous section. However, the satellite and receiver clocks are generally not synchronized. The receiver clock will generally have a bias error from system time. Further, satellite frequency generation and timing is based on a highly accurate free running cesium or rubidium atomic clock, which is typically offset from system time. Thus, the range determined by the correlation process is denoted as the pseudorange . The measurement is called pseudorange because it is the range determined by multiplying the signal propagation velocity, c, by the time difference between two nonsynchronized clocks (the satellite clock and the receiver clock). The measurement contains (1) the geometric satellite-to-user range, (2) an offset attributed to the difference between system time and the user clock, and (3) an offset between system time and the satellite clock. The timing relationships are:

- T_s = System time at which the signal left the satellite
- T_u = System time at which the signal reached the user receiver
- t = Offset of the satellite clock from system time [advance is positive; retardation (delay) is negative]
- t_u = Offset of the receiver clock from system time
- $T_s + t$ = Satellite clock reading at the time that the signal left the satellite
- $T_u + t_u$ = User receiver clock reading at the time the signal reached the user receiver
- c = speed of light

- Geometric range, $r = c\,(T_u - T_s) = c\Delta t$
- Pseudorange $R_p = c\,[(T_u + t_u) - (T_s + \delta t)] = c\,(T_u - T_s) + c\,(t_u - \delta t) = r + c\,(t_u - \delta t)$

Therefore, r can be rewritten as:

$$R_p - c\,(t_u - \delta t) = ||\underset{\rightarrow}{s} - \underset{\rightarrow}{u}|| \tag{1.4}$$

where t_u represents the advance of the receiver clock with respect to system time, Δt represents the advance of the satellite clock with respect to system time, and c is the speed of light.

The satellite clock offset from system time, Δt, is composed of bias and drift contributions. The GPS ground-monitoring network determines corrections for these offset contributions and transmits the corrections to the satellites for rebroadcast to the users in the navigation message. These corrections are applied within the user receiver to synchronize the transmission of each ranging signal to system time. Therefore, we assume that this offset is compensated for and no longer consider Δt an unknown. (There is some residual offset, but in the context of this discussion we assume that this is negligible.) Hence, the preceding equation can be expressed as

$$R_p - ct_u = ||\underset{\rightarrow}{s} - \underset{\rightarrow}{u}|| \tag{1.5}$$

Calculation of User Position In order to determine user position in three dimensions (p_x, p_y, p_z) and the offset t_u, pseudorange measurements are made to four satellites resulting in the system of equations

$$R_p k = ||\underset{\rightarrow}{s} - \underset{\rightarrow}{u}|| + ct_u \tag{1.6}$$

where k ranges from 1 to 4 and references the satellites. The previous equation can be expanded into the following set of equations in the unknowns p_x, p_y, p_z, and $b = c \cdot t_u$:

$$R_{pk} = \sqrt{(x_k - p_x)^2 + (y_k - p_y)^2 + (z_k - p_z)^2} + b = D_k + b, \tag{1.7}$$

where x_k, y_k, and z_k denote the k-th satellites position in three dimensions.

These nonlinear equations can be solved for the unknowns by employing either (1) closed-form solutions , (2) iterative techniques based on linearization, or (3) Kalman

filtering. (Kalman filtering provides a means for improving PVT estimates based on optimal processing of time sequence measurements) Linearization is illustrated in the following paragraphs. If we know approximately where the receiver is, then we can denote the offset of the true position (p_x, p_y, p_z) from the approximate position ($\hat{p}_x$,$\hat{p}_y$,$\hat{p}_z$) by a displacement (Δx,Δy,Δz). By expanding the previous equation in a Taylor series about the approximate position, we can obtain the position offset (Δx_u, Δy_u, Δz_u) as linear functions of the known coordinates and pseudorange measurements. This process is described next. Let a single pseudorange be represented by

$$R_{pk} = \sqrt{(x_k - p_x)^2 + (y_k - p_y)^2 + (z_k - p_z)^2} + b = D_k + b = f\left(p_x, p_y, p_z, b\right), \quad (1.8)$$

Using the approximate position location ($\hat{p}_x$, $\hat{p}_y$, $\hat{p}_z$) and time bias estimate $\hat{t}_u$, an approximate pseudorange can be calculated:

$$\hat{R}_{pk} = \sqrt{(x_k - \hat{p}_x)^2 + (y_k - \hat{p}_y)^2 + (z_k - \hat{p}_z)^2} + \hat{b} = \hat{D}_k + \hat{b} = f\left(\hat{p}_x, \hat{p}_y, \hat{p}_z, \hat{b}\right), \quad (1.9)$$

As stated earlier, the unknown user position and receiver clock offset is considered to consist of an approximate component and an incremental component:

$$\begin{aligned} p_x &= \hat{p}_x + \Delta x \\ p_y &= \hat{p}_y + \Delta y \\ p_z &= \hat{p}_z + \Delta z \\ b &= \hat{b} + \Delta b \end{aligned} \quad (1.10)$$

Therefore, we can write

$$f\left(p_x, p_y, p_z, b\right) = f(\hat{p}_x + \Delta x, \hat{p}_y + \Delta y, \hat{p}_z + \Delta z, \hat{b} + \Delta b) \quad (1.11)$$

This latter function can be expanded about the approximate point and associated predicted receiver clock offset ($\hat{p}_x$,$\hat{p}_y$,$\hat{p}_z$) using a Taylor series:

$$\begin{aligned} &f(\hat{p}_x + \Delta x, \hat{p}_y + \Delta y, \hat{p}_z + \Delta z, \hat{b} + \Delta b) \cong \\ &f(\hat{p}_x, \hat{p}_y, \hat{p}_z, \hat{b}) + \frac{\partial}{\partial \hat{p}_x} f(\hat{p}_x, \hat{p}_y, \hat{p}_z, \hat{b})\Delta p_x + \\ &\frac{\partial}{\partial \hat{p}_y} f(\hat{p}_x, \hat{p}_y, \hat{p}_z, \hat{b})\Delta p_y + \frac{\partial}{\partial \hat{p}_z} f(\hat{p}_x, \hat{p}_y, \hat{p}_z, \hat{b})\Delta p_z + \frac{\partial}{\partial \hat{b}} f(\hat{p}_x, \hat{p}_y, \hat{p}_z, \hat{b})\Delta b \end{aligned} \quad (1.12)$$

The expansion has been truncated after the first-order partial derivatives to eliminate nonlinear terms. The partial derivatives evaluate as follows:

$$\begin{aligned}
\frac{\partial}{\partial \hat{p}_x} f(\hat{p}_x, \hat{p}_y, \hat{p}_z, \hat{b}) &= -\frac{x_k - \hat{p}_x}{\hat{D}_k} \\
\frac{\partial}{\partial \hat{p}_y} f(\hat{p}_x, \hat{p}_y, \hat{p}_z, \hat{b}) &= -\frac{y_k - \hat{p}_y}{\hat{D}_k} \\
\frac{\partial}{\partial \hat{p}_z} f(\hat{p}_x, \hat{p}_y, \hat{p}_z, \hat{b}) &= -\frac{z_k - \hat{p}_z}{\hat{D}_k} \\
\frac{\partial}{\partial \hat{b}} f(\hat{p}_x, \hat{p}_y, \hat{p}_z, \hat{b}) &= 1
\end{aligned} \tag{1.13}$$

where

$$\hat{D}_k = \sqrt{(x_k - \hat{p}_x)^2 + (y_k - \hat{p}_y)^2 + (z_k - \hat{p}_z)^2} \tag{1.14}$$

The first three derivatives denote the direction cosines of the unit vector pointing from the approximate user position to the k-th satellite, and we denote them by $(a_k, b_k, c_k\ )$. Substituting and rearranging this expression with the known quantities on the left and unknowns on right we yield to

$$R_{pk} = \hat{R}_{pk} + a_k \Delta x + b_k \Delta y + c_k \Delta z + \Delta b. \tag{1.15}$$

These equation can be put in matrix form by making the definitions

$$\underline{\Delta R_p} = \begin{bmatrix} \Delta R_{p1} \\ \Delta R_{p2} \\ \Delta R_{p3} \\ \Delta R_{p4} \end{bmatrix}; \underline{\underline{H}} = \begin{bmatrix} a_1 & b_1 & c_1 & 1 \\ a_2 & b_2 & c_2 & 1 \\ a_3 & b_3 & c_3 & 1 \\ a_4 & b_4 & c_4 & 1 \end{bmatrix}; \underline{\Delta x} = \begin{bmatrix} \Delta x \\ \Delta y \\ \Delta z \\ \Delta b \end{bmatrix}; \tag{1.16}$$

Finally, one obtains:

$$\underline{\Delta R_p} = \underline{\underline{H}} \times \underline{\Delta x} \tag{1.17}$$

which has the solution

$$\underline{\Delta x} = \underline{\underline{H}}^{-1} \times \underline{\Delta R_p} \tag{1.18}$$

Once the unknowns are computed, the users coordinates p_x, p_y, p_z and the receiver clock offset t_u are then calculated. This linearization scheme will work well as long as the displacement (Δp_x, Δp_y, Δp_z) is within close proximity of the linearization point. The acceptable displacement is dictated by the users accuracy requirements. If the

displacement does exceed the acceptable value, this process is reiterated with being replaced by a new estimate of pseudorange based on the calculated point coordinates p_x, p_y, and p_z. In actuality, the true user-to-satellite measurements are corrupted by uncommon (i.e., independent) errors, such as measurement noise, deviation of the satellite path from the reported ephemeris, and multipath. These errors translate to errors in the components of vector Δx, as shown here:

$$\underline{\epsilon_x} = \underline{\underline{H}}^{-1} \times \underline{\epsilon_{meas}} \tag{1.19}$$

where ϵ_{meas} is the vector containing the pseudorange measurement errors and ϵ_x is the vector representing errors in the user position and receiver clock offset. The error contribution ϵ_x can be minimized by making measurements to more than four satellites, which will result in an overdetermined solution set of equations similar to the one just shown. Each of these redundant measurements will generally contain independent error contributions. Redundant measurements can be processed by least squares estimation techniques that obtain improved estimates of the unknowns. Various versions of this technique exist and are usually employed in todays receivers, which generally employ more than four user-to-satellite measurements to compute user PVT.

Chapter 2

Accuracy Limits for Time-Of-Arrival (TOA) Estimation

Timing recovery represents the most critical function in every radio-location systems, including those based on satellite positioning. In particular, positioning accuracy depends on the accuracy in time delay estimation (TDE) between transmitted codes and local replicas, to find the absolute time-of-arrival (TOA) of the first ones. In this scenario, it is apparent that the more accurate the TOA estimation is, the more precise the user position will be. This thesis proposes some criteria to calculate and improve TDE or TOA estimation accuracy of SS signals, focusing on the properties of the transmitted signal, with particular emphasis on investigating the fundamental limits of tracking performance. The aim of the Chapter is thus to give a close picture of TOA estimation accuracy and its maximization through signal design, providing a deep insight into its Cramér-Rao lower bound (CRB) and its Ziv-Zakai lower bound (ZZB) and their modified versions. In particular, after recalling the bases on estimation theory in Sect. 2.2 and specifically on the CRB and on the ZZB in 2.3 and 2.4, respectively, we will fix the problem of measuring TOA estimation accuracy for different signal formats in Sect. 2.5. In fact, specific formulas of the bounds for TDE in an AWGN channel will be discussed, and in particular Sect. 2.5.3 will investigate the interpretation of the same CRB and ZZB formulations as functions of the spectral properties of digitally modulated signal, showing their matching in specific conditions, and revealing to be the key-point for optimizing different signal

modulations irrespectively from how they are generated. Finally, some considerations on the applicability of the bounds are addressed.

2.1 Motivations

Global navigation satellite systems GNSS are based on the capability of a receiver to estimate the propagation times of a set of spread-spectrum SS signals broadcast by multiple satellites placed at known locations [41]. When at least four propagation times are available, the receiver can unambiguously obtain its own spatial coordinates and the time reference [51].

This thesis is specifically focused on the problem of improving positioning accuracy for GNSS, directly improving TDE. In particular, time synchronization can easily be cast into a conventional parameter estimation problem [46], to be tackled with the tools of estimation theory [42]. Although acquisition and tracking issues for spreading codes in the field of satellite positioning are well documented in the literature [13, 48], their fundamental limits are relatively less investigated. Many activities [4, 35, 37] aiming at enhancing the overall navigation performance are currently ongoing. This is typically performed by designing enhanced signals compared to those available today, e.g., by optimizing the modulation schemes. This can be achieved either introducing novel chip waveforms [4, 35] or combining existing signals, as is taken for the multiplexed binary offset carrier (MBOC) modulation [37], or finally adopting different modulation schemes.

This thesis proposes some criteria to improve TDE accuracy of SS signals [52], focusing on the properties of the transmitted signal. The problem is thus assessed using conventional parameter estimation and signal synchronization tools [42], which makes the proposed analysis suitable for both navigation and communication systems and independent of the particular receiver configuration. In the remainder of the thesis, we focus on satellite positioning, but the results can easily be readapted to wireless communication by replacing the satellite with the communication terminal.

Following these aims, this Chapter poses the theoretical bases on TDE for signal optimization. The fundamental limits in time synchronization are here recalled and further investigated in an AWGN channel. The results of this Chapter either comes from the literature or can be easily predicted, but are not easy to be explicitly found

in a unique text.

2.2 Estimation theory

This section recalls the fundamental performance limits on the estimation accuracy of a *scalar* parameter [42]. Let λ to be the deterministic parameter to be estimated and $\mathbf{r}$ to be the random vector of the observable samples (or data or outcomes) that depend on λ. The generic estimation process based on the observation of a realization of $\mathbf{r}$ will be denoted hereafter by $\hat{\lambda}(\mathbf{r})$ or simply by $\hat{\lambda}$.

An estimator is a function that maps a *sample design* to a set of sample estimates. A *sample design* can be thought of as an ordered pair $(\mathbf{r}, p(\mathbf{r}, \lambda))$ where $p(\mathbf{r}, \lambda)$ is the probability density function (pdf). The pdf maps the set of $\mathbf{r}$ to the closed interval [0,1], and has the property that the sum (or integral) of the values of $p(\mathbf{r}, \lambda)$, over all elements in $\mathbf{r}$, is equal to 1. The pdf is *parameterized* by the unknown parameter λ, i.e, there is a class of pdf where each one is different due to a different value of λ [42]. When the pdf is viewed as a function of the unknown parameter (with $\mathbf{r}$ fixed), it is termed the *likelihood function*.

Intuitively the "sharpness" of the likelihood function determines how accurately we can estimate the unknown parameter. To quantify this notion it can be observed that the sharpness is effectively measured by the negative of the second derivative of the logarithm of the likelihood function at its peak. This is the curvature of the *log-likelihood function*.

As such, $\hat{\lambda}(\mathbf{r})$ is a random variable, since it depends on the particular observation $\mathbf{r}$, and thus different observations lead to different estimates. As a random variable, $\hat{\lambda}(\mathbf{r})$ is characterized by its statistical properties, whose main definitions and properties are being reported. For all the properties below, the value λ, the estimation formula, the set of samples, and the set probabilities of the collection of samples, can be considered fixed. Yet since some of the definitions vary by sample (yet for the same set of samples and probabilities), we must use r in the notation. Hence, the estimate for a given sample r is denoted as $\hat{\lambda}(r)$.

We have the following definitions and attributes.

1. For a given sample r, the error ε of the estimator $\hat{\lambda}$ is defined as

$$\varepsilon = \hat{\lambda}(r) - \lambda. \tag{2.1}$$

Note that the error depends not only on the estimator (the estimation formula or procedure), but also on the sample itself.

2. The mean squared error of $\hat{\lambda}$ is defined as the expected value (probability-weighted average, over all samples) of the squared errors; that is,

$$\mathrm{MSE}(\hat{\lambda}) = \mathrm{E}[(\hat{\lambda} - \lambda)^2]. \tag{2.2}$$

It is used to indicate how far, on average, the collection of estimates are from the single parameter being estimated.

3. For a given sample r, the sampling deviation of the estimator $\hat{\lambda}$ is defined as

$$\hat{\lambda}(r) - \mathrm{E}(\hat{\lambda}), \tag{2.3}$$

where $\hat{\lambda}(r)$ is the estimate for sample r, and $\mathrm{E}(\hat{\lambda})$ is the expected value of the estimator. Note that the sampling deviation depends not only on the estimator, but also on the sample itself.

4. The variance of $\hat{\lambda}$ is simply the expected value of the squared sampling deviations; that is,

$$\mathrm{var}(\hat{\lambda}) = \mathrm{E}[(\hat{\lambda} - \mathrm{E}(\hat{\lambda}))^2]. \tag{2.4}$$

It is used to indicate how far, on average, the collection of estimates are from the expected value of the estimates. Note the difference between MSE and variance.

5. The bias of an estimator $\hat{\lambda}$ is defined as

$$b(\lambda) = \mathrm{E}(\hat{\lambda}) - \lambda. \tag{2.5}$$

It is the distance between the average of the collection of estimates, and the single parameter being estimated. It also is the expected value of the error, since $\mathrm{E}(\hat{\lambda}) - \lambda = \mathrm{E}(\hat{\lambda} - \lambda)$. The relationship between bias and variance is analogous to the relationship between accuracy and precision.

6. An estimator $\hat{\lambda}$ is an *unbiased estimator* of λ if and only if $b(\lambda) = 0$. Note that bias is a property of the estimator, not of the estimate. Often, people refer to a "biased estimate" or an "unbiased estimate", but they really are talking about an "estimate from a biased estimator", or an "estimate from an unbiased estimator".

7. The MSE, variance, and bias, are hence related:

$$\mathrm{MSE}(\hat{\lambda}) = \mathrm{var}(\hat{\lambda}) + (b(\lambda))^2, \tag{2.6}$$

   i.e. mean squared error = variance + square of bias.

8. The *standard deviation* of an estimator of λ (the square root of the variance), or an estimate of the standard deviation of an estimator of λ, is called the *standard error* or *RMSE* of λ.

2.3 Cramér-Rao bound (CRB) and Modified Cramér-Rao bound (MCRB)

2.3.1 The Cramér-Rao lower bound (CRB)

The Cramér-Rao lower bound (CRB) is a fundamental lower bound on the variance of any estimator [16, 56] and, as such, it serves as a benchmark for the performance of actual estimators [2, 42, 46] .

For a scalar parameter λ, the CRB states that the variance (or covariance) of any estimator of λ with bias function $b(\lambda)$ is lower bounded by [16, 56]

$$\mathrm{var}(\hat{\lambda}) = \mathrm{E}[(\hat{\lambda} - \mathrm{E}(\hat{\lambda}))^2] \geq CRB(\lambda) \tag{2.7}$$

where $CRB(\lambda)$ denotes the *true* CRB, given by [16, 54, 56]

$$CRB(\lambda) = \frac{\left[1 + \frac{db}{d\lambda}\right]^2}{\mathbb{E}_{\mathbf{r}}\left\{\left[\frac{\partial \ln p(\mathbf{r}|\lambda)}{\partial \lambda}\right]^2\right\}}. \tag{2.8}$$

The $p(\mathbf{r}|\lambda)$ is the pdf of the observations $\mathbf{r}$ when λ is the true value and $\mathbb{E}_{\mathbf{r}}\{\cdot\}$ in (2.7) and (2.8) denotes statistical expectation wrt the pdf $p(\mathbf{r})$.

Obviously, when the estimator is unbiased, the CRB simply reduces to

$$CRB(\lambda) = \frac{1}{\mathbb{E}_{\mathbf{r}}\left\{\left[\frac{\partial \ln p(\mathbf{r}|\lambda)}{\partial \lambda}\right]^2\right\}} \tag{2.9}$$

or, equivalently, to

$$CRB(\lambda) = \frac{1}{-\mathbb{E}_{\mathbf{r}}\left\{\frac{\partial^2 \ln p(\mathbf{r}|\lambda)}{\partial \lambda^2}\right\}}. \tag{2.10}$$

2.3.2 The Modified Cramér-Rao lower bound (MCRB)

The CRB is well known and widely adopted for its simple computation, but its close-form evaluation becomes mathematically intractable when the vector of observables contains, in addition to the parameter to be estimated, also some *nuisance parameters*, i.e., other unknown random quantities whose values we are not interested in (information data, random chips of the code of a ranging signal etc.), but that concurs to shape the actual values of the observables. To encompass the problem, it has been shown in [17] that in the presence of nuisance parameters, the variance of any unbiased estimator is lower bounded by the so-called Modified Cramér-Rao lower bound (MCRB), which is much simpler to evaluate than the *true* CRB. As proven in [17] the MCRB is in general looser than the true CRB, but it has been also demonstrated that in a few specific cases of synchronization parameter estimation, the MCRB is essentially as tight as the true CRB.

To better understand the problem, lets assume that the observable is given by a received waveform in an AWGN channel, whose baseband equivalent (or complex envelope) is

$$r\left(t\right) = x\left(t\right) + n\left(t\right), \tag{2.11}$$

and which is observed over an interval T_{obs}. In (2.11) $x\left(t\right)$ is the information-bearing signal and $n\left(t\right)$ represents the complex-valued additive white Gaussian noise with two-sided power spectral density $2N_0$. If we now assume that the signal is known in most of its basic characteristics (nominal carrier frequency, modulation format, signaling interval and so on), the remaining unknown parameters can be divided into two groups: the group of the parameter/parameters to be estimated and the group of unwanted parameters. Limiting to the case of estimating one parameter, denoted by λ, all other parameters, including the data, are collected in a random vector $\mathbf{u}$ having a known pdf $p(\mathbf{u})$ which does not depend on λ. An exact representation of the observed waveform $r\left(t\right)$ would require infinite-dimensional vector spaces, but it is realistic to assume that a finite-dimensional vector $\mathbf{r}$ can be found to represent $r\left(t\right)$ with adequate accuracy. It follows that the observation vector $\mathbf{r}$ is thus given by

$$\mathbf{r} = \mathbf{x}(\lambda, \mathbf{u}) + \mathbf{w}. \tag{2.12}$$

To compute the CRB as in (2.9) the pdf $p(\mathbf{r}|\lambda)$ is needed. In principle it can be

computed from the integral

$$p\left(\mathbf{r}|\lambda\right)=\int_{-\infty}^{+\infty}p\left(\mathbf{r}|\mathbf{u},\lambda\right)\cdot p\left(\mathbf{u}\right)d\mathbf{u}, \tag{2.13}$$

where $p\left(\mathbf{r}|\mathbf{u},\lambda\right)$, the conditional probability density function of $\mathbf{r}$ given $\mathbf{u}$ and λ, is easily available, at least for additive Gaussian channels. Unfortunately, in most cases of practical interest, the computation of (2.9) is impossible because either the integration in (2.13) cannot be carried out analytically or the expectation in (2.9) poses insuperable obstacles. It is in this case that the MCRB reveals fundamental. The MCRB in fact is defined as follows

$$MCRB\left(\lambda\right)=\frac{1}{\mathbb{E}_{\mathbf{r},\mathbf{u}}\left\{\left[\frac{\partial\ln p(\mathbf{r}|\mathbf{u},\lambda)}{\partial\lambda}\right]^2\right\}} \tag{2.14}$$

or, equivalently,

$$MCRB\left(\lambda\right)=\frac{1}{\mathbb{E}_{\mathbf{u}}\left[\mathbb{E}_{\mathbf{r}|\mathbf{u}}\left\{\left[\frac{\partial\ln p(\mathbf{r}|\mathbf{u},\lambda)}{\partial\lambda}\right]^2\right\}\right]} \tag{2.15}$$

and it reveals much easier to compute. In fact, for the Gaussian channel as in (2.12), the pdf is

$$p(\mathbf{r}|\mathbf{u},\lambda)=\exp\left(-\frac{1}{2\sigma_w^2}\left|\mathbf{r}-\mathbf{x}(\lambda,\mathbf{u})\right|^2\right)=\exp\left(-\frac{1}{2N_0}\left|\mathbf{r}-\mathbf{x}(\lambda,\mathbf{u})\right|^2\right) \tag{2.16}$$

and the MCRB reduces to [17]

$$MCRB\left(\lambda\right)=\frac{N_0}{\mathbb{E}_{\mathbf{u}}\left\{\left|\frac{\partial\mathbf{x}(\lambda,\mathbf{u})}{\partial\lambda}\right|^2\right\}}. \tag{2.17}$$

Coming back to the problem of computing the CRB for the signal $r\left(t\right)$ (2.11), in [56] it is shown that in the limit, as the number of dimensions of $\mathbf{r}$ tends to infinity, a formula like (2.17) does still apply provided that $p(\mathbf{r}|\mathbf{u},\lambda)$ is replaced by the likelihood function

$$\Lambda(\mathbf{u},\lambda)=\exp\left(-\frac{1}{2N_0}\int_{T_obs}\left|r\left(t\right)-x\left(t\right)\right|^2dt\right), \tag{2.18}$$

and the expectation over $\mathbf{r}$ is replaced by the expectation over the noise process $n\left(t\right)$. With this changes (2.17) becomes

$$MCRB\left(\lambda\right)=\frac{1}{\mathbb{E}_{n,\mathbf{u}}\left\{\left[\frac{\partial\ln\Lambda(\mathbf{u},\lambda)}{\partial\lambda}\right]^2\right\}} \tag{2.19}$$

and substituting (2.18) into (2.19) one gets after some manipulations [17],

$$MCRB\left(\lambda\right)=\frac{N_0}{\mathbb{E}_{\mathbf{u}}\left\{\int_{T_{obs}}\left|\frac{\partial x(t)|\mathbf{u}}{\partial\lambda}\right|^2dt\right\}} \tag{2.20}$$

Note that the MCRB is much simple to evaluate than the CRB.

For completeness, we report the CRB expression when no nuisance parameters are present for the signal (2.11). Starting from (2.9), after some manipulation we get

$$CRB\left(\lambda\right)=\frac{N_0}{\int_{T_{obs}}\left|\frac{\partial x(t)}{\partial\lambda}\right|^2dt} \tag{2.21}$$

whose numerical value clearly depends only on the type of modulation, on the time of observation and on the parameter to estimate.

2.4 Ziv-Zakai bound (ZZB) and Modified Ziv-Zakai bound (MZZB)

2.4.1 The Ziv-Zakai lower bound (ZZB)

The ZZB is a theoretical performance limit in signal parameter estimation, for both biased and unbiased estimators [11], [59] representing a lower benchmark for the mean squared error (MSE). The Ziv-Zakai formulation of the bound comes out from the detection theory and it is based on the probability of deciding correctly between two possible values h and $h+\Delta$ of the parameter to estimate. The ZZB belongs to the family of so-called *Bayesian* bounds which are adopted to compute the theoretical performance of *random parameters estimators* and which take into account the *a priori* information (pdf) about the parameters space. In this frangent we consider only one parameter to be estimated with a uniform pdf in [0,D], even though the theory proposed here can be expanded for a set of parameters and other distributions could be adopted [7].

Lets assume that the observable is given by a received waveform in an AWGN channel, whose baseband equivalent (or complex envelope) is

$$r\left(t\right)=x\left(t\right)+n\left(t\right), \tag{2.22}$$

and which is observed over an interval T_{obs}. In (2.22) $x(t)$ is the information-bearing signal which is a (non-linear) function of a random parameter λ to estimate $(x(t,\lambda))$ and $n(t)$ represents the complex-valued additive white Gaussian noise with two-sided power spectral density $2N_0$.

The Ziv-Zakai lower bound (ZZB) states that the MSE of any estimator of λ is lower bounded by

$$\mathrm{MSE}(\hat{\lambda}) = \mathrm{E}[(\hat{\lambda}-\lambda)^2] \geq ZZB(\lambda) \tag{2.23}$$

where $ZZB(\lambda)$ denotes the *true* ZZB, given by [11]

$$ZZB(\lambda) = \frac{1}{D}\int_0^D \Delta \int_0^{D-\Delta} P_e(h, h+\Delta)\, dh d\Delta \tag{2.24}$$

where $P_e(h,h+\Delta)$ is the minimum probability of error in deciding between the signals $x(t,h)$ and $x(t,h+\Delta)$, with h and $h+\Delta$ trial values of the λ, uniformly distributed on the uncertainty range [0,D]. Observing the (2.24), the computation of ZZB needs a double integration and it appears as a two dimensional average of the probability of error function weighted by the Δ function, evaluated for all the pairs of trial values. The (2.24) can be further enhanced by [7,8,59]

$$ZZB(\lambda) = \frac{1}{D}\int_0^D \Delta G\left[\int_0^{D-\Delta} P_e(h, h+\Delta)\, dh\right] d\Delta \tag{2.25}$$

where $G[\cdot]$ is a nonincreasing function of Δ obtained by filling the valleys (if there are any) in the bracketed function, obtaining a tighter bound than the basic one.

Assuming that one of the two replicas of the signal is transmitted, each one with equal probability, the minimum probability of detection error is given by [56]

$$P_e(h, h+\Delta) = Q\left(\sqrt{\frac{d^2(\Delta, h)}{2N_0}}\right) \tag{2.26}$$

where

$$Q(x) = \frac{1}{\sqrt{2\pi}}\int_x^{+\infty} \exp\left(-\frac{z^2}{2}\right) dz \tag{2.27}$$

and with the squared distance between the (baseband equivalent) signal replicas defined as

$$d^2(\Delta, h) = \frac{\int_0^{T_{obs}} |x(t,h) - x(t,h+\Delta)|^2\, dt}{2} \tag{2.28}$$

where T_{obs} is the time of observation.

Under these assumptions the improved version of the bound results

$$ZZB(\lambda) = \frac{1}{D}\int_0^D \Delta G\left[\int_0^{D-\Delta} Q\left(\sqrt{\frac{d^2(\Delta,h)}{2N_0}}\right)dh\right]d\Delta. \tag{2.29}$$

If the error probability is independent of trial h ($P_e(h,h+\Delta) = P_e(\Delta)$), i.e. the distance does not depend on h, the (improved) ZZB can be reduced to the form

$$ZZB(\lambda) = \frac{1}{D}\int_0^D \Delta G\left[(D-\Delta)\,Q\left(\sqrt{\frac{d^2(\Delta)}{2N_0}}\right)\right]d\Delta \tag{2.30}$$

which requires a single integration and can be easier carried out.

2.4.2 The Modified Ziv-Zakai lower bound (MZZB)

The ZZB results relatively easy to compute, but its evaluation becomes mathematically intractable when the received signal contains, in addition to the parameter to be estimated also the "stray" (nuisance) parameters. As for the CRB and MCRB reported in Sect. 2.3, here we define a *modified* version of the ZZB which results much simpler to evaluate than the *true* ZZB. As we proof hereafter, the Modified Ziv-Zakai lower bound (MZZB) is in general looser than the true ZZB, by definition, but it has been also demonstrated that in the specific cases of interest, the MZZB is essentially as tight as the true ZZB, [19, 20].

Recalling the scenario depicted in Sect. 2.3.2, the observable is given by a received waveform in an AWGN channel, whose baseband equivalent (or complex envelope) is

$$r(t) = x(t) + n(t), \tag{2.31}$$

and which is observed over an interval T_{obs}. The received signal contains the λ to estimate and other unknown parameters with a known pdf, collected in a random vector $\mathbf{u}$, i.e. the *nuisance parameters* vector.

Retracing the steps seen before, and indicating with $P_e(h,h+\Delta|\,\mathbf{u})$ the minimum probability of detection error between $x(t,h|\mathbf{u})$ and $x(t,h+\Delta|\mathbf{u})$ as in (2.26), we can

find a *conditional* bound, assuming that $\mathbf{u}$ is known:

$$\begin{aligned} &\mathrm{MSE}(\hat{\lambda}|\mathbf{u}) = \mathrm{E}_{\mathrm{r}|\mathbf{u}}[(\hat{\lambda}-\lambda)^2] \\ &\geq ZZB\,(\lambda|\mathbf{u}) = \frac{1}{D}\int_0^D \Delta G\left[\int_0^{D-\Delta} P_e\,(h, h+\Delta|\mathbf{u})\,dh\right]d\Delta \end{aligned} \tag{2.32}$$

where we have applied the non increasing "valley-filling" function $G\,[\cdot]$ according to [8,59]. We obtain the final ZZB, including the nuisance parameters effect, averaging (2.32) over all possible values of the vector $\mathbf{u}$

$$\begin{aligned} &\mathrm{E}_{\mathrm{r},\mathbf{u}}[(\hat{\lambda}-\lambda)^2] = \mathrm{E}_{\mathbf{u}}\{\mathrm{E}_{\mathrm{r}|\mathbf{u}}[(\hat{\lambda}-\lambda)^2]\} \\ &\geq \mathrm{E}_{\mathbf{u}}\,\{ZZB\,(\lambda|\mathbf{u})\} = ZZB\,(\lambda) \end{aligned} \tag{2.33}$$

To simplify, we can define the $\mathbf{u}$-conditioned squared distance, and we can cast the expression of the bound (2.33) into

$$ZZB(\lambda) = \frac{1}{D}\int_0^D \Delta G\left[\int_0^{D-\Delta} \mathrm{E}_{\mathbf{u}}\left\{Q\left(\sqrt{\frac{d^2\,(\Delta, h|\mathbf{u})}{2N_0}}\right)\right\}dh\right]d\Delta \tag{2.34}$$

that can be further simplified if the distance is independent of h as in (2.30).

Unluckily, the calculation of (2.34) proves to be very heavy due to the presence of the expectation on $\mathbf{u}$. If K is the size of the nuisance parameters vector $\mathbf{u}$, the computation of the $ZZB\,(\lambda)$ requires an integration on K+2 dimensions. This could be carried out numerically only for low K, while for large sets of parameters, the integration is computationally heavy, and at times inaccurate. For this reason, it is expedient to find some mathematical "tricks" to solve this "impasse".

A similar situation has been solved for the well known Cramér-Rao Bound (CRB) in the presence of nuisance parameters. As fully explained in [17], the MCRB is derived from the original CRB with nuisance parameters by exploiting i) some properties of the conditional CRB with respect to $\mathbf{u}$, ii) the convexity of the function $\phi\,(x)$=$-ln\,(x)$ on $\mathbb{R}^+$, and iii) the well-known *Jensen's inequality* [17], [15]. We can adopt a similar approach here:

$$\begin{aligned} &\mathrm{E}_{\mathrm{r},\mathbf{u}}[(\hat{\lambda}-\lambda)^2] = \mathrm{E}_{\mathbf{u}}\{\mathrm{E}_{\mathrm{r}|\mathbf{u}}[(\hat{\lambda}-\lambda)^2]\} \geq \mathrm{E}_{\mathbf{u}}\,\{ZZB\,(\lambda|\mathbf{u})\} \\ &= ZZB\,(\lambda) = \frac{1}{D}\int_0^D \Delta G\left[\int_0^{D-\Delta} \mathrm{E}_{\mathbf{u}}\left\{Q\left(\sqrt{\frac{d^2\,(\Delta, h|\mathbf{u})}{2N_0}}\right)\right\}dh\right]d\Delta \end{aligned} \tag{2.35}$$

$$\geq \frac{1}{D}\int_0^D \Delta G\left[\int_0^{D-\Delta} Q\left(\sqrt{\frac{E_{\mathbf{u}}\{d^2(\Delta,h|\mathbf{u})\}}{2N_0}}\right)dhd\Delta\right] \triangleq MZZB(\lambda) \tag{2.36}$$

where the first inequality is derived from the application of the ZZB to λ for a given vector $\mathbf{u}$, while the last one comes from *Jensen's inequality* [15]. In our case, the strictly convex function $\phi(x)$ can be easily proved to be $Q(\sqrt{x})$, and consequently

$$Q\left(\sqrt{\frac{E_{\mathbf{u}}\{d^2(\Delta,h|\mathbf{u})\}}{2N_0}}\right) \leq E_{\mathbf{u}}\left\{Q\left(\sqrt{\frac{d^2(\Delta,h|\mathbf{u})}{2N_0}}\right)\right\} \tag{2.37}$$

so that (2.35),

$$MZZB(\lambda) \leq ZZB(\lambda). \tag{2.38}$$

To sum-up, the expression of the modified ZZB runs as follows:

$$MZZB(\lambda) \triangleq \frac{1}{D}\int_0^D \Delta G\left[\int_0^{D-\Delta} Q\left(\sqrt{\frac{E_{\mathbf{u}}\{d^2(\Delta,h|\mathbf{u})\}}{2N_0}}\right)dhd\Delta\right] \tag{2.39}$$

that can again be simplified if the distance is independent of h. It is very apparent that this expression is computationally less heavy than (2.34), since it only requires the calculation of $E_{\mathbf{u}}\left\{d^2|\mathbf{u}\right\} = \int_{-\infty}^{+\infty}(d^2|\mathbf{u})p_{\mathbf{u}}(\mathbf{u})\,d\mathbf{u}$ with a K-dimensional integration only. In addition, such computation can often be closed analytically when the statistics of the nuisance parameters are known and sufficiently simple, as we will show in the Chapter 5 with some case of study.

2.5 CRB and ZZB in TOA estimation

2.5.1 Motivation

As clearly stated in the Introduction, this thesis deals with topics in signal analysis for TOA estimation, with particular application to satellite positioning. In particular, SS modulated signals will be analyzed throughout, as insight to actually adopted GNSS signals and alternative modulations for future signal-in-space (SIS). In fact, as delineated in Sect .1.6.3, the modulation actually adopted is GNSS is a DS-SS linear modulation, thanks to which signals coming from different satellite are univocally determined by the code sequence associated to each satellite. For this reason, in the

sequel we will focus on the class of SS modulations, deeply investigating on spread-spectrum continuous-phase-modulation and multicarrier signals. Performance of the different SS modulated signals will be thus discussed in details, focusing on TOA estimation accuracy together with some other parameters of analysis that has to be taken into account in GNSS systems.

As far as TOA estimation accuracy is concern, the MCRB and MZZB will be used as performance benchmark, since it is independent from the receiver structure, and thus it can be used to characterize different signal modulations, relying only on the signal structure itself.

2.5.2 Signal model

In this section, we formalize the lower bounds in TOA estimation for a generic digitally modulated signal.

In particular we focus on a bandpass signal, whose format is

$$x_{BP}(t) = \mathfrak{Re}\left\{x(t)\, e^{j(2\pi f_0 t+\varphi)}\right\}, \tag{2.40}$$

where $\mathfrak{Re}\{\cdot\}$ denotes the real part of a complex-valued argument; f_0 and φ are the carrier frequency and phase, respectively and $x(t)$ is the complex signal with average transmitted power P_x, digitally modulated by the vector $\mathbf{a} = \{a_n\}$. The vector $\mathbf{a}$ represents the data-modulated spreading code, given by the product of the binary data symbols with the spreading code ranging sequence $\mathbf{c} = \{c_n\}_{n=0}^{N-1}$ assigned to each satellite.

In the sequel we will adopt this notation, using the subscript BP when referring to the real bandpass signal, while nothing will be added when referring to the baseband equivalent (complex) signal.

In this section, we restrict the study of TOA estimation fundamental limits to a frequency-flat channel, which represents an acceptable approximation for the satellite communication channel [29].

Hence, assuming ideal coherent demodulation (thus with the realistic assumption that during signal tracking the carrier frequency f_0 and the carrier phase φ are known to a sufficient accuracy), the baseband-equivalent of the received SS signal reduces to

$$r(t) = x(t-\tau) + n(t), \tag{2.41}$$

where $x(t)$ is the complex-valued SS signal; τ is the group delay experienced by the radio signal when propagating from the satellite to the receiver (as seen in the reference time of the receiver) [41] to estimate; and $n(t)$ represents the complex-valued AWGN with two-sided power spectral density $2N_0$.

It is worth noting that the following analysis is focused on detecting a single satellite during the tracking stage (corresponding to single-user detection in a communication scenario). As a result, although the effects of other users should be explicitly included in a multiuser model, considering those effects in $n(t)$, as done in (2.41), represents a good approximation in view of the central limit theorem.

For the sake of simplicity, the transmitted signal is assumed to be an unmodulated signal, in the sense of data-less signal: $\mathbf{a} = \mathbf{c}$. This is equivalent to consider either a pilot signal, or a data signal in which the data modulation is removed prior to the tracking stage. This approach does not reduce the generality of the problem, since the effects of data modulation can be neglected when considering modulated SS signals with high processing gain N, as is typical in the field of satellite navigation. Moreover, when secondary codes are used, the following analysis can easily be applied considering the vector $\mathbf{c}$ as the product of the primary code with the secondary code. As a result, the received signal (2.41) can be seen as the combination of noise with a "*spreading signature waveform* $x(t)$" defined as a function

$$x(t) = f(\mathbf{c}, p(t), T_c), \tag{2.42}$$

thus depending on the type of modulation $f()$, code sequence $\mathbf{c}$, chip-rate $1/T_c$ and pulse shape $p(t)$ adopted.

2.5.3 Characterization of (M)CRB and (M)ZZB in TOA estimation

In this section we recall the main results analyzed in the previous sections specializing them for the TOA estimation problem. Assuming the signal model depicted in the Sect. 2.5.2, the parameter τ to be estimated is the time-of-arrival of the radio signal $x(t)$ which propagates in the AWGN channel. Hence, following the same notation of the previous sections, $\lambda = \tau$ and $x(t)$ is the transmitted signal. The CRB and the MCRB become [17, 46], in absence and in presence of nuisance parameters,

respectively

$$CRB\left(\tau\right)=\frac{N_0}{\int_{T_{obs}}\left|\frac{\partial x(t-\tau)}{\partial\tau}\right|^2dt} \tag{2.43}$$

and

$$MCRB\left(\tau\right)=\frac{N_0}{\mathbb{E}_{\mathbf{u}}\left\{\int_{T_{obs}}\left|\frac{\partial x(t-\tau|\mathbf{u})}{\partial\tau}\right|^2dt\right\}} \tag{2.44}$$

remembering that these limits are benchmarks for the unbiased estimators variance, in the estimation of the scalar parameter τ, and that the expressions would change if biased algorithms are adopted [16, 54, 56].

Let us assume now the *parametric random process* $x\left(t\right)$, in which the sequence of (symbols) chips assumed binary random is the only nuisance parameter ($\mathbf{u}=\mathbf{c}$). If the (2.44) can not be easy computed in the *time domain*, the MCRB can be either computed in the *frequency domain* [2, 27, 63], in particular for filtered or bandlimited signals.

To attain an accurate approximation of the bound, specifically, we have to assume T_{obs} very large, so that by applying the Parçeval theorem to the (2.44),

$$MCRB\left(\tau\right)=\frac{N_0}{T_{obs}4\pi^2\int\limits_{-\infty}^{\infty}f^2S_x\left(f\right)df}=\frac{B_{eq}T_c}{4\pi^2\cdot\frac{E_c}{N_0}\beta_x^2} \tag{2.45}$$

where $S_x\left(f\right)$ is the PSD of the complex signal, β_x is the root second-order moment of the signal spectrum, normalized to the complex signal power $\int\limits_{-\infty}^{\infty}S_x\left(f\right)df=2P_x$, i.e. the (squared) Gabor bandwidth; and defined by

$$\beta_x^2\triangleq\frac{\int\limits_{-\infty}^{\infty}f^2S_x\left(f\right)df}{\int\limits_{-\infty}^{\infty}S_x\left(f\right)df}, \tag{2.46}$$

$E_c=P_x\cdot T_c$ is also the average signal energy per chip, and $B_{eq}=1/2T_{obs}$ is the (one-sided) noise bandwidth of a closed-loop estimator equivalent to an open-loop estimator operating on an observation time equal to T_{obs}. From (2.45)-(2.46), we conclude that the MCRB depends on the second-order moment of the PSD of the complex signal, independent of the type of signal format (modulation, spreading, etc.) that is adopted. In particular, we see that signals with the same PSD have the

same MCRB even if generated by different modulations. As a proof of it, in Chapter 4 we will demonstrate the equivalence of the MCRB for a single carrier signal and a multicarrier signal with the same PSD.

For the mean squared error (MSE) benchmark of biased or unbiased τ estimators the ZZB and the MZZB can be computed in absence and in presence of stray parameters, respectively by

$$ZZB\left(\lambda\right)=\frac{1}{T_x}\int_0^{T_x}\Delta\, G\left[\left(T_x-\Delta\right)Q\left(\sqrt{\frac{d^2\left(\Delta\right)}{2N_0}}\right)\right]d\Delta \tag{2.47}$$

and

$$MZZB(\tau)\triangleq\frac{1}{T_x}\int_0^{T_x}\Delta\, G\left[\left(T_x-\Delta\right)Q\left(\sqrt{\frac{E_{\mathbf{u}}\{d^2(\Delta|\mathbf{u})\}}{2N_0}}\right)\right]d\Delta \tag{2.48}$$

where $[0,T_x]$ is the uncertainty range of the τ with uniform pdf, chosen according to the TOA estimation stage, with the ($\mathbf{u}$-conditioned) squared distance

$$\begin{aligned} d^2\left(\Delta,h|\mathbf{u}\right)&=\frac{\int_0^{T_{obs}}\left|x\left(t-h|\mathbf{u}\right)-x\left(t-h-\Delta|\mathbf{u}\right)\right|^2dt}{2} \\ &\approx\frac{\int_0^{T_{obs}}\left|x\left(t|\mathbf{u}\right)-x\left(t-\Delta|\mathbf{u}\right)\right|^2dt}{2}=d^2\left(\Delta|\mathbf{u}\right)=2E_{T_{obs}}(1-\rho_{T_{obs}}\left(\Delta|\mathbf{u}\right)) \end{aligned} \tag{2.49}$$

where the approximation holds when the time of observation T_{obs} is large enough, lightening the MZZB computation by an integration; and where the (conditional) signal correlation function

$$\rho_{T_{obs}}\left(\Delta|\mathbf{u}\right)=\frac{\mathfrak{Re}\left\{\int_0^{T_{obs}}x\left(t|\mathbf{u}\right)x^*\left(t-\Delta|\mathbf{u}\right)dt\right\}}{2E_{T_{obs}}} \tag{2.50}$$

is normalized to the signal energy $E_{T_{obs}}=P_xT_{obs}$ with P_x the band-pass (transmitted) signal power (which is usually also called C).

If we assume binary random sequence of i.i.d. (symbols) chips as nuisance parameter ($\mathbf{u}=\mathbf{c}$), with a long time of observation, when we apply the expectation $E_{\mathbf{c}}\{\cdot\}$ to (2.49), computing the MZZB, the (2.50) becomes the (normalized) theoretical signal correlation function $R_x\left(\Delta\right)$. Hence when the computation of the MZZB could result heavy in the time domain and easier in the frequency one, an alternative formulation can be adopted. In the argument of the Q function in (2.48), assuming a large

time of observation, the **c**-averaged distance can be re-formulated in the frequency domain [59] by applying the Parçeval theorem,

$$E_{\mathbf{c}}\{d^2(\Delta|\mathbf{c})\} \approx 2P_x T_{obs} \frac{\int_{-\infty}^{\infty} S_x(f)\,[1-cos(2\pi f\Delta)]\,df}{\int_{-\infty}^{\infty} S_x(f)\,df} \tag{2.51}$$

particularly useful for filtered or bandlimited signals, adjusting the integrations limits. Finally using (2.51), the MZZB can be rewritten as

$$MZZB(\tau) \triangleq \frac{1}{T_x}\int_0^{T_x} \Delta G\left[(T_x-\Delta)\,Q\left(\sqrt{\frac{1}{B_{eq}T_c}\frac{E_c}{N_0}\frac{\int_{-\infty}^{\infty} S_x(f)\,sin^2(\pi f\Delta)df}{\int_{-\infty}^{\infty} S_x(f)\,df}}\right)\right]d\Delta \tag{2.52}$$

Analyzing this alternative formulation some general results can be found [7, 8, 59]:

1. For (very) low E_c/N_0 (SNR), the MSE of any estimator tends to $\sigma_\tau^2 = T_x^2/12$, i.e. the variance of a uniform random variable in [0, T_x]. In this region, the optimum estimator actually uses the a priori information on τ, estimating the random variable with its mean value, and neglecting the received noisecorrupted data. This result can be easy found noting that when $\frac{E_c}{N_0}\rightarrow 0$, $Q\left(\sqrt{\alpha\frac{E_c}{N_0}}\right)\rightarrow 1/2$ and $MZZB\rightarrow\sigma_\tau^2$.

2. However, for high SNR ratios can be proof that the MZZB tends to the MCRB. In particular, observing that $sin^2(\pi f\Delta) \leq (\pi f\Delta)^2$ and (2.46), with some mathematics [7, 59], can be found that

$$MZZB(\tau) \geq \frac{1}{T_x}\int_0^{T_x} \Delta G\left[(T_x-\Delta)\,Q\left(\sqrt{\frac{\pi^2}{B_{eq}T_c}\frac{E_c}{N_0}\beta_x^2\Delta^2}\right)\right]d\Delta \tag{2.53}$$

$$=\frac{1}{T_x}\int_0^{T_x}\Delta(T_x-\Delta)\,Q(\Delta\mu)d\Delta = \frac{1}{\mu^2}\frac{1}{\mu T_x}\int_0^{\mu T_x} y(\mu T_x - y)\,Q(y)d\Delta$$

with $\mu^2 = \frac{\pi^2}{B_{eq}T_c}\frac{E_c}{N_0}\beta_x^2$, which for large SNR ($\mu T_x \gg 1$) approaches the limit

$$\hookrightarrow \frac{1}{4\mu^2} = \frac{B_{eq}T_c}{4\pi^2\cdot\frac{E_c}{N_0}\beta_x^2} = MCRB(\tau) \tag{2.54}$$

3. The boundary of the two regions is a threshold which depends on the characteristics of the signaling waveform adopted.

The CRB and the ZZB are functions of the particular values of the "*spreading signature waveform* $x(t)$" (2.42). Equations (2.43)-(2.48) give a practical criterion to numerically assess the performance in terms of position accuracy by TOA accuracy. Thus, designing a signal (2.42) that minimizes the CRB and ZZB appears to be a motivated approach for improving positioning performance. Therefore, improving TOA estimation accuracy translates into minimizing (2.43)-(2.48).

As we have underlined, the transmitted signal $x(t)$ can be thought as a "*spreading signature waveform* $x(t)$" as in (2.42), thus minimizing the bounds can be achieved by either modifying the code sequence $\mathbf{c}$ or the shaping pulse $p(t)$ separately, or by selecting code sequence and shaping pulse jointly in an optimization process of the entire "*spreading signature waveform*" (2.42). This process can imply also to use a different modulation format, that is, a different function $f(\cdot)$ in (2.42).

In the next chapters, we propose different methods to improve TOA estimation accuracy for future GNSSs based on signal design at the transmitter side, deeply discussing the SS-CPM and multicarrier signals. For this reason, in the next chapters the CRB and ZZB will be specifically re-formulated case by case depending on the modulation format under investigation.

Obviously, when the signal model will imply nuisance parameters $\mathbf{u}$, TOA accuracy will be studied making use of the MCRB (2.44) and MZZB (2.48), otherwise the *true* bounds will be adopted.

2.5.4 Considerations on the applicability of the bounds

In the previous sections, we have recalled the basics of the estimation theory, giving particular emphasis to the CRB and ZZB for TOA estimation. Particularities of the bounds applied to different signal formats, will be discussed in later chapters, as soon as they will be used. We here mention some general characteristics on the existence and applicability of such bounds, as coming from the literature.

First of all, the *true* CRB is never below the MCRB so that the MCRB is in general looser than the *true* CRB. However, it was shown in [17] that in a few specific cases

of synchronization parameter estimation, the MCRB is essentially as tight as the true CRB at high signal-to-noise ratio (SNR).

Moreover, in [47] it is proven that the MCRB equals the asymptotic CRB at high SNR when the parameter to be estimated is not coupled with the nuisance parameters, finding that for considerably many cases of signal synchronization the asymptotic CRB is essentially the same as the MCRB.

In particular, in [17] it is shown that approximate equality between the CRB and MCRB is found to occur for estimation of τ when the carrier frequency f_0, the carrier phase φ and data are known.

On the other hand, the CRB and the MCRB are known to yield poor results for small SNR ratios. To this regard, alternative bounds such as the ZZB [11], [60] could be investigated, as they are known to be tighter bounds at low SNR. At high SNR ratios the CRB and ZZB performs the same tightness [7, 58, 59], whereas for medium values of SNR, ZZB again results tighter than CRB showing a threshold behavior which depends on the characteristics of the signaling waveform adopted [23, 24, 58, 59].

Similarly to the CRB case, the *true* ZZB is never below the MZZB so that the MZZB is in general looser than the *true* ZZB. However, it was shown in [19, 20] that in a few specific cases of practical interest, when the number of nuisance parameters is high enough, the MZZB and the ZZB match each other in every SNR regions, with a very important gain in terms of computation.

Anyhow, in the sequel, we will deal with problems for which the SNR values belong to a range of medium-high SNR (e.g. tracking stage), for which the CRB/MCRB validity is ensured, and also we will investigate applications for which the SNR can span from low to high values (e.g. acquisition stage) for which the ZZB/MZZB will be adopted.

A second point to be clarified is that the valid application of the (M)CRB (2.9) requires that the signaling waveform be sufficiently smooth [60], since it has to exist the second derivative of the signal. To this regard, we can anticipate that in the cases of practical interest reported in this thesis, this condition results satisfied. Moreover, for the few cases in which this condition is not fulfilled, an alternative expression of the bound can be used, since it relies on the signal properties in the frequency domain. On the other hand, the (M)ZZB can be computed for every signaling waveform adopted not showing any constraint in these terms, except for the complexity in

its computation.

Finally, it has to be mentioned that, even if the (M)CRB recalled up till now are applied when estimating a scalar parameter, they can be used also for the estimation of a uniformly distributed random variable, as it is our case of interest. (Simply the reader can note that the tracking process is fulfilled immediately after the acquisition stage and thus the time delay to be estimated is known to belong to a certain time interval). In fact, when the estimation of a random variable is quite accurate, the CRB/MCRB expression for a scalar parameter, can be used as good approximation of the real expressions [56, 60]. In particular, rigourously speaking, if the *a priori* pdf of the variable τ to be estimated is known, the performance becomes the ones of an estimator of a random variable, showing that the lower bound of the mean squared estimation error (MSEE) is set to [56]

$$E\left\{[\hat{\tau}-\tau]^2\right\} \geqslant \frac{N_0}{E_\tau\left\{\int\limits_{T_{obs}}\left[\frac{\partial x(t-\tau)}{\partial \tau}\right]^2 dt - \frac{\partial^2 \ln p_\tau(\tau)}{\partial \tau^2}\right\}}. \tag{2.55}$$

It follows that the inequality requires the signal being "smooth" (as before), and also the function $\frac{\partial^2 \ln p_\tau(\tau)}{\partial \tau^2}$ existing. When the parameter τ is uniformly distributed, (and consequently the pdf $p_\tau(\tau)$ holds jump discontinuities), the bound can be reformulated avoiding the discontinuities in $p_\tau(\tau)$, obtaining [56], [60]

$$E\left\{[\hat{\tau}-\tau]^2\right\} \geqslant \frac{N_0}{\int\limits_{T_{obs}}\left[\frac{\partial x(t-\tau)}{\partial \tau}\right]^2 dt}, \tag{2.56}$$

valid when the estimation is accurate, that is, for high SNR values. It can be observed that, under such hypothesis, (2.56) coincides with (2.44). In the sequel, we will refer always to formula (2.44), intending either that there is no knowledge on the *a-priori* distribution of the τ or, if τ is uniformly distributed, that the approximation (2.56) is implied.

By definition, the (M)ZZB in (2.47) and (2.48) do not require any approximation for the estimation of uniformly distributed random parameters [7, 11, 19, 23]. The computation of the bounds needs the knowledge of the *a priori* uncertainty of the τ to estimate. As it will be investigated in the Chapter 5, the uncertainty interval will be chosen according to the signaling waveform and the application. In particular

the TOA estimation is addressed, in its acquisition and tracking stages, assuming different uncertainty ranges within which the exact delay value has to be found by the estimators.

2.6 Conclusions

This chapter investigated on the ultimate accuracy limits, defined by signal synchronization and estimation theory, for time delay estimation (TDE) of a generic digitally modulated signal, posing also the basis for some theoretical performance analysis on specific modulation formats that will be discussed in the following chapters. To this aim, specific inside have been given to the expressions of Cramér-Rao lower bound (CRB) and Ziv-Zakai lower bound (ZZB) and their modified versions in presence of nuisance parameters, applying them for TDE of a signal embedded in the additive white Gaussian noise (AWGN) channel. In fact, the CRB is the lower bound on the variance of an estimator and, as such, can be used as a design signal parameter, since signals minimizing TDE bound correspond to signals maximizing positioning accuracy. The same considerations can be done for the ZZB which is a theoretical mean squared error (MSE) benchmark, which can be adopted for biased or unbiased estimators, and whose formulation highlight a correspondence between the correlation/spectral properties of the signal to its TDE performance. Deeply investigating on the two bounds, the convergence of both limits to the same value is addressed, showing that the *spectral shaping and placement in frequency* of the signal can heavily affect TOA accuracy and so, positioning accuracy.

Chapter 3

TOA Estimation with SS-CPM signals for GNSS

In this Chapter, we investigate the performance of a subset of spread spectrum continuous-phase-modulated (SS-CPM) signals, characterized by a modulation index h greater than one, considering the architecture of a simplified digital signal tracker for GNSS. After a general description of signal spectral properties, we focus on the problem of ranging code synchronization (code tracking), presenting few low-complex chip timing recovery loops based on an OQPSK approximation of the signal. The relative performance of the proposed recovery loops are analyzed in terms of RMS tracking error and multipath (MP) robustness.

3.1 Introduction

New GNSSs [51] such as Galileo [26] and modernization of GPS will soon become a reality, exhibiting higher performance wrt older GNSSes like GPS first generation. Improvements have been achieved taking full advantage of the gains obtained in the last years on concepts and technologies, such as new materials and components for spacecraft or advanced digital signal processing [26], just to cite a few. Nevertheless, even if at the time of writing Galileo is still not fully operational, the need for more systems and signals is already pushing the researchers to prospect new solutions for future advanced GNSSes.

To resume the problem, the ultimate goal of satellite positioning systems is enhanced user position accuracy, that is directly related to the accuracy of time-of-arrival (TOA)

estimation of ranging signals [50]. Current activities aim at enhancing the overall navigation performance by providing better navigation signals to those available today, i.e., by optimizing modulation schemes. Present-day ranging signals are based on DS-SS modulation and thus signal optimization can be achieved by either improving the code sequences [33], or multiplexing existing signals like multiplexed binary offset carrier (MBOC) [9], [37], or introducing new modulation chip waveforms [35], [4], [14] or, optimizing a *signature waveform* eventually given by an optimal combination of code and chip waveform as in [62], [28] and [4]. As a result of these studies, several DS-SS signal options have been proposed, aiming at improving tracking performance both in an AWGN channel and in a channel affected by multipath (MP), while maintaining good acquisition and multiple access properties. Another relevant signal design constraint is the need to guarantee a modulation scheme preserving a constant envelope. This feature is particularly critical when looking at GNSSes, where the use of highly non-linear HPA contrasts with severe specifications in terms of OOB emission for certain services [6], [53], [14].

One of the solutions to the considerations above can be the use of ranging signals based on robust constant envelope modulations. Spread spectrum continuous-phase-modulated (SS-CPM) [3] signals are constant envelope modulations by definition and this ensures insensitivity to nonlinear distortions induced by the transmitter HPA operated at saturation region.

Specifically, this contribution analyzes SS-CPM signals applied to satellite positioning, in terms of signal generation, signal spectral properties, tracking performance and multipath robustness.

As is known, time delay estimation (TDE) or TOA estimation (hereafter assumed synonymous) tracking accuracy, and thus positioning accuracy, is related to the second order moment of the PSD of the ranging signal [42], [28], [31]: the higher the second order moment, the better the performance. The BOC modulations [9], [37] used for Galileo were chosen, among other features, for their characteristic of shifting the power at the edge of the band (and thus ensuring higher PSD second order moment) by means of subcarriers modulation. For the sake of completeness we here mention that similar goal is achieved in [6] by multiplying Minimum-Shift-Keying (MSK) and Gaussian Minimum-Shift-Keying (GMSK) chip waveform with a BOC(m,n) modulation. In this chapter, we present some expedients to achieve this goal by means of general SS-CPM ranging signal design (note that MSK and GMSK are particular

CPM subclasses). Setting the modulation index h to semi-integer values with $h > 1$ allows the SS-CPM signal to behave like having a subcarrier, exactly in the same way as it happens for the BOC modulation, but with the inherent advantage of preserving the constant envelope transmission.

In the following sections, once defined the signal properties, some tracking algorithms suitable for SS-CPM signals are studied and compared to the relevant CRB. In particular, some TDE algorithms already presented for Spread-Spectrum Generalized-Minimum-Shift-Keying (SS-GenMSK) timing synchronization and data detection in communication systems [34], are here generalized and analyzed as applied to signal tracking. SS-GenMSK modulation is a specific subset of SS-CPM signals, obtained when the modulation index h is set to $h = 0.5$. We extend here such algorithms [34] to the case of semi-integer values h ($h = H + 1/2, H \in \mathbb{N}$) with $h > 1$.

Finally, this contribution addresses the issue of mapping two different services onto a single SS-CPM signal. As case study, two different services are envisioned, either at the same chiprate (same-rate-services, SRS), or at two different chiprates (two-rate-services, TRS).

The chapter is organized as follow: Sect. 3.2 theoretically describes the signal modulations and the service mapping and analyzes the signal correlation and spectral properties; In Sect. 3.3 SS-CPM tracking loops are described, while different types of SS-CPM signal configurations are tested in terms of tracking performance in AWGN (Sect. 3.4.1) and MP resistance (Sect. 3.4.2). Considerations on the use of variable chip-rates services are then drawn in Sect. 3.4.3 and finally a complete summary of performance results is reported in Sect. 3.4.4. General comments conclude the chapter in Sect. 3.5.

3.2 Signal design

3.2.1 Signal definition

The baseband equivalent of a CPM signal with binary symbols is [3]

$$x_{CPM}(t) = \sqrt{2P_x} \exp\left\{ j \left[2\pi h \sum_k \alpha_k q(t - kT_c) + \phi_0 \right] \right\} \tag{3.1}$$

where P_x is the signal power, T_c is the symbol-time, h is the modulation index, α_k are the binary symbols, ϕ_0 is the initial phase and $q(t)$ is the phase pulse related to the finite-support frequency pulse $g(t)$ by the relation

$$q(t) = \int_{-\infty}^{t} g(\beta)\, d\beta \tag{3.2}$$

The phase response $q(t)$ is normalized such that

$$q(t) = \begin{cases} 0 & t \leq 0 \\ 1/2 & t \geq LT_c \end{cases} \tag{3.3}$$

where L, the integer duration of $g(t)$ as measured in symbol times, is called response length, and represents the system memory. In the following, CPM signals will be identified by the response length L and the type of frequency pulse, in the common short form $LPULSE$ [3]. As an example, the CPM using a rectangular pulse with support $L = 1$ will be denoted as $1REC$. A special case of CPM is the popular minimum shift keying (MSK) signal ($h = 1/2$, $L = 1$, $q(t) = t/2T_c$ for $0 < t < T_c$), that can be interpreted as a Quadrature Phase-Shift Keying (QPSK) signal with an in-phase-quadrature-phase (I-Q) timing offset of T_c (Offset QPSK) and, as such, can be demodulated by a simple I-Q linear receiver. This property reduces receiver complexity, and thus CPM signals bearing this feature are highly desirable.

Generalized Minimum-Shift-Keying (Gen-MSK) [3], is a particular subset of CPM, with $h = 0.5$ that can be demodulated using linear MSK-type receivers with limited loss in performance compared to optimum demodulation. Various ideas for selecting detection filters for MSK-type receivers are analyzed in the literature [43], [45], while digital modem architecture for spread spectrum communications employing Gen-MSK modulated signals have also been studied in [34].

It is also well-known that the Offset QPSK (OQPSK) approximation of Gen-MSK can be generalized for any constant amplitude binary phase modulation [43], as any CPM signal can be expressed as a sum of a finite number of time-limited amplitude modulated pulses (AMP decomposition) and the approximation is often good just considering a "main pulse" only (as happens with Gen-MSK). In particular, for semi-integer values of the modulation index h or for phase response with full length ($L = 1$), the main pulse is the first component of Laurent's decomposition [43], and the computation of the approximated signal is simplified. In this chapter, we will focus

on this particular subset of CPM, that is on CPM signals such that

$$L = 1 \text{ or } h = H + 1/2,\ H \in \mathbb{N}, \tag{3.4}$$

and we will name them "Semi-integer MSK (SiMSK)" from now on, extending the Gen-MSK with the schemes with a semi-integer modulation index greater than 0.5.

For this defined family the CPM signal can be well approximated by

$$x_{CPM}(t) \cong \sqrt{2P_x} \sum_{n=-\infty}^{N} J^{A_{0,n}} C_0 (t - nT_c) \tag{3.5}$$

where the complex-valued, unit-amplitude coefficient $J^{A_{0,n}}$ associated to the main pulse C_0 at time nT_c is

$$J^{A_{0,n}} = (\exp\{jh\pi\})^{A_{0,n}} = (\exp\{jh\pi\})^{\sum_{i=-\infty}^{n} a_i} \tag{3.6}$$

and the main pulse C_0 of length $(L+1)T_c$ is

$$C_0(t) = \prod_{i=0}^{L-1} S_i(t) = \prod_{i=0}^{L-1} S_0(t + iT_c) = \prod_{i=0}^{L-1} \left[\frac{\sin(\psi(t + iT_c))}{\sin(h\pi)}\right], 0 \le t \le (L+1)T_c \tag{3.7}$$

with $\psi(t)$, the so-called generalized phase pulse function, derived from the phase response function $q(t)$ as follows:

$$\psi(t) = \begin{cases} 2\pi h q(t) & t < LT_c \\ \pi h - 2\pi h q(t - LT_c) & t \ge LT_c. \end{cases} \tag{3.8}$$

The generalized phase pulse function $\psi(t)$ has nonzero values only for $0 \le t \le 2LT_c$ and it is still more important than $q(t)$ itself, since it allows the definition of the basis of the Laurent decomposition.

Elaborating the general form (3.5), the CPM signal can also be represented as an OQPSK, that is,

$$x_{CPM}(t) \cong \sqrt{2P_x} \left[\sum_m \gamma_{2m-1} C_0 (t - 2mT_c + T_c) + j \sum_m \gamma_{2m} C_0 (t - 2mT_c)\right] \tag{3.9}$$

where γ_k is the I-Q symbol sequence generated by the symbols α_k in (3.1) through differential coding

$$\alpha_k = (-1)^k \gamma_{k-1} \gamma_k (-1)^{\frac{2h-1}{2}}. \tag{3.10}$$

In equation (3.1), we left unspecified the role of the binary "symbols" α_k. In data transmission, they represent the information bits to be sent on a wireless channel, and T_c represents the bit time. With minor modifications, we can define a spread spectrum CPM (SS-CPM) signal as depicted in Fig.3.1.

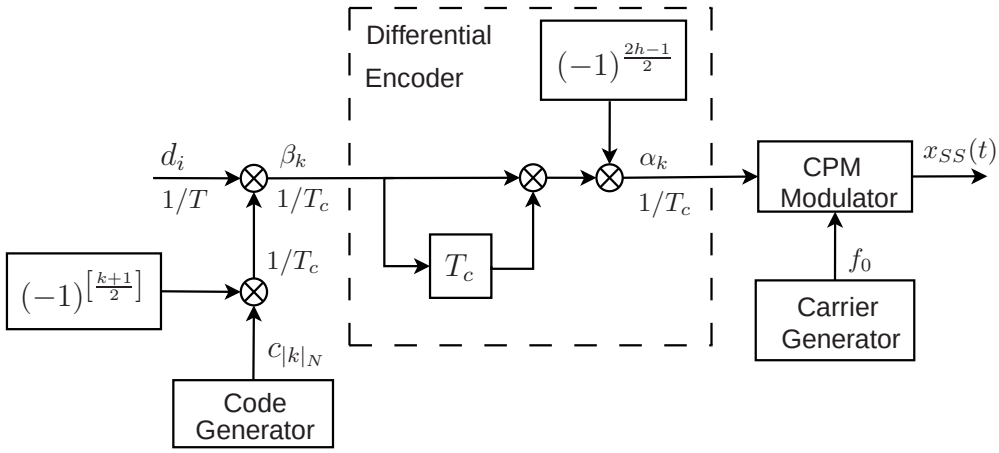

Figure 3.1: *SS-CPM Signal generator.*

In the scheme the incoming binary data symbols $\{d_i\}$ at the bit rate $1/T$ are encoded by a binary spreading code $\{c_k\}$ at the chip rate $1/T_c = M/T$ after an alternate chip sign inversion. The resulting chip-rate symbols $\beta_k = d_{k//M} \cdot c_{|k|_N} (-1)^{\left[\frac{k+1}{2}\right]}$ are finally mapped onto the CPM symbols $\alpha_k = \beta_{k-1}\beta_k \, (-1)^{\frac{2h-1}{2}}$ of (3.1), as shown in Fig.3.1, where $k//M$ denote the integer part of k/M ($M = T/T_c$ is the spreading factor) and $|k|_N$ represents the remainder of k/N (N being the code length).

This generalized explanation allows us now to define the traditional elements of a signal used in satellite navigation. Clearly the code sequence $\{c_k\}$ corresponds to the ranging code sequence associated to each satellite, while the symbols sequence $\{d_i\}$ can be associated either to the symbols of the navigation message (if we are considering the transmission of the data component) or to a fictitious sequence of all "one-symbols" $\{d_i = 1\}$ (if we are considering the transmission of the pilot component).

Our SS-CPM signal has now exactly the same form as (3.9)

$$x_{SS-CPM}(t) \cong \sqrt{2P_x}\left[\sum_m \gamma_{2m-1} C_0(t-2mT_c+T_c) + j\sum_m \gamma_{2m} C_0(t-2mT_c)\right] \tag{3.11}$$

with T_c the chip duration and $\gamma_k \triangleq d_{k//M} \cdot c_{|k|_N}$ coming out by the β_k and α_k definitions.

Equations (3.11), (3.10), (3.7) can be seen as a generalization of the SS-GenMSK presented in [34]. Under condition (3.4) OQPSK approximation loss at the receiver is almost negligible (example depicted in Sect. 3.2.2). Besides equation (3.11) becomes a perfect equality and not an approximation if $L=1$ and $h=H+1/2$.

In the sequel, we will consider only SS-CPM under condition (3.4), namely "SS-SiMSK" and we will refer indifferently to (3.1) or to its approximated version (3.11) depending on the needs.

3.2.2 OQPSK approximation validation

In general, using only the first component of the Laurent's decomposition instead of complete AMP can cause a performance degradation. Under condition (3.4), the main pulse $C_0(t)$ is sufficient to ensure a good approximation. To prove this, signal approximation losses have been analyzed in terms of degradation of the correlation function. Figure 3.2 reports the normalized auto-correlation function $R_{CPM}(\tau)$ of the CPM signal defined in (3.1), and the normalized cross-correlation function $R_{CPM-OQPSK}(\tau)$ of the transmitted CPM signal (3.1) with its OQPSK version (3.11), for the case of Gaussian pulse with $L = 4$ and for two instances of the modulation index h.

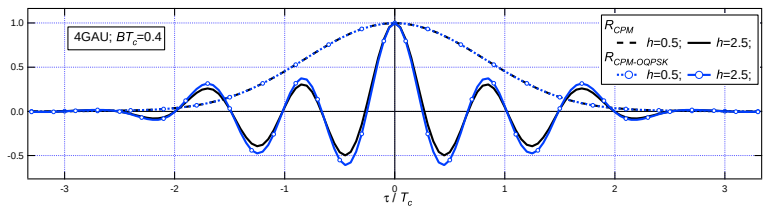

Figure 3.2: *Comparison of normalized correlation functions, for $h = 0.5$ and $h = 2.5$.*

PRN codes (ideally random, independent, identically distributed (i.i.d.) and equiprobable) are assumed for both CPM and OQPSK version. It is evident that for $h = 0.5$ the two correlation functions coincide, showing optimal approximation. For $h = 2.5$ the use of the approximated filter translates into a gap of 1 dB in terms of peak-to-peak correlation loss. We here mention that the correlation function of a generic CPM depends on the frequency pulse, on the response length L and on the code distribution. However, when chips are binary and i.i.d., as in our case, the correlation function $R_{CPM}(\tau)$ is zero for $\tau \geq (L+1)T_c$ and relies only on the shape of the frequency pulse. As a final remark, we recall here that the signal is transmitted exactly as a CPM (3.1), while its OQPSK interpretation is exploited only at receiver side. In this way the losses due to this approximation do not affect the constant envelope of the signal and other spectral characteristics at transmission, avoiding in particular spectral regrowth at the HPA output.

3.2.3 Mapping to services

Our SS-CPM signal can be used as a ranging signal for GNSS applications. In particular, we will consider here pilot SS-CPM signal containing no navigation data and a primary code only [26] ($d_i = 1$ and thus $\gamma_k = c_{|k|_N}$). As such, this contribution will not deal with problems related to data detection.

Mapping a unique code (chip) sequence c_k (and thus a unique service) into a CPM signal (3.1) is trivial. Nonetheless, for the type of CPM we consider here, i.e. subject to (3.4), the OQPSK approximation (3.11) applies, and two services can be easily accommodated by using two different spreading codes on the two I-Q components. Therefore, the CPM pilot signal (3.11) can easily bear either

- a single service at rate $f_c = 1/T_c$ (where $\gamma_k = c_{|k|_N}$, with $\{c_i\}$ being the ranging code sequence of length N), or
- two (orthogonal) services at half rate $f'_c = 1/(2T_c)$ each, where $\gamma_{2m} = c^{(2)}_{|m|_{N_2}}$ and $\gamma_{2m-1} = c^{(1)}_{|m|_{N_1}}$, with $\left\{c^{(1)}_i\right\}$ and $\left\{c^{(2)}_i\right\}$ two (orthogonal) sequences of length N_1 and N_2, relative to two different services.

When the two code sequences $\left\{c^{(1)}_i\right\}$ and $\left\{c^{(2)}_i\right\}$ run at the same rate f'_c, we will speak of same-rate-service (SRS).

When instead one out of the two code sequences $\left\{c_i^{(1)}\right\}$ and $\left\{c_i^{(2)}\right\}$ is given by the repetition of each code element for "N_{rep}" times, then the configuration will be defined as two-rate-service (TRS). We will show in the following that, although the signal still belong to the general class of CPM, for the TRS case we can identify a wideband spectral component related to the high-rate service, and a narrowband component for the low-rate service. In Sect. 3.4.3 we will better analyse the TRS case, underlining its main characteristics.

3.2.4 Signal spectral analysis

The spectral characteristics of the signal play a crucial role: as it will be discussed in Sect. 3.3 on one hand it is desirable having a signal with power concentrated at the edge of the band to ensure better performance in terms of TDE accuracy and multipath (MP) resistance [38], and on the other hand it is necessary a signal spectrum that is sufficiently confined in order to guarantee lower OOB emissions. The PSD of CPM signals can be found following the approach in [3]. The results of such computation for conventional rectangular (1REC, 2REC), raised cosine (1RC, 2RC) and Gaussian (4GAU)[1] frequency pulses are presented wrt the normalized frequency in Figs. 3.3a, 3.3b, 3.4a, 3.4b, 3.5, respectively, as a function of the modulation index $h = H + 1/2, H \in \mathbb{N}$.

The modulation index h plays a role similar to the modulation depth in analog FM. The main characteristic for which continuous-phase-modulations (CPMs) are considered in wireless communication is their spectral efficiency, and consequently CPMs have been intensively studied for values that preserve spectral compactness (that is, for $h < 1$) [3], while spectral characterization has not been usually considered for $h > 1$ ($H > 0$). On the contrary, for navigation applications, CPM signals with $h > 1$ may reveal interesting, since they result in a spectrum bearing a sort of subcarrier frequency, thus enhancing performance by shifting the power far from the carrier. In particular, from the spectral shapes of Fig. 3.3a, 3.3b, 3.4a, 3.4b, 3.5, we see that the main lobe of the spectra is shifted exactly at $f = h/2T_c$ for the case of $1REC$, $2REC$,

[1] The value of the normalized Gaussian filter bandwidth $BT_c = 0.4$ and the GMSK frequency pulse length $L = 4$ adopted in the example, were selected according to the relation $L = max\lfloor 2/BT_c - 1, 1\rfloor$. This ensures that the truncation of the frequency pulse has a negligible effect on the spectrum of the signal wrt the case of the theoretically infinitely-long pulse.

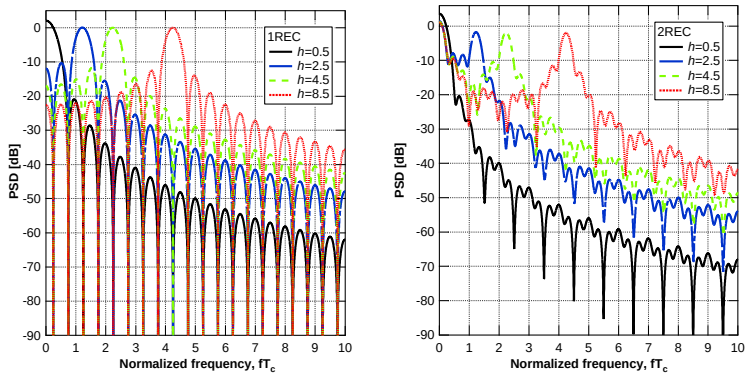

(a) $L = 1$ **(b)** $L = 2$

Figure 3.3: *PSD of the LREC CPM.*

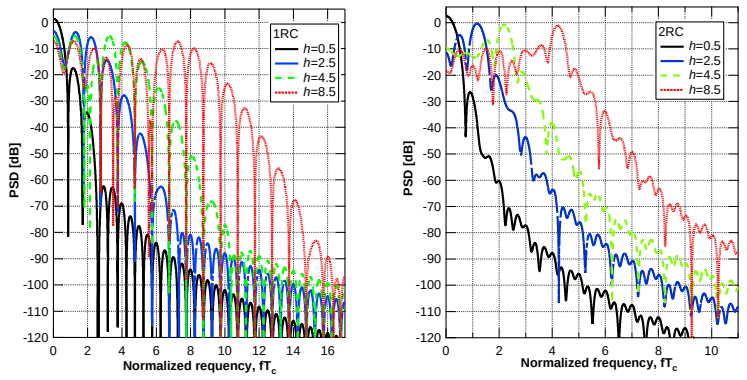

(a) $L = 1$ **(b)** $L = 2$

Figure 3.4: *PSD of the LRC CPM.*

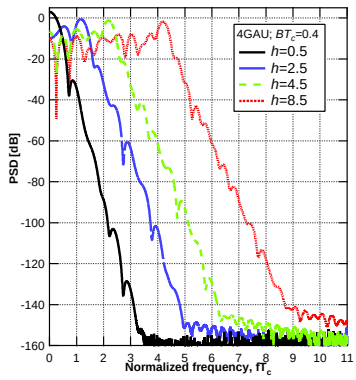

Figure 3.5: *PSD of the LGAU CPM, $L = 4$.*

$2RC$, and Gaussian, while it is only spread around such frequencies for the $1RC$ case. As a result, increasing H will directly increase performance in terms of second order moment of the spectra (or Gabor bandwidth), even if at the expense of higher sidelobe levels, when T_c is kept constant. Elaborating on this behaviour, we show in Fig.3.6 the spectrum of what we have called Binary Offset Carrier-CPM (BOC-CPM) or, more properly, Square Wave-CPM (SQW-CPM), where the frequency pulse (depicted in Fig.3.7) is given by

$$g_{SQW}(t) = \frac{1}{2LT_c}\left\{1 + 8A \cdot n \cdot \text{sign}\left(\cos\left(\frac{2\pi tn}{T_c}\right)\right)\right\} \text{rect}\left(\frac{t - LT_c/2}{LT_c}\right) \tag{3.12}$$

where A and n are two integer parameters defining the amplitude and the frequency of the square-wave subcarrier, and, consequently, the position and the width of the lobes of the spectral function, as shown in Fig.3.6.

3.2.5 Comparison between SS-CPM and BOC formats

A fair comparison between the new SS-CPM ($LPULSE$, h) signals and the conventional BOC(m,n) formats as envisaged in modernized GPS and GALILEO is a bit problematic, owing to the fundamental different features of the two signals, and is out of the scope of the work. We try here to consider a few specific cases, just to give a hint about how that comparison should be done. In Fig.3.8 we show the spectra of the standard BOC(2,1) modulation together with a number of spectra

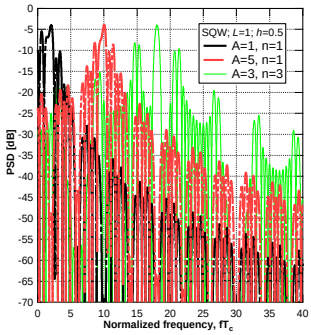

Figure 3.6: *PSD of the LSQW CPM, $L = 1$.*

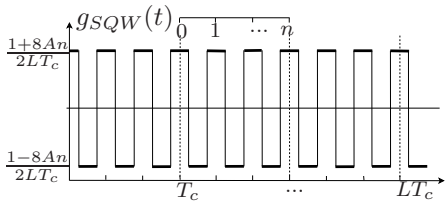

Figure 3.7: *Square Wave (SQW) frequency pulse.*

of SS-CPM with Gaussian pulse and with a modulation index $h = 2.5$, for different values of the normalized Gaussian filter bandwidth BT_c (and consequently for different values of the pulse response length $L = max\lfloor 2/BT_c - 1, 1\rfloor$). Values of BT_c in the literature vary between 0.3 and 0.5, but if $BT_c = 0.3$ ($L = 5$) the spectrum would be too "flat" loosing the "subcarrier" effect that was created on purpose with $h > 1$. On the contrary if $BT_c = 0.5$ ($L = 3$) the "subcarrier" effect is larger, but OOB would increase. To have a fair comparison, the parameters of CPM are chosen so as to "match" the BOC PSD shape. This means that, once the modulation index $h = 2.5$ is fixed, an *ad hoc* chip rate is chosen for SS-CPM according to the constraint $h/2T_c = mf_g$ ($f_g = 1.023MHz$), i.e. assuming the same "subcarrier" value for both modulations. As we see in Fig.3.8a, the spectra of the Gaussian CPM, although not strictly bandlimited, are very well confined in a narrow band wrt the chip rate, irrespective of the value of BT_c. Conversely the BOC(2,1) PSD decays with a slow rate due to its rectangular shape in time. We can also see that, as expected, the spectral efficiency of SS-CPM increases with lower values of BT_c. On the other hand,

low values BT_c also entail a loss of the "bimodality" feature of the spectrum, causing a decrease in the Gabor bandwidth. In the specific case that we present in Fig. 3.8, all CPM signals have a bandwidth occupancy of $10.23MHz$, so a fair comparison would be with a *filtered* BOC(2,1) occupying the same bandwidth. If we do this, the BOC(2,1) has a Gabor bandwidth slightly greater than that of CPMs (by just $0.6dB$), but its correlation sidelobes are higher than those of LGAU CPM, as is documented in Fig.3.8b that depicts the relevant autocorrelation functions. In addition, filtered BOC turns out not to have a constant envelope, contrary to SS-CPM.

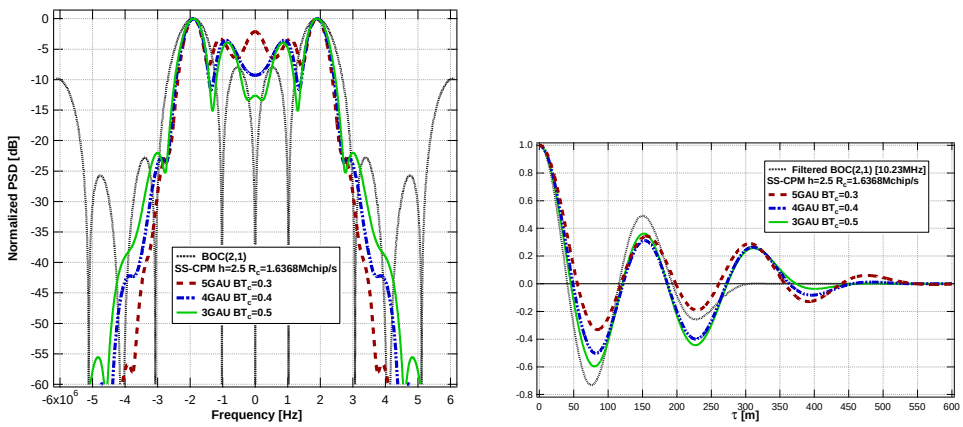

(a) PSD **(b)** Correlation function

Figure 3.8: *SS-CPM vs BOC*

Concerning receiver complexity, the processing rate in any receiver primarily depends on the bandwidth of the signal. Hence once the occupied signal bandwidth is fixed (e.g. $B_{99\%}$, B_{xdB}), the receiver complexity will be similar for (filtered) BOC and for SS-CPM. The conclusion is that by carefully selecting proper values for the chip pulse, the chip rate, and the modulation index, we can find a (constant-envelope) SS-CPM signals whose characteristics are as good as or better than those of existing formats.

3.3 Delay tracking performance

In this section we deal with the tracking performance of the proposed SS-CPM signals in terms of accuracy of TDE. In particular, tracking performance depends on the signal format and on the specific estimator implemented in the receiver. To characterize the signal format only, tracking performance will be evaluated in terms of MCRB, while specific analysis on receiver performance and complexity will be assessed for some proposed time-delay estimators.

The MCRB [17] for a CPM signal is a function of the frequency pulse shape as in [46]

$$MCRB(\tau) = \frac{T_c^2}{\frac{E_c}{N_0} 8\pi^2 L_0 \zeta} \tag{3.13}$$

where the observation time is $T_0 = L_0 T_c$ and $\zeta = C_2 h^2 T_c \int_{-\infty}^{\infty} g^2(t)\, dt$ is a dimensionless parameter, playing the same role as the normalized Gabor bandwidth that appears in the MCRB expression for conventional DS-SS modulations [46], and where $C_2 = \mathbb{E}\left\{{c_i}^2\right\} = 1$ in our case.

When the observation time is sufficiently large, the CRB can be computed in the frequency domain letting

$$\zeta \cong \xi = \frac{T_c^2 \int_{-\infty}^{\infty} f^2 S_x(f)\, df}{\int_{-\infty}^{\infty} S_x(f)\, df}, \tag{3.14}$$

where $S_x(f)$ denotes the PSD of the signal.

The approximated expression of the MCRB using (3.14) is easier to compute than (3.13) when the received signal is subject to band limitation, since the effect of filtering directly affects $S_x(f)$. As anticipated in Sect. 3.2.4, signals with energy shifted at the edge of the allocated band have better tracking performance.

3.3.1 Code Tracking loop

We can show that the signal formats we are considering can be tracked by a simple loop, considering the approximated OQPSK version of the signal.

The baseband equivalent of the SS-CPM tracking loop is depicted in Fig. 3.9, where, using complex envelope notation, the signal at the output of the matched filter is:

$$r\left(t\right)= \ y\left(t\right)\otimes h_{MF}\left(t\right)=e^{j\vartheta}\ x\left(t\right)\otimes h_{MF}\left(t\right)+\ n\left(t\right) \tag{3.15}$$

$$n\left(t\right)= \ w(t)\otimes h_{MF}(t)=\left[w_c\left(t\right)+jw_s\left(t\right)\right]\otimes h_{MF}(t) \tag{3.16}$$

$$h_{MF}\left(t\right)=\frac{1}{T_c}C_0\left(-t\right) \tag{3.17}$$

where $w(t)$ is complex-valued AWGN whose components are mutually independent and have a PSD $S_{w_c}\left(f\right)=S_{w_s}\left(f\right)=N_0$, ϑ is the carrier phase offset introduced during base band conversion, and $C_0\left(t\right)$ is the approximated pulse as defined in (3.7). Assuming that coarse delay estimation (signal acquisition) has already occurred, the circuit is a classical digital non-coherent early-late code tracking loop [34], [32]. The received signal $r(t)$ is sampled at the frequency $2/(\Delta T_c)$ (where $\Delta\in(0,1)$ is the normalized correlator spacing), it is matched filtered, and (possibly) decimated to obtain the sets of prompt samples r_k, early samples $r_{k+\Delta/2}$ and late samples $r_{k-\Delta/2}$, all running at chip rate $1/T_c$, that are passed as input to the code tracking loop. [2] The early-late detector outputs the error signal

$$e_m=\left|\ z_m^-\right|^2-\left|\ z_m^+\right|^2 \tag{3.18}$$

where

$$z_m^+=\left[\ r_{k+\Delta/2}\gamma_k\right]\otimes h_{b,k} \tag{3.19}$$

$$z_m^-=\left[\ r_{k-\Delta/2}\gamma_k\right]\otimes h_{b,k} \tag{3.20}$$

$$\left|\overline{H}_b\left(f\right)\right|=\frac{1}{\lambda}\left|\frac{\sin\left(\pi\lambda fT_c\right)}{\sin\left(\pi fT_c\right)}\right| \tag{3.21}$$

and where we assumed that the branch filters $\overline{H}_b\left(f\right)$ are moving-average smoother on a windows length λ.

[2] The sampling rate $2/(\Delta T_c)$ to obtain $r_{k\pm\Delta/2}$ is only "conceptual". Other, more efficient DSP arrangements based on digital interpolation to provide the prompt and the early late samples with the desired spacing Δ can be found.

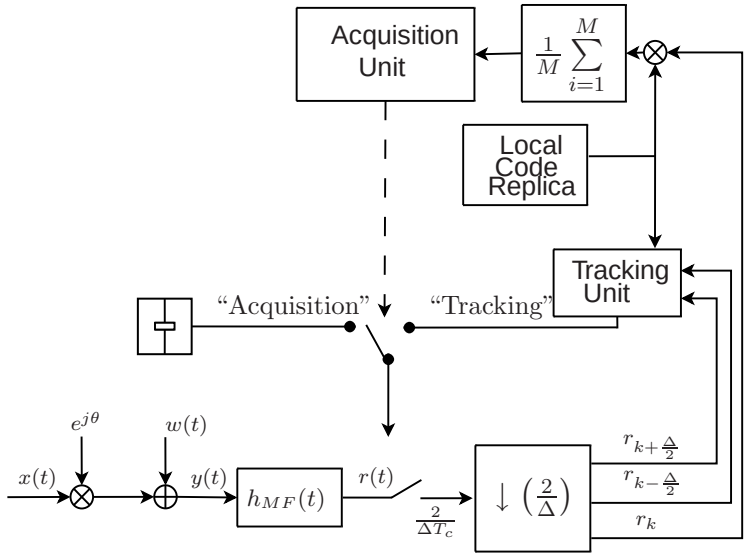

Figure 3.9: *SS-CPM Delay Estimator.*

The loop recursively updates the time delay error ε_m estimate on the basis of the current sample of the error signal e_m, as follows:

$$\varepsilon_{m+1} = \varepsilon_m - \varphi e_m \tag{3.22}$$

where φ is the step-size of the algorithm. From (3.18)-(3.20) we see that the error detector of Fig. 3.10a (hereafter labeled DDLL1) relies on the a priori knowledge of the entire sequence of the code symbols γ_k, given by the interleaving of both sequences of the two services, as defined in (3.9)-(3.11). A variant to the DDLL1 scheme, that can be used autonomously by each service, is shown in Fig. 3.10b (labeled DDLL2). The DDLL2 calls for the a priori knowledge of only one sequence (and thus one service) at a time. The DDLL2 exploits the characteristics of the CPM signals decomposed in the OQPSK form (3.11), delivering the early/late samples to the DDLL at the rate $f_c' = 1/2T_c$ instead of the rate $1/T_c$, thus reducing the error detector complexity and allowing separation of the tracking of the I and Q components. As a further variant of the DDLL2, Fig. 3.10c depicts what we call DDLL3 in which two identical (half-rate) DDLL2 detectors are used in parallel, one operating on the odd samples $r_{2k+1+\Delta/2}$ and the other operating on the even samples $r_{2k+\Delta/2}$, k being the index

of the symbol rate $1/T_c$. The outputs are then used to form the overall loop error e_m. As for the DDLL1, the DDLL3 needs a-priori knowledge of both service sequences, but, differently from DDLL1 and DDLL2, it yields higher performance, as will be highlighted later.

3.4 Performance results

After the theoretical definition of the code tracking loops given in the previous section, the performance of these estimators are shown here from different points of view. First, performance in AWGN are assessed in terms of RMSE, secondly effects of multipath channels are considered in terms of MPEE, then a subsection investigates an example of two-rate services SS-CPM performance and finally an overview of the main performance results is reported.

3.4.1 Performance in the AWGN channel

The performance of the three proposed DDLL schemes are reported in Figures 3.11a, 3.11b and 3.12 in terms of average error characteristic (S-curve) and of root mean square error estimation (RMSEE), respectively. The average error characteristic (S-curve) of the loop, denoted by $\eta(\varepsilon)$, is a function of the chip timing error ε and is defined as the average of the error detector output e_m when the loop is kept open (that is, (3.22) is not implemented) and the receiver is operated with a constant chip timing error ε, that is

$$\eta(\varepsilon) \triangleq \langle \mathbb{E}\{e_m | \varepsilon_m = \varepsilon\} \rangle \tag{3.23}$$

where the operator $\langle \cdot \rangle$ stands for "time average over a code period" and $\mathbb{E}\{\cdot\}$ is the statistical expectation taken over the Gaussian noise. The S-curve determines the operating range of the synchronizer, but it can be used to find the variance of the estimator as well. In fact, the main performance parameter of the accuracy of the code tracking loop is the root mean square error estimation (RMSEE) σ_ε , that is, the RMS value of the time delay error ε_m. Resorting to standard linear analysis of the loop, it is found

$$\sigma_\varepsilon \cong \frac{1}{A}\sqrt{2B_L T_a S_N(0)} \tag{3.24}$$

where $S_N(0)$ is the DC-value of the open-loop error signal PSD:

$$S_N(f) \triangleq \sum_{n=-\infty}^{\infty} R_e(n) e^{-j2\pi n f T_a} \tag{3.25}$$

$$R_e(n) \triangleq < E\left\{ e_m e_{m+n} |\ \varepsilon_m = 0 \quad \forall m \right\} > \tag{3.26}$$

and $B_L T_a$ represents the one-sided equivalent noise bandwidth of the loop, normalized to the updating time T_a of the loop equation (3.22). Referring to the proposed DDLL1-DDLL3 schemes of Figures 3.10a-3.10c, the updating time T_a of the loop error is set to $T_a = \lambda T_c$ for DDLL1, whereas it is $2\lambda T_c$ for DDLL2 and DDLL3. In particular, for the first order time delay locked loop, the normalized loop noise bandwidth is

$$B_{eq} T_a = \frac{\varphi A}{2(2 - \varphi A)}, \tag{3.27}$$

where A is the slope of the S-curve function nearby the zero error, $A = \left.\frac{d\eta(\varepsilon)}{d\varepsilon}\right|_{\varepsilon=0}$. Figure 3.12 reports the variance of the proposed schemes for some signal formats, together with the relevant modified Cramér-Rao bound (MCRB) (3.13), as a reference. In our numerical calculations of the RMSEE, the loop noise bandwidth is $B_L = 1Hz$, a typical value for satellite navigation systems, and the bandwidth of the branch filter $\overline{H}_b(f)$ is chosen with the constraint $T_a \ll 1/B_L$. In particular, a value of $\lambda = 10000$ is considered for simulations. Once B_L and λ (thus T_a) are set, the step-size φ can be found trough (3.27) after computation of the S-curve.

For each RMSEE figure, the correspondent MCRB is computed as in (3.13)-(3.14) considering an equivalent observation time $T_{obs} = L_{eq} T_c = \frac{1}{2B_L}$. Finally, computation of (3.24) is carried out after evaluation of $S_N(0)$ via simulation. The RMSEE curves are shown here only for the CPM signals with Gaussian frequency pulses, with two modulation indices ($h = 0.5$ and $h = 2.5$), with normalized bandwidth $BT_c = 0.4$ and support $L = 4$, chip time value $T_c = 195.5ns$ ($R_c = 5.115Mchip/s$) and correlator spacing $\Delta = 0.2$. Performance with different pulses or different modulation index h present the same qualitative behavior and the correspondent RMSEE curves can be easily considered as a "vertical translation" of the "basic" curves depicted in Fig. 3.12. In particular, the relative behavior of the three proposed tracking schemes reveals independent of the selected signal. As can be seen from Fig. 3.12, irrespective of the modulation index h, the DDLL1 and DDLL2 present the same performance, while the DDLL3, as expected, exhibits a 3 dB gain.

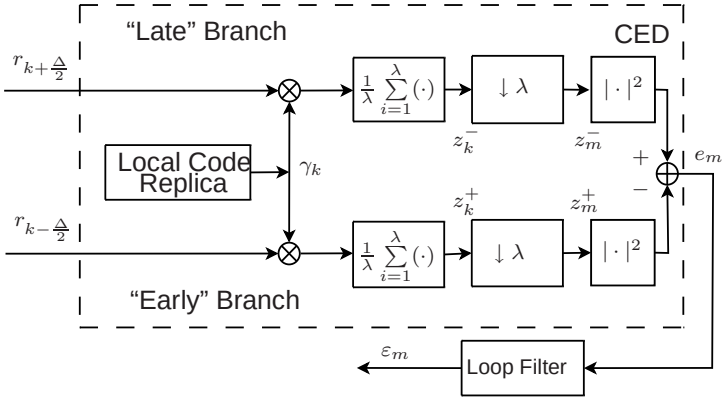

(a) DDLL1.

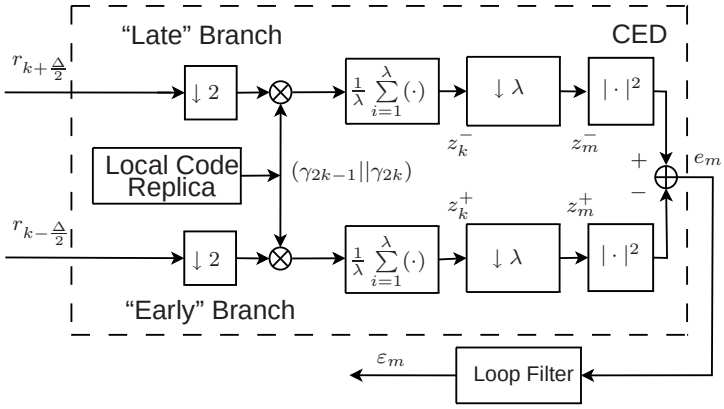

(b) DDLL2.

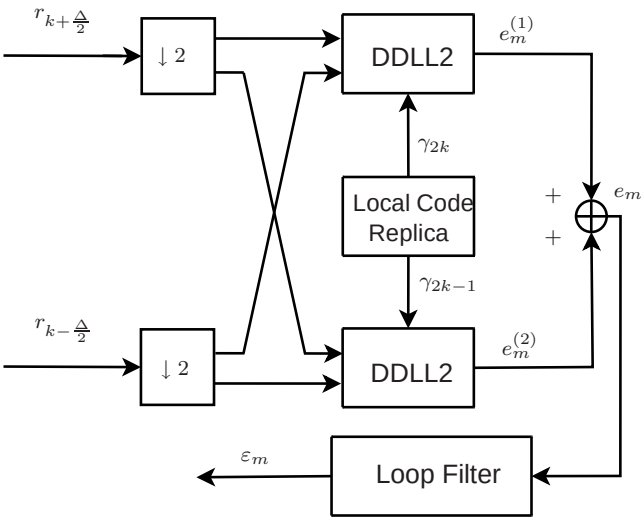

(c) DDLL3.

Figure 3.10: *Digital Delay Lock Loop code tracking loops.*

As was anticipated, a higher modulation index induces a higher second order moment of the spectrum and, thus, better tracking accuracy. As depicted in Fig. 3.12, for example, the MCRB relative to $h = 2.5$ exhibits a C/N_0 gain of 14 dB wrt the MCRB relative to $h = 0.5$. Figure 3.12 also shows that the tracking performance of the DDLL3 practically equals its own MCRB for high C/N_0 both when $h = 0.5$ and when $h = 2.5$.

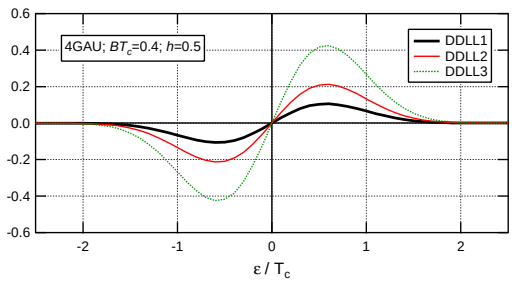

(a) $h = 0.5$

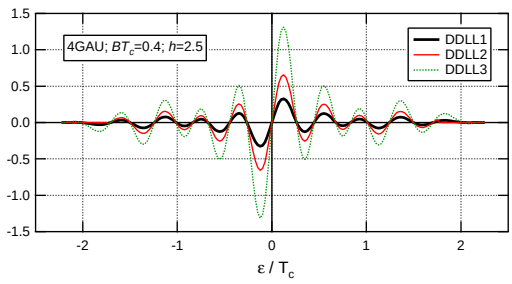

(b) $h = 2.5$

Figure 3.11: *S-curve function of the different DDLL schemes. Simulation for 4GAU frequency pulse.*

3.4.2 Performance in the multipath channel

The signal design analysis described so far is suitable for AWGN channels. However, multipath still remains the dominant factor in a GNSS error budget. Currently, it is customary to evaluate the MP performance of a given signal/estimator combination by its MPEE plot [37], [38]. The MPEE plot reflects the performance of a two-ray multipath channel (line-of-sight + one reflected ray), by showing the bias induced by

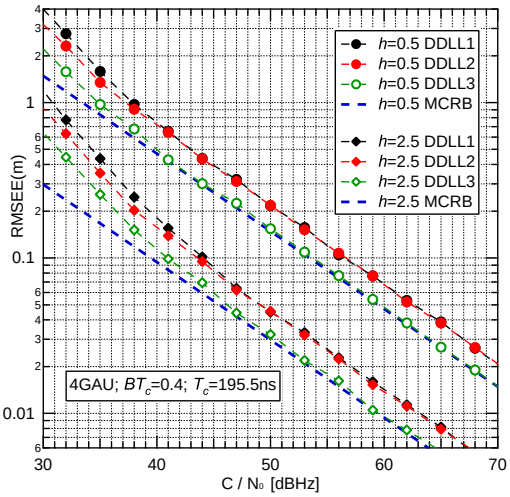

Figure 3.12: *RMSEE for the proposed DDLL schemes. Simulation for* 4*GAU frequency pulse for* $h = 0.5$ *and* $h = 2.5$.

the non-line-of-sight path onto TDE. The bias is computed establishing a receiver configuration (TDE estimator, early-late spacing) as a function of the reflected path delay, and with the MP (relative) amplitude kept constant. As an example, Fig. 3.13 shows the MPEE of CPM modulations for the particular frequency pulse $4GAU$. The curves are computed considering the non-coherent DDLL1, with an early-late spacing $\Delta = 0.01$ and for different values of h. The signal-to-multipath ratio (SMR) is equal 6 dB, a typical value for ranging systems. For each signal configurations, two lines are plotted, corresponding to the two worst cases of in-phase reflected signals, whilst the cases with intermediate phase shifts that lie in between are not considered. The figure reports the bias error expressed in chip as a function of the delay of the specular ray expressed in chip as well.

The MPEE curves show smaller errors when the modulation index h of the CPM signal is higher, i.e. when the bandwidth is larger and RMSEE is smaller.

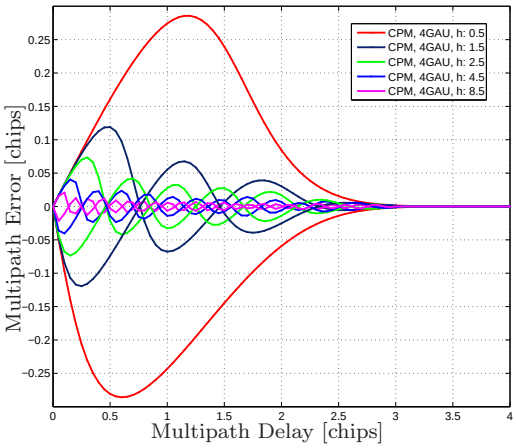

Figure 3.13: *MPEE figures of SS-CPM for different modulation indices.*

3.4.3 Two-rate-service (TRS) performance

As anticipated in Sect. 3.2.3, a TRS signal is characterized by two different chip rates on the two I-Q components. Figure 3.14 shows the spectrum on the I and Q branches of a TRS signal characterized by an I branch with $N_{rep} = 10$, and $1REC$ CPM with a chip time $T_c = 97.75ns$ ($R_c = 10.23Mchip/s$). In this case, therefore, the "slow" and the "fast" service chip rates result $1.023Mchip/s$ and $10.23Mchip/s$, respectively on the I and Q branches. Considering the OQPSK approximation of CPM, the I-Q components can be considered as two independent pulse amplitude modulation (PAM), with basic time pulses bearing different duration. The "expansion" of the time pulse on the I component by a factor N_{rep}, causes a compression of its spectrum, resulting in a narrower main lobe wrt the (fast) Q-branch. In particular the width of the spectral main lobe is inversely proportional to N_{rep}. Unfortunately, considering only a narrow band around the first main lobe in the I-branch receiver, causes a non-negligible out of band power loss (≈ 6 dB).

Figure 3.15 shows the MCRB for TRS TDE with 1REC frequency pulse and modulation index $h = 0.5$, considering in the calculation independent I-Q branches and assuming (coherent) estimators with different spectrum bandwidths. In our computations, we considered a few cases: slow-rate I-branch with bandwidth equal to that

of the first lobe, 5 lobes and 13 lobes, and with the fast-rate Q-branch at the 1st lobe or with infinite bandwidth spectrum. It can be seen that bounds for I-branch fall far from Q-branch ones, depending on number of spectrum lobes considered. The advantage in using a TRS is related to the possibility of receiving the slow-rate service with a narrow band mass-market receiver.

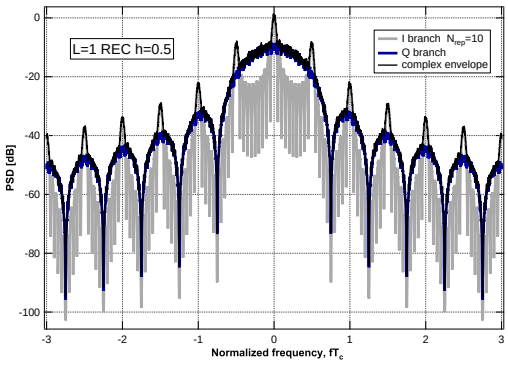

Figure 3.14: *PSD of SS-CPM for Two-Rate-Service (TRS), $N_{rep} = 10$, for the I and Q branches and the total complex envelope.*

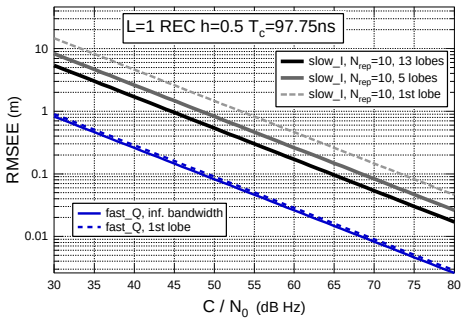

Figure 3.15: *MCRB of SS-CPM for Two-Rate-Service (TRS), $N_{rep} = 10$. MCRBs for slow I-branch 1st lobe, 5 and 13 lobes spectrum, fast Q-branch 1st lobe and infinite bandwidth spectrum.*

3.4.4 Summary of performance results

Due to our parametric analysis, some general conclusions can be drawn.

For all types of frequency pulses, the higher the L, the better the spectral efficiency, at the expenses of a higher receiver complexity. For our test cases, solutions like 1REC, 2REC, 1RC, 2RC, 3GAU, 4GAU and 5GAU can be easily implemented.

In AWGN channel, the relative behavior of the three proposed tracking schemes reveals independent of the selected signal. Irrespective of the modulation index h, the DDLL1 and DDLL2 present the same performance (RMSEE), while the DDLL3 exhibits a 3 dB gain achieving the MCRB. For all the sub-classes of analyzed SS-CPM signals, a higher modulation index induces a higher signal Gabor bandwidth and, thus, better tracking accuracy.

In the MP channel, performance in terms of MPEE enhance when h increases for all the types of frequency pulses.

Examining these results and also the spectral and correlation properties, the effects of increasing the modulation index h can be compared to the ones induced by an higher m/n ratio in the $BOC(m,n)$ modulations, thus allowing for higher tracking performance and MP rejection, at the expense of an increase of autocorrelation sidelobes and receiver complexity.

Interestingly, some new frequency pulses like the square wave (SQW) frequency pulse can be designed to allow the desired spectral shaping, while some trivial tricks can be used to allocate two services.

In conclusion, after analyzing SS-CPM we have seen that they allow much more flexibility than what expected, by simply tuning the design parameters. When comparing to traditional DS-SS modulations (like the $BOC(m,n)$) it is thus appearing the same intrinsic binomium between tracking accuracy and acquisition performance and receiver complexity: since the two aspects are inversely related to the relative position of the main spectral lobes into the signal bandwidth, thus we cannot improve one aspect without deteriorating the other one. With this respect, the analyzed SS-CPM generally behave as the $BOC(m,n)$, while intrinsically ensuring a constant envelope.

Detailed design and specific comparison among the different SIS classes can be achieved only when having defined specific system constraints. A possible application of this design could be foreseen for any new ranging application, like for example the

C-band usage [14], [6], [53]. In particular in [6], [53] already some MSK and GMSK cases have been exploited as option to fulfill their system design.

3.5 Conclusions

This chapter has shown how a constant-envelope spread-spectrum CPM signal could be effectively used as a ranging signal in future-generation GNSS systems. Let us outline the main conclusions from the sections above:

- The constant-envelope feature of a CPM signal is desirable to get rid of the detrimental spectral-regrowth effect caused by high-power amplification of a non-constant-envelope signal;
- Conventional CPM formats are geared towards spectrum-efficient data communications. In a GNSS system, the focus of SIS design is accurate time-delay estimation, that calls for a different spectral distribution of the signal power, namely, an high second-order moment. Semi-integer values of the modulation index like $h = H + 1/2$,H natural, meet the requirement above when increasing h to values $h > 1$;
- A semi-integer CPM signal can be easily approximated (via Laurent's decomposition) with an Offset-QPSK signal, making detection and TDE very easy with conventional DDLL algorithms;
- The DDLL algorithms mentioned in the chapter come very close to their TDE CRB in terms of AWGN RMSEE;
- Two-rate services with different chip-rate/bandwdith can be combined into the same CPM signal via easy I-Q multiplexing and chip code repetition without constant envelope loss.

The effects of increasing the modulation index h can be compared to the ones induced by an higher m/n ratio in the $BOC(m,n)$ modulations, thus allowing for higher tracking performance and MP rejection, at the expense of an increase of autocorrelation sidelobes and receiver complexity. SS-CPM with ad-hoc settings of frequency pulse, of T_c and of h could be suitable for forthcoming satellite positioning systems [6], [53], thanks to their characteristics of spectral flexibility and of constant

envelope, once requirements from system design are set. More work can and has to be done in terms of i) optimization of the CPM shaping pulse; ii) reduction of the performance loss due to out-of-band power of the low-rate service in the two-rate signal arrangement.

Chapter 4

TOA Estimation with SS-FMT signals for GNSS

In this Chapter, we investigate the performance of spread spectrum filtered multitone (SS-FMT) signals, characterized by a strictly bandlimited basic pulse, considering the architecture of a standard digital signal tracker for GNSS. After a general description of signal properties in time and frequency domain, we focus on the problem of ranging code synchronization (code tracking), presenting a standard chip timing recovery loop based on the multicarrier signal property to be seen as a single carrier modulation and so to be tracked with standard delay lock loops. The relative performance of the proposed recovery loop is analyzed in terms of RMS tracking error and multipath (MP) robustness.

4.1 Motivation

Current Global Navigation Satellite Systems (GNSSs) state-of-the art is based on (NRZ) square-chip pulses, that, when digitally generated leads in practice to non-constant envelope SIS and slow out-of-band spectral decay. Thus, the interest of considering SIS designs with band-limited waveforms as it is the case in today's telecommunication payloads (e.g., DVB-S and DVB-S2) but without compromising navigation performance is steadily growing. Not too long ago, the need of innovation and the endless demand of optimal performance pushed the researchers to look for new solutions for future advanced GNSSs also in the field of multicarrier schemes [27], [21], [22]. Among the advantages of MC techniques, the robustness to

frequency selective fading, the resistance to inter-symbol-interference and high data rates are indeed interesting characteristics. In this context the application of the FMT technique [12] to satellite navigation seems appealing not only for the characteristics previously listed but also for full spectral flexibility and the limited OOB emissions. This chapter discusses a number of advantages of using multicarrier (MC) signal as a possible option for future global navigation satellite systems (GNSSs).

Multicarrier signal could be an interesting "motherboard" on which design every solution, for its several degrees of freedom in its design. It contains a large set of constituent parameters as the basic pulse, the number of subcarriers, the subcarriers frequency spacing, the power distribution within the subcarriers, the ranging code sequence, and each of these factors has an influence on the resulting signal performance. The best advantage of a multicarrier technique is thus its full spectral flexibility. Basically the number of subcarriers and the power distribution on them (also by switching off some of them) can be designed in order to obtain a Power Spectral Density (PSD) shaping which takes into account the constraints and requirements of the particular application (e.g. time of arrival (TOA) estimation tracking and acquisition performance, intersystem and intra-system interference, multipath resistance). The interest of this chapter is focused on a particular multicarrier scheme known as Filtered multitone (FMT), characterized by the strictly bandlimited Square Root Raised Cosine (SRRC) basic pulse and a subcarrier spacing that allows complete orthogonality in the frequency domain.

A theoretical formulation of the MC signal is developed focusing on the FMT technique. The correlation and spectral properties are analyzed and theoretical expressions are formulated in time and frequency domains highlighting FMT advantages, such as the full flexibility and the disadvantages related to its non-constant envelope are investigated. The chapter reports on a number of multicarrier properties which allow different applications both in navigation and communication systems. In particular the applicability of the FMT technique for navigation purposes is investigated in different scenarios. FMT modulation is investigated to synthesize (theoretically) bandlimited PSD signals or more simply any filtered signals. Existing, new and "esoteric" modulations can be reproduced with the desired accuracy and growing bandwidth resolution playing on the FMT signal setting. Interferences mitigation and coexistence with existing Signal-In-Space are possible adopting an appropriate FMT adaptive spectra management, for instance filling the gaps of spectra with

new compatible components moving the available transmission power from interfered notches to interference-free subcarriers. Finally an Early-Late Delay Lock Loop (DLL) estimator [56], which comes out from Maximum-Likelihood (ML) theory is tested on a number of FMT schemes, ensuring its full applicability by comparing its performance in TOA estimation in Additive White Gaussian Noise (AWGN), in terms of mean square error (MSE) and variance with the well known modified Cramér-Rao bound (MCRB) [27].

The modulation performance is also tested in a standard two-ray multipath channel (line-of-sight plus one reflected ray) analyzing the simulation results with different signal settings in terms of induced bias on TOA estimation with respect to AWGN results.

The chapter is organized as follow: Sect. 4.2 theoretically describes the signal modulation, analyzes the signal correlation and spectral properties; In Sect. 4.3 a SS-FMT tracking loop is described, while different types of signal configurations are tested in terms of tracking performance in AWGN (Sect. 4.4.1) and MP resistance (Sect. 4.4.2) and finally a complete summary of performance results is reported in Sect. 4.4.3. General comments conclude the chapter in Sect. 4.5.

4.2 Signal Design

4.2.1 Signal definition

The baseband equivalent of a Spread-Spectrum Multicarrier (SS-MC) signal can be written as:

$$x_{SS-MC}(t) = \sqrt{2P_x} \sum_{k \in D_f} \sqrt{w_k} x_k(t) e^{j2\pi k f_k t} = \tag{4.1}$$

$$\sqrt{2P_x} \sum_{k \in D_f} \sqrt{w_k} \left[\sum_{n=-\infty}^{+\infty} \gamma_n^{(k)} g(t - nT_s) \right] e^{j2\pi(kf_{sc}+\Delta_f)t}$$

where the coefficient w_k identifies the fraction of total power transmitted on the k-th subcarrier centered in f_k with $\sum_{k \in D} w_k = 1$, D_f is the set of active subcarrier centers, $\gamma_n^{(k)}$ is the symbol/chip (or chip-data product $\gamma_n^{(k)} = d_n^{(k)} c_n^{(k)}$) on the k-th subcarrier, $P_x = C$ is the real total power, f_{sc} is the subcarrier frequency spacing, Δ_f is a frequency offset, T_s is the multicarrier (MC) symbol time, $T_s = NT_c$, with

N the number of equally spaced subcarriers and T_c the chip (symbol) time. The multicarrier signal is also identified by its basic pulse $g(t)$, which defines a number of signal properties and it can be for instance time limited or bandlimited. This generalized explanation allows us now to define the traditional elements of a signal used in satellite navigation. Clearly the code sequence $\{c_k\}$ corresponds to the ranging code sequence associated to each satellite, while the symbols sequence $\{d_i\}$ can be associated either to the symbols of the navigation message (if we are considering the transmission of the data component) or to a fictitious sequence of all "one-symbols" $\{d_i = 1\}$ (if we are considering the transmission of the pilot component). In data

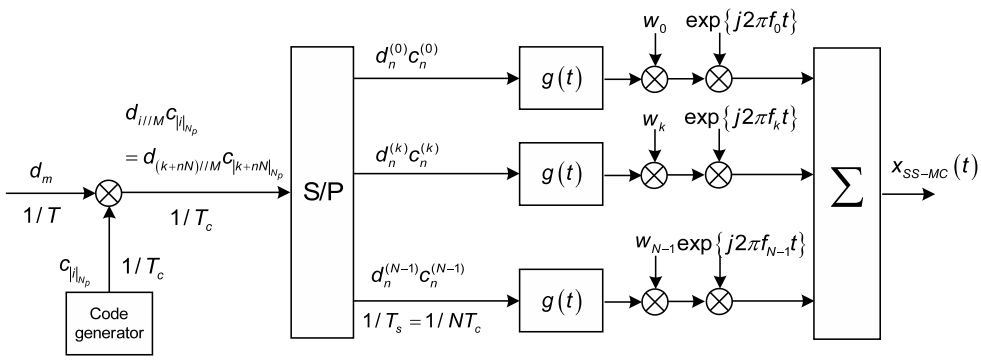

Figure 4.1: *General Spread-Spectrum Multicarrier Transmitter.*

transmission, γ represents the stream of information symbols to be sent on a wireless channel. After the mapping of the bits of information into the information symbols, with T_c the *short* symbol time, they are sent to a serial-to-parallel (S/P) converter and transmitted on the sub-channels with a *long* MC symbol time T_s. Let us consider for the sake of simplicity only binary data, remembering that all the results found can be easily generalized to an M-ary modulation case. Figure 4.1 depicts the general scheme of a SS-MC transmitter. The data stream is spread by the code sequence with a spreading factor M, and Np is the code length. The main stream is divided into N sub-streams, then they are shaped by the basic pulse, transmitted on the N subcarriers and finally summed before to be transmitted.

In this section a Spread spectrum filtered multitone (SS-FMT) transmission scheme is considered, where the subcarrier spacing is $f_{sc} = \frac{1+\alpha}{T_s}$, chosen as the minimum

which allows orthogonality between the subcarriers, using a Squared-Root Raised-Cosine (SRRC) pulse with the roll-off factor α. In this case, the Continuous Fourier Transform (CFT) of $g(t)$ is defined as $G(f)=T_s\sqrt{\frac{G_N(f)}{T_s}}$ with the Raised Cosine pulse $G_N(f)=CFT\{g_N(t)\}$ with $G_N(0)=T_s$ and a bandwidth equal to $BW_{sc}=\frac{1+\alpha}{T_s}$. The bandwidth of the total multicarrier signal so defined can be found as the sum of the N sub channels' bandwidths: $BW=(1+\alpha)/T_c=N(1+\alpha)/T_s=NBW_{sc}$. From (4.1), the baseband model specific for the FMT modulation becomes

$$x_{FMT}(t)=\sqrt{2P_x}\sum_{k\in D}\sqrt{w_k}x_k(t)e^{j2\pi\left(k\frac{(1+\alpha)}{T_s}+\Delta f\right)t}= \tag{4.2}$$

$$\sqrt{2P_x}\sum_{k\in D}\sqrt{w_k}\left[\sum_{n=-\infty}^{+\infty}\gamma_n^{(k)}g_{SRRC}(t-nT_s)\right]e^{j2\pi\left(k\frac{(1+\alpha)}{T_s}+\Delta f\right)t} \tag{4.3}$$

where the frequency offset Δf and the power distribution are defined according to the spectrum and correlation function design.

4.2.2 Signal analysis

Multicarrier signal is constituted by the superposition of N sub-channels. Their (complex) amplitudes $\sqrt{w_k}\gamma_n^{(k)}$ can be modeled as independent and uncorrelated random variables belonging to a QAM or PSK constellation. The N components are orthogonal in the frequency domain and instantaneously they have a different "phase" due to the different symbols/chips on each subcarrier, so they are non-coherently summed in time, resulting in a "multilevel" modulation. Fig.4.2 plots the I/Q components of a representative example of FMT signal, with odd N=127, flat power distribution with $w_k=1/N$, $\gamma_n^{(k)}\in\{\pm1\}$, $\Delta f=0$ and $D=\left\{-\frac{(N-1)}{2}:\frac{(N-1)}{2}\right\}$.

Obviously according to the power distribution and the set of parameters chosen the waveforms will be instantaneously different, but statistically similar. The main disadvantage in using a MC modulation is its non-constant envelope that causes distortion on the signal at the High Power Amplifier (HPA) output and consequently inter carrier, inter symbol and inter chip interferences. To evaluate this feature, the statistical characteristics and the histogram of the absolute value of the envelope is depicted in Fig.4.3 for the previous FMT example. The result reported is qualitative but enough to understand how not constant is the envelope of this modulation, when

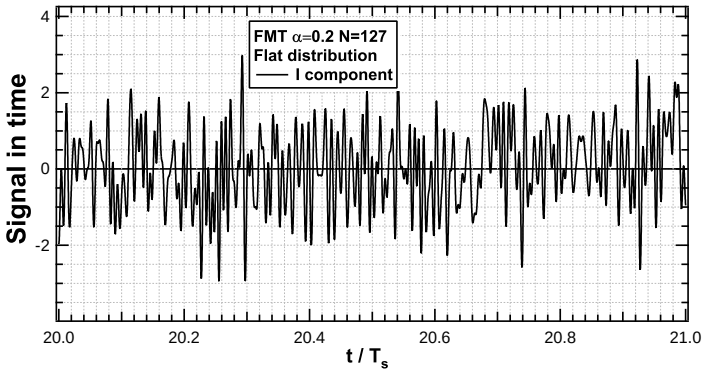

(a) In-phase component

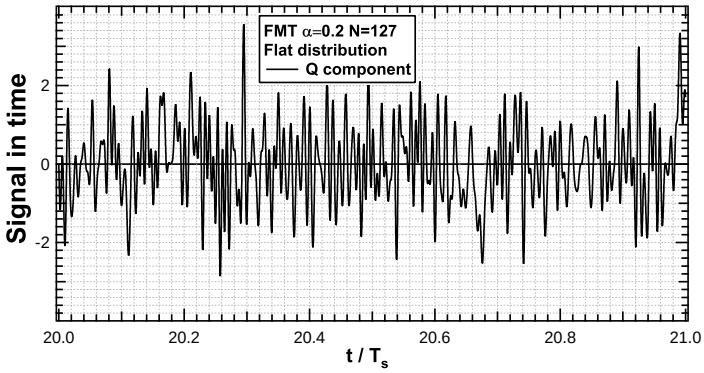

(b) Quadrature component

Figure 4.2: *I/Q components of FMT with flat power distribution, N=127 and* $\alpha = 0.2$.

a not optimized PN code was transmitted on the subcarriers. Peak, Root mean square (Rms), Peak to Average Power Ratio (PAPR), mean, variance and standard deviation are reported in the chart with the normalized envelope histogram.

The PAPR is greater than one for any power distribution (the optimum for a constant envelope is equal to 1), but a better insight is given by the distribution of probability of the absolute value of the envelope approximated with its histogram. If one observes the definition of a multicarrier signal (4.1), the I-Q branches samples are obtained as a sum of N terms with a similar density of probability with finite mean and variance. This is the hypothesis for the Central Limit Theorem (CLT) which

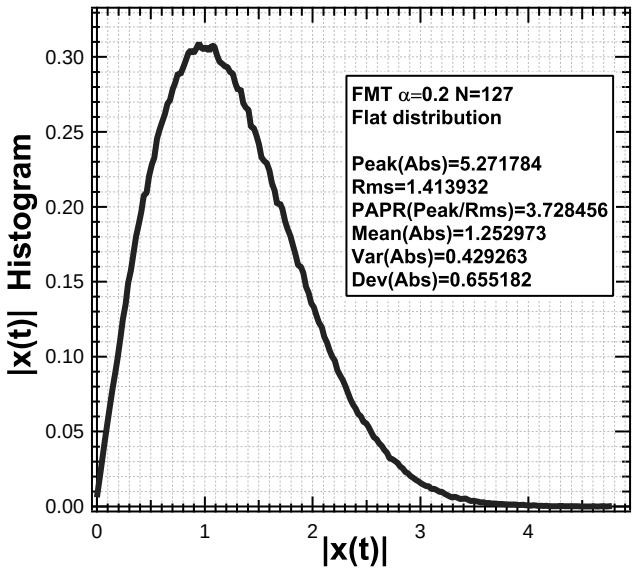

Figure 4.3: *Histogram of the FMT signal envelope.*

states conditions under which a sum of a sufficiently large number of independent random variables, each with finite mean and variance, will tend to be distributed according to a Gaussian distribution. The absolute value is calculated as the sum of the squares of I and Q values which for the CLT are Gaussian random variable, so its density of probability (histogram) tends to a Rayleigh distribution for N enough great. Statistical characteristics (mean value, variance, rms) are approximately constant for N greater than 10 (CLT). Statistically the Peak appears with a very low probability and by considering only the PAPR could be not fair. A significant performance parameter for HPA behavior could be the product between the PAPR and the standard deviation normalized by the RMS. In this way different modulation schemes can be compared each other with respect to this complete parameter, which takes into account both the PAPR and the envelope distribution. A number of algorithms for PAPR reduction are present in the literature [44]: weighting the input sequences with optimized coefficients; using ad hoc code sequences distributed in time or frequency domains [57]; the design of additional ad hoc subcarriers. One general countermeasure could be the selection of a specific set of interdependent subcarrier waveforms [39],

optimizing the total signal according to the constraints of the system.

4.2.3 Correlation analysis

This section describes some properties of the FMT correlation function. In particular the subset of signals with symmetric power distribution and identical (symbol) constellation on the equally spaced subcarriers is here analyzed. For the cyclostationary property, the correlation function is given by:

$$R(\tau) = \frac{1}{T_0}\int_{T_0} \bar{R}(t,\tau)dt = \frac{1}{T_0}\int_{T_0} E\left\{x(t)\,x^*(t-\tau)\right\}dt \tag{4.4}$$

where T_0 is the period of the cyclostationarity of $\bar{R}(t,\tau)$, and the expectation is done on the data/chips considered here random and uncorrelated. Under the hypothesis of a symmetric power distribution within the subcarriers, centered around zero, inserting (4.2) in (4.4) the FMT correlation function can be written as:

$$R_{FMT}(\tau) = 2P_x C_2 g_N(\tau)\left[\sum_{k\in D} w_k \cos\left(2\pi\left(k\frac{(1+\alpha)}{T_s}+\Delta f\right)\tau\right)\right] \tag{4.5}$$

with $C_2 = E\left\{|\gamma|^2\right\}$, which is the power of the symbols/chips (or chip-data product), $g_N(\tau)$ is the autocorrelation function of the SRRC pulse, i.e. the RC pulse. In general the autocorrelation in (4.5) can be written as the product of two independent terms

$$R_{FMT}(\tau) \propto R_{subcarrier-pulse}(\tau)\cdot R_{Pdistr}(\tau, D, \Delta f) \tag{4.6}$$

i.e. the correlation function of the basic pulse and the "array factor" which is a periodic function and depends on the power distribution and the set of subcarrier centers. For the sake of simplicity, only two possible FMT configurations for the subcarriers centers are here analyzed:

- one subcarrier centered on f=0 and $\Delta f = 0$, with an odd number of subcarriers N, with the set of centers which run in $k = -\frac{(N-1)}{2} : \frac{(N-1)}{2}$;
- no subcarrier on f=0, maintaining the symmetric distribution with an even number of subcarriers, the centers of the subcarriers shifted by $\Delta f = -\frac{(1+\alpha)}{2T_s}$ and $k = -\frac{N}{2}+1 : \frac{N}{2}$.

A number of other different schemes can be adopted, according to the particular systems constraints. The charts in Fig.4.4 depict the correlation function composition expressed in (4.6) for the FMT signal with flat power distribution, N=67 and N=66 and $\alpha = 0.25$. The array function has the maximum absolute value in multiples

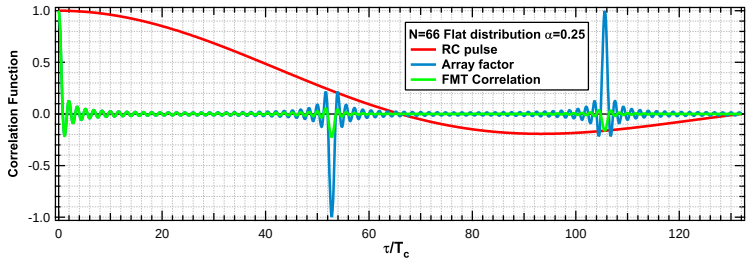

(a) Even number of subcarriers

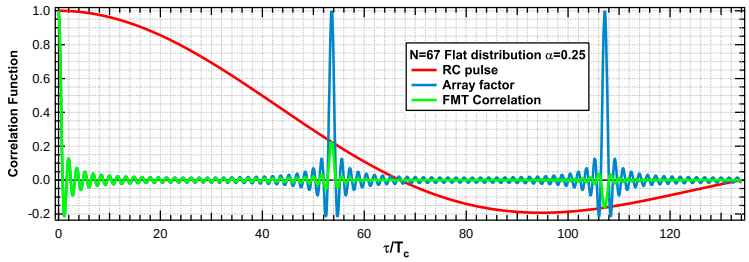

(b) Odd number of subcarriers

Figure 4.4: *FMT correlation composition*

of $T_s/(1+\alpha) = NT_c/(1+\alpha)$. If N is odd the function is periodic of $T_s/(1+\alpha)$, whereas if N is even the function is periodic of $T_s/(1+\alpha)$ with alternate sign. In this case of study the RC pulse represents the "envelope" and it is multiplied by the array factor to obtain the final correlation. As it can be seen from the plots, the multicarrier correlation function shows secondary lobes near and far to the zero delay. It will be explained in the last chapter how these lobes constraint respectively the tracking and acquisition performance.

Regarding the correlation shape and the sidelobes near the zero, they practically depend only on the array function because the correlation of the basic pulse appears locally constant. Hence, they can be properly designed choosing the power distribution within the subcarriers, once the set of centers is chosen. The array function

repeats every $T_s/(1+\alpha)$, with changed sign if N is even, leading to residual (far) sidelobes dimmed by the basic pulse correlation. These secondary peaks could be deleted setting properly the basic pulse, so that the maxima of the array factor fall on the zeros of the basic pulse. In the case of study, the RC pulse has its nulls on the multiples of $T_s = NT_c$, so for the FMT with SRRC basic pulse there will be no far side lobes adopting an $\alpha = 0$, i.e. selecting a rectangular pulse in the frequency domain. This theoretical result can be only approximated for a realistic truncated pulse in time. In general, the lower is the roll-off the lower the "far" secondary peaks, the higher is the filters design complexity. Besides, the higher is α the easier the synchronization of the signal and TOA estimation. For the cases reported in Fig.4.4 a realistic trade-off value of α was adopted, maintaining the residual sidelobes lower than 20% of the main peak. Obviously optimized basic pulses with "tails" shorter than the RC pulse ones, together with one ad hoc power distribution within the subcarriers could be designed.

4.2.4 Signal spectral analysis

Consider the correlation function in (4.5). The correspondent equivalent baseband power spectral density (PSD) of FMT signal, supposing random (i.i.d.) code sequences on the subcarriers, is defined as

$$S_{FMT}(f) = 2P_x C_2 \left[\sum_{k \in D} w_k G_N \left(f - \frac{k(1+\alpha)}{T_s} - \Delta f \right) \right] \tag{4.7}$$

with

$$G_N(f) = \left\{ \begin{array}{cc} T_s & |f| \leq \frac{1-\alpha}{2T_s} \\ \frac{T_s}{2}\left[1 + \cos\left(\frac{\pi T_s}{\alpha}\left(|f| - \frac{1-\alpha}{2T_s}\right)\right)\right] & \frac{1-\alpha}{2T_s} \leq |f| \leq \frac{1+\alpha}{2T_s} \\ 0 & otherwise \end{array} \right\} \tag{4.8}$$

The main characteristics of the FMT signal and more in general of multicarrier modulations are:

- Limited out of band (OOB) emission;
- Full spectral flexibility.

The SRRC pulse has theoretically no OOB emissions, being strictly bandlimited by definition, but it should be unlimited in time. In practice, the realistic basic pulse

has a limited time support. As a consequence $G_N(f)$ in (4.8) has to be substituted by the squared convolution between $G_T(f)/\sqrt{T_s}$ and $T_w sinc(fT_w)$, where T_w is the truncated time window. In spite of this, the OOB emission is still very limited if the T_w is chosen long enough. Once the bandwidth is set, the spectrum can be modified acting on the number of subcarriers and on the power distribution within the subcarriers, obtaining the desired frequency resolution and the desired PSD shaping, respectively, according to the particular system constraints. The FMT modulation allows a complete freedom of design regarding its spectrum and its corresponding autocorrelation. According to the scenario analyzed a fraction of the subcarrier can be attenuated (also switching off some of them), shifting the power to the other active subcarriers.

Fig.4.5 reports a number of examples with different masks of power distributed within the same active subcarriers with flat, triangular and "dovetail" shaping. The OOB emission (about 80dB) of the cases in Fig.4.5 is obtained with a particular truncation window T_w of 60 symbol times, which in general can be problematic. If the OOB is not a determinant system constraint, a narrow time window could be chosen, decreasing the processing time at the transmitter side. Other interesting cases

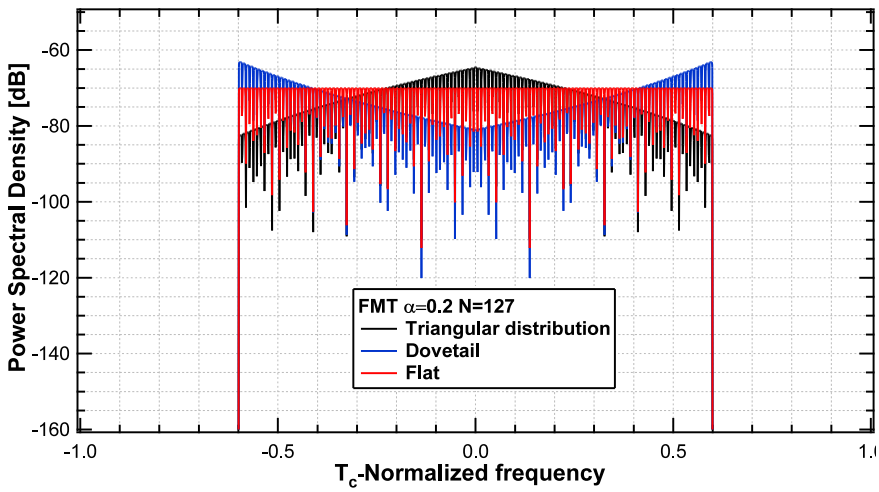

Figure 4.5: *Masks of power distribution.*

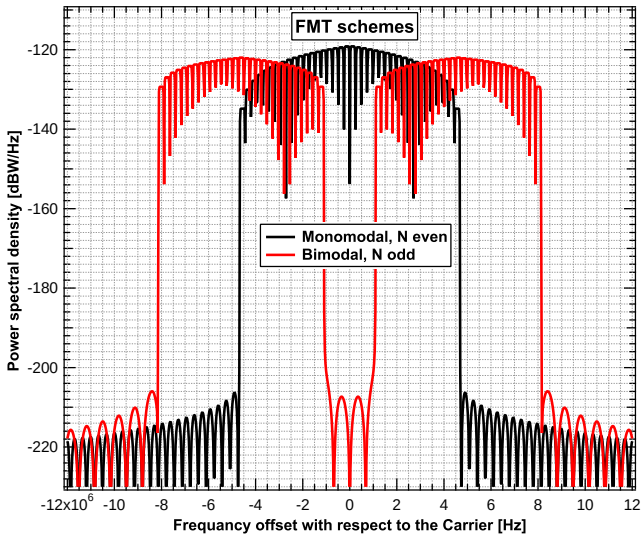

Figure 4.6: *Monomodal and bimodal schemes.*

are reported in the fig.4.6, where two different FMT schemes are plotted in the same chart labeled as monomodal and bimodal. These simple schemes, eventually with a different shaping, can be adopted for example, in case of high-pass and low-pass preexisting systems occupying the same bandwidth.

4.2.5 Multicarrier flexibility exploitation

In this section we investigated on a number of multicarrier purposes which come out of the signal characteristics reported in the previous sections. The main signal property that we have developed is the spectral flexibility. Thanks to the power distribution freedom degree we can "synthesize" any PSD of any bandlimited or filtered signal. The group of charts in Fig.4.7 depict an example of FMT synthesis of the $BOC(6,1)$ signal filtered. The samples of the analog PSD are normalized and adopted for the shaping of the FMT power profile directly on the subcarriers. In the reported example the number of active subcarriers selected was $N = 60$. In the lower side of the Fig.4.7 the synthesis autocorrelation function is reported. Due to its MC nature, the FMT correlation of the synthesized waveform presents further sidelobes than the analog

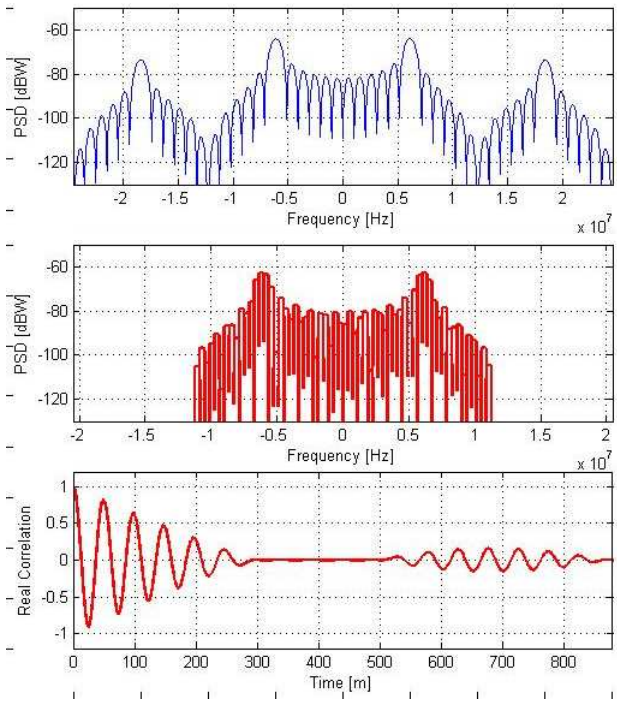

Figure 4.7: *Theoretical $BOC(6,1)$ PSD - FMT synthesis of filtered $BOC(6,1)$.*

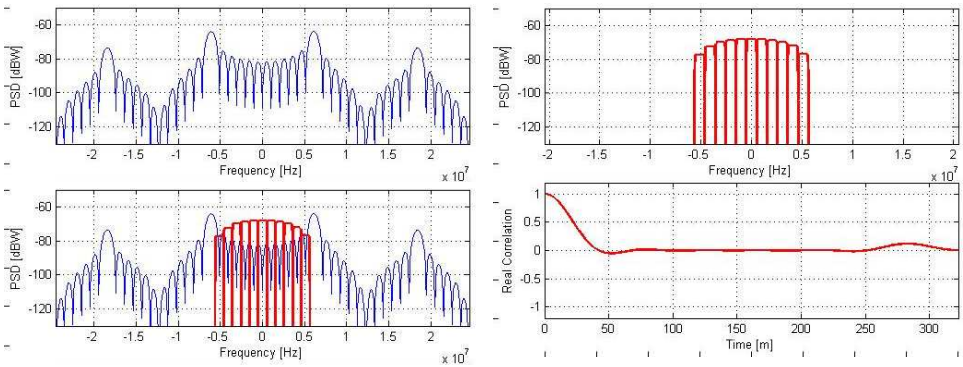

Figure 4.8: *Theoretical $BOC(6,1)$ PSD - Low-pass FMT solution to minimize inter-systems interference.*

$BOC(6,1)$ on the multiple of $NT_c^{FMT}/(1+\alpha)$, where attenuated replicas of the *basic correlation* are centered. A greater N can be chosen to shift the secondary lobes far according to the requirements. Another possible aim of the spectral flexibility can be the design of innovative PSDs minimizing the interference with an existing signal or group of system's signals. In the Fig.4.8 the $BOC(6,1)$ is considered as the pre-existing system on which we have to design a new signal. The FMT synthesis of the signal is realized choosing the power distribution in inverse proportion to the samples of the BOC PSD. Besides, the subcarriers centers can be placed on the zeros of the BOC spectrum, filling its gaps to decrease the mutual interference. The respective autocorrelation function, reported in the lower chart of the Fig.4.8, has not sidelobes near zeros, but only the "usual" sidelobes due to the contribution of the MC (periodic) array factor emphasized in (4.6). For both the examples reported, the number of subcarrier has to be defined according to the requirements of the system. The accuracy of the synthesis both in the frequency domain both in time on the correlation function will depend on the number of "samples" (subcarriers) adopted for a fixed bandwidth. A proof of this is explained with an example reported in the Fig.4.9a with a synthesis of the $BPSK(1)$ PSD, where the number of subcarriers has been increased from 19 to 41. The (far) sidelobes move from zero proportionally to N and naturally the FMT resolution in the frequency domain gets better. A parallel enhancement of the synthesis can be obtained when it is possible, increasing the

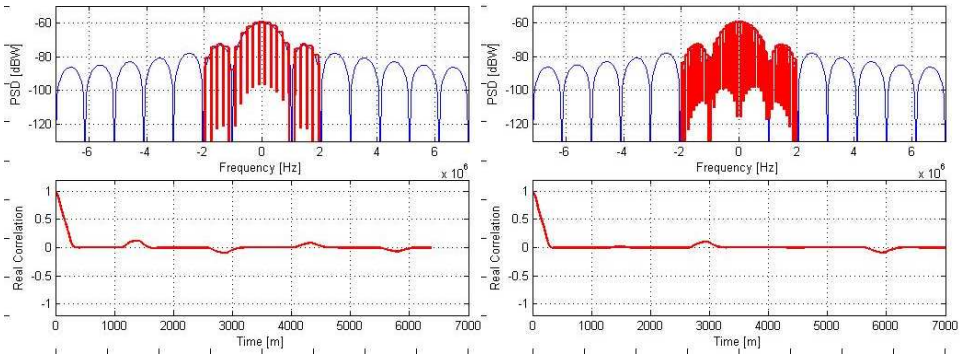

(a) Filtered $BPSK(1)$ synthesis with growing number of subcarriers.

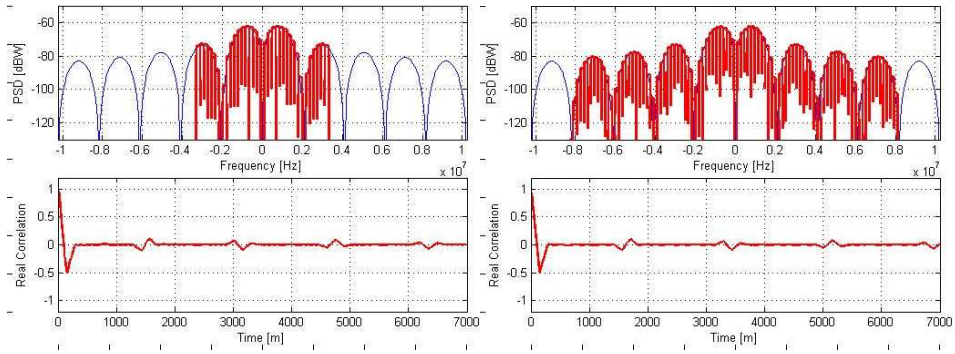

(b) Filtered $BOC(1,1)$ synthesis with growing available bandwidth.

Figure 4.9: *Enhancement of the PSD synthesis.*

available bandwidth of the signal as in the $BOC(1,1)$ example in Fig.4.9b, maintaining the same subcarrier spacing and increasing the number of subcarriers from 37 to 97. The scenarios in which the FMT can be adopted are different and its spectral flexibility can be the key factor to solve problems like mitigation of the interference or coexistence with other preexisting Signal-In-Space. In the group of chart of Fig.4.10 a very simplified (stylized) example explains how the MC waveform replies to different kind of interferences. In the upper part there is the PSD of the FMT signal with flat distribution, which can be considered as the state of the waveform in absence of interference. If the system implemented is capable to do some sort of spectrum sensing to detect the interferences the power distribution can be changed according to

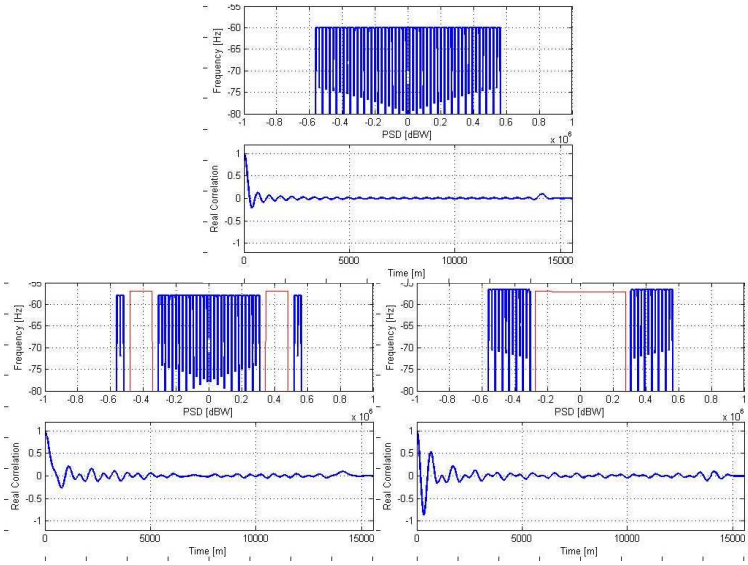

Figure 4.10: *FMT power spectral flexibility - no interference, high-pass and low-pass interference cases.*

these, maintaining the other parameters of the waveform. Two cases of interference are reported in the Fig.4.10, bandpass and lowpass respectively. Supposing spectrum sensing by the receiver, the channel scenario could be sent to the transmitter side, where the waveform could be reshaped as seen in the charts, moving the available transmission power from interfered notches to interference-free subcarriers, or also with other power profiles minimizing the interference in accord to other requirements in frequency and in time. In accord to this the receiver will change the modulation parameters too. If only the receiver knows the channel scenario, it can re-allocate the power on the interference-free subcarriers of the signal replica, loosing from one side useful power on the interfered subcarriers received, but on the other hand amplifying the remaining subcarriers, avoiding the deleterious interference.

4.2.6 Mapping to services: Time and Frequency domain ranging codes

In the previous sections random codes are considered to characterize the averaged properties of a multicarrier signal. The ranging sequences adopted in actual positioning systems based on single carrier waveform are (optimized) codes which try to approximate a random behavior and which ensure low autocorrelation sidelobes and low cross-correlation, to maximize the acquisition performance and to minimize the multiple access interference (MAI) introduced by the contemporary presence of more than one satellite code at the receiver side, respectively,. In the case of multicarrier signaling waveform, the design of a ranging code is more critical than the case of a single carrier signal. The performance will depend on the particular code sequence, as in the single carrier case, but also on the distribution of the same code chips on the active subcarriers in frequency, and in the symbol intervals in time, "twisting" the property of a normal "one-dimension" code. The design of the *two-dimension* code has to be performed jointly with the power distribution between the subcarrier, and in particular with the distribution scheme of the chips in time and frequency, considering the system constraints to be obtained. In this thesis a single satellite scenario is analyzed, not dealing with the code optimization. For the cases analyzed Golden codes are adopted, which are sequentially distributed from the first active subcarrier to the last one, and the full code length is divided on an integer number of MC symbol intervals depending on the number of subcarriers.

4.3 Delay tracking performance

In this section we deal with the tracking performance of some proposed SS-FMT signals in terms of accuracy of TOA estimation. In particular, tracking performance depends on the signal format and on the specific estimator implemented in the receiver. To characterize the signal format only, tracking performance will be evaluated in terms of MCRB, while specific analysis on receiver performance and complexity will be assessed for some proposed time-of-arrival estimators.

The MCRB for an FMT signal [27] is a function of the basic pulse shape, as in [46], and of the power distribution within the subcarriers and their centers. Assuming the code sequence as an array of nuisance parameters, and so averaging on all the possible

binary code sequences one obtains

$$MCRB\left(\tau\right)=\frac{T_s^2}{8\pi^2\frac{C}{N_0}LT_s\left[\xi_g^2+\frac{(1+\alpha)^2}{N}\sum\limits_{k=-\frac{N-1}{2}}^{+\frac{N-1}{2}}k^2w_k\right]} \tag{4.9}$$

for $\Delta f=0$ and N odd, whereas

$$MCRB\left(\tau\right)=\frac{T_s^2}{8\pi^2\frac{C}{N_0}LT_s\left[\xi_g^2+\frac{(1+\alpha)^2}{N}\sum\limits_{k=-N/2+1}^{+N/2}\left(k-\frac{1}{2}\right)^2w_k\right]} \tag{4.10}$$

for $\Delta f=-\frac{1+\alpha}{2T_s}$ and N even, where L is the number of MC symbols in the observation time $T_{obs}=LT_s=LNT_c$. The ξ_g^2 is the so-called Pulse Shape Factor (PSF), an adimensional parameter defined in [46], which represents normalized Gabor bandwidth of the basic pulse defined as

$$\xi_g^2\triangleq\frac{T_s^2\cdot\int\limits_{-\infty}^{\infty}f^2\cdot\left|G\left(f\right)\right|^2df}{\int\limits_{-\infty}^{\infty}\left|G\left(f\right)\right|^2df}=\frac{T_s^2\cdot\int\limits_{-\infty}^{\infty}f^2G_N\left(f\right)df}{\int\limits_{-\infty}^{\infty}G_N\left(f\right)df}=\frac{1}{12}+\alpha^2\left(\frac{1}{4}-\frac{2}{\pi^2}\right) \tag{4.11}$$

and in turn the content of the square brackets in 4.9 and 4.10 represents the normalized signal Gabor bandwidth which can be labeled as ξ_x^2. The MCRB can be evaluated through the use of the signal shaping in time, otherwise when the observation time is sufficiently large, the limit can be computed in the frequency domain, especially to evaluate the performance of filtered or bandlimited spectra such as this case, as defined in the Sect. 2.5. Obviously the particular ranging code adopted could have slightly different performance compared to the theoretical bound. Anyway, if the length of the code is large enough and if only (PN) sequences suitable for ranging are considered, every sequence can be assumed as statistically equal and its performance will match the averaged behavior. Finally, in accordance with what one evinces in the 4.9 and the 4.10, and as anticipated in the previous chapters, signals with energy shifted at the edge of the allocated band have better tracking performance. The best result in this case can be obtained switching off all the power coefficients w_k except for the two more distant from the centrum, which will have a power coefficient equal to $w_k=1/2$ and minimize the expressions discussed before.

4.3.1 Code tracking loop

The bound evaluated in the previous section depends only on the signal shaping, and it represents the optimum performance in terms of RMSE for any (unbiased) estimator. Let us show how the multicarrier signal can be tracked by a standard loop, considering a particular design in which the received signal can be processed as a *single carrier* waveform, without acting on each subcarrier's code sequence segment.

In communication a number of algorithms use a particular code sequence of preamble, to estimate the time delay. Each subcarrier code segment can be processed after its baseband demodulation and correlated with the matched filter of the basic subcarrier pulse. The error output which comes out of each subcarrier can be combined to the others for the delay estimation according to a specific algorithm. This could result convenient, like in the case of an OFDM modulation, when an efficient demodulation scheme is adopted, e.g. the Fast Fourier Transform (FFT), such as at the transmitter side, and if this constraint is more binding than the timing estimation performance itself. In fact, if the FFT scheme precedes the matched filtering, a loss in the performance occurs for the Gabor bandwidth (GB) losses of each subcarrier. An alternative scheme [21, 22, 61] preserves the theoretical GB of the signal, exploiting coherently the frequency offsets of each subcarrier, and achieving the optimum in the AWGN scenario. This time delay estimator, applying a standard *Maximum Likelihood* technique, simply processes the full signal correlating the received signal with a local replica of the transmitted waveform.

The scheme consists in an Early-Late (E-L) estimator applied to the FMT waveform, obtained by a particular (time-frequency) ranging code sequence transmitted within the N_a active subcarriers and an integer number L of FMT symbol times (T_s). The technique does not depend on the particular MC set of parameters adopted, and is general for all the waveforms designed. The FMT pilot signal results a periodic function, with a period multiple of the code length, $T_p = qN_{code}T_c = qLNT_c$ where N_{code} is the code length (in chip) and q is the minimum integer value which makes integer the number $qL\,(1+\alpha)$. In this way, the FMT signal can be considered as a repetition of a *basic window*, eventually modulated by a data sequence, assuming each data spread on M chips, with M an ad-hoc spreading factor, equal to a multiple of the N_{code}. Hence the received signal can be filtered by the *basic period* matching filter and processed as a standard single carrier waveform.

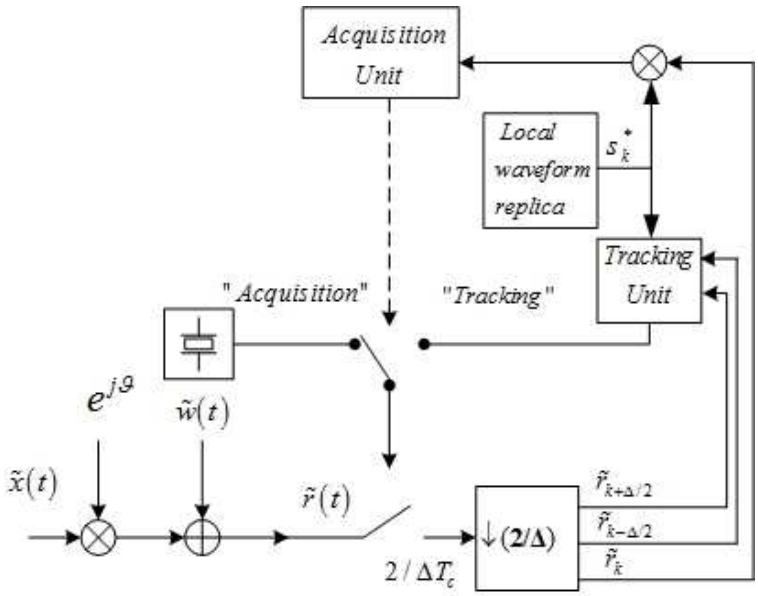

Figure 4.11: *SS-FMT Receiver*

The baseband equivalent of the SS-FMT receiver is depicted in Fig.4.11, where, using complex envelope notation, the received signal before to be sampled is

$$r(t) = e^{j\vartheta} x(t) + w(t) \tag{4.12}$$

$$w(t) = [w_c(t) + jw_s(t)] \otimes h_{LP}(t) \tag{4.13}$$

where $w(t)$ is complex-valued AWGN whose components are mutually independent and have a PSD $S_{w_c}(f) = S_{w_s}(f) = N_0$, ϑ is the carrier phase offset introduced during the (non coherent) base band conversion. The received signal $r(t)$ is sampled at the frequency $2/(\Delta T_c)$ (where $\Delta \in (0,1)$ is the normalized correlator spacing), and (possibly) decimated to obtain the sets of prompt samples r_k, early samples $r_{k+\Delta/2}$ and late samples $r_{k-\Delta/2}$, all running at the samplimg rate $f_{sa} = 1/T_{sa}$, that are passed as input to the code tracking loop. [1] Assuming that coarse delay estimation

[1] The sampling rate $2/(\Delta T_c)$ to obtain $r_{k\pm\Delta/2}$ is only "conceptual". Other, more efficient DSP arrangements based on digital interpolation to provide the prompt and the early late samples with the desired spacing Δ can be found.

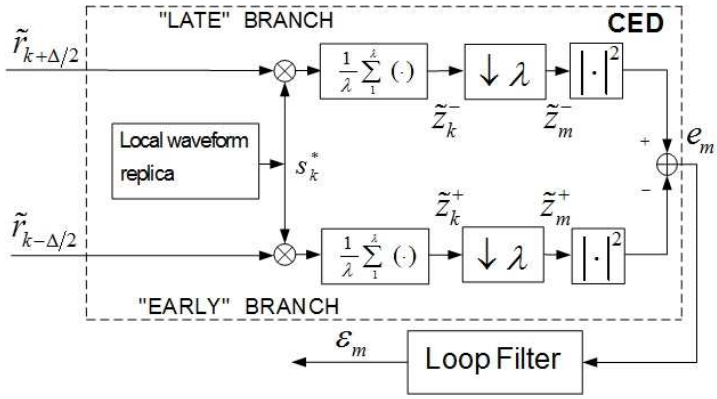

Figure 4.12: *Non coherent E-L DDLL.*

(signal acquisition) has already occurred, the tracking circuit adopted is a classical digital non-coherent early-late code tracking loop. Hence, the digital delay lock loop (DDLL) shown in the Fig.4.12 is designed insensitive to residual phase offset. From the analog discriminator function, the digital version of a non coherent E-L discriminator output [34], [32] becomes

$$e_m = \frac{\left|\int_{mT_{\text{int}}}^{(m+1)T_{\text{int}}} r\left(t+\hat{\varepsilon}_m+\frac{\Delta}{2}\right) s^*(t)\,dt\right|^2 - \left|\int_{mT_{\text{int}}}^{(m+1)T_{\text{int}}} r\left(t+\hat{\varepsilon}_m-\frac{\Delta}{2}\right) s^*(t)\,dt\right|^2}{T_{\text{int}}^2} \tag{4.14}$$

$$= \frac{\left|\sum_{m\lambda}^{(m+1)\lambda} r_{k+\Delta/2} s_k^*\right|^2 - \left|\sum_{m\lambda}^{(m+1)\lambda} r_{k-\Delta/2} s_k^*\right|^2}{\lambda^2}$$

where $T_{int} = \lambda \cdot T_{sa}$ is the integration time, which represents the window on which the early and late versions of the received signal are correlated with the local signal replica, and subtracted each other to produce the discriminator output error further filtered to recover from the current time delay error $\hat{\varepsilon}_m$. In the case of perfect phase estimation ($\vartheta = 0$), a coherent version of the discriminator can be adopted substituting the (squared) absolute value block with the one which computes the real part of the input, as reported in Fig.4.13.

The loop recursively updates the time delay error ε_m estimate on the basis of the

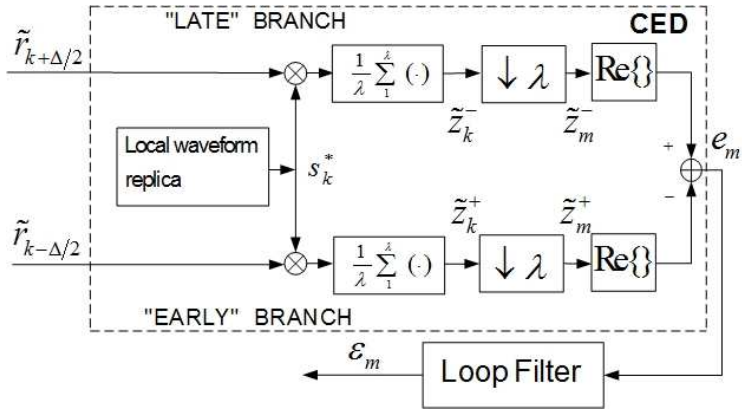

Figure 4.13: *Coherent E-L DDLL.*

current sample of the error signal e_m, as follows:

$$\varepsilon_{m+1} = \varepsilon_m - \varphi e_m \tag{4.15}$$

where φ is the step-size of the algorithm and where 4.15 represents the differential equation (state equation) of the first order loop filter adopted in this analysis.

4.4 Performance results

After the theoretical definition of the code tracking loops given in the previous section, the performance of the DDLL is shown here from different points of view. First, performance in AWGN are assessed in terms of root mean square error (RMSE), secondly effects of multipath channels are considered in terms of multipath error envelope (MPEE).

4.4.1 Performance in the AWGN channel

Recalling the results reported in the Sect. 3.4.1, the average error characteristic (S-curve) of the loop, can be computed averaging the error detector output e_m when the loop is kept open (that is, (4.15) is not implemented) and the receiver is operated with a constant timing error ε.

The S-curve determines the operating range of the synchronizer, and resorting to standard linear analysis of the loop it can be used to find the variance of the estimator as well. In this analysis the loop is closed, computing the RMSE performance directly from the time delay estimates. Besides, for the first order time delay locked loop analyzed, the normalized loop noise bandwidth is

$$B_{eq}T_a = \frac{\varphi A}{2\,(2-\varphi A)}, \tag{4.16}$$

where A is the slope of the S-curve function nearby the zero error, normalized by the updating time T_a of the loop equation (4.15) which in this case corresponds also to the integration time T_{int} of the early and late correlators.

In our numerical calculations of the RMSEE, the loop noise bandwidth is $B_{eq} = 1Hz$, a typical value for satellite navigation systems, and the integration time is chosen with the constraint $T_{int} = T_a \ll 1/B_L$. Once B_L and T_a are set, the step-size φ can be found trough (4.16) after computation of the S-curve. The DDLL is here adopted to track FMT waveforms with different characteristics.

Flat and Bimodal formats case of study

Let us consider two FMT signal formats labeled as *Flat* and *Bimodal*, whose spectra and correlation function are depicted in Fig.4.14 and Fig.4.15. Both the solutions show to be strictly bandlimited, thanks to the SRRC basic pulse which shapes every subcarriers. A standard flat power distribution is compared with a bimodal one, in which only a fraction of the total subcarriers is activated at the edges of the signal bandwidth, to test the performance of the proposed DDLL for MC signals. In the analysis, the SRRC roll-off is set to $\alpha = 0.4$ and an odd number of subcarriers $N = 1023$ with symmetric power distributions within the active subcarriers centered in zero is adopted. The E-L delta spacing chosen for the simulation is less than a half of the correlation width $\Delta = 0.5T_c$. The integration time is equal to one code period, using a PN Gold sequence of 10230 chips divided on the N subcarriers and on $L = 10$ symbol times. The chip rate is chosen equal to $1.023Mchip/s$ and consequently the signal bandwidth is $BW = (1+\alpha)/T_c = 1.4322MHz$.

The bimodal distribution of the power causes a more oscillating correlation function compared to the flat one. From one hand, the Gabor bandwidth of the bimodal signal is greater than the flat one, but from the other hand the large number of ambiguities in the correlation function will have a negative impact on the acquisition performance.

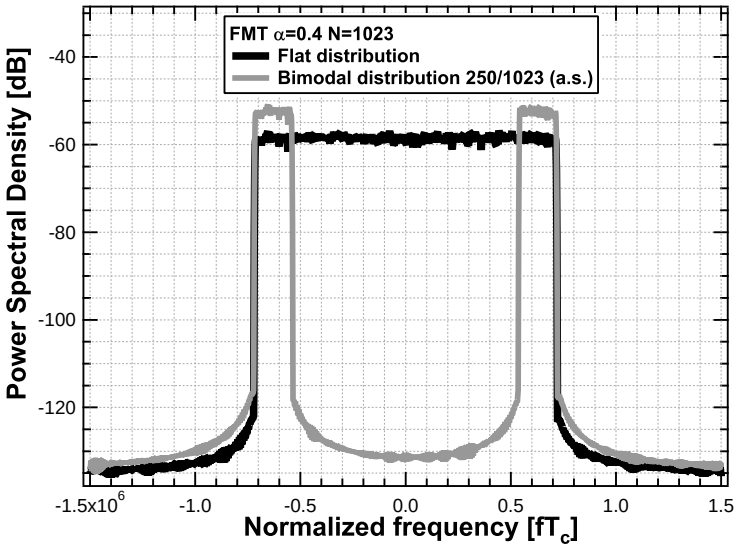

Figure 4.14: *Power spectral density of the FMT schemes.*

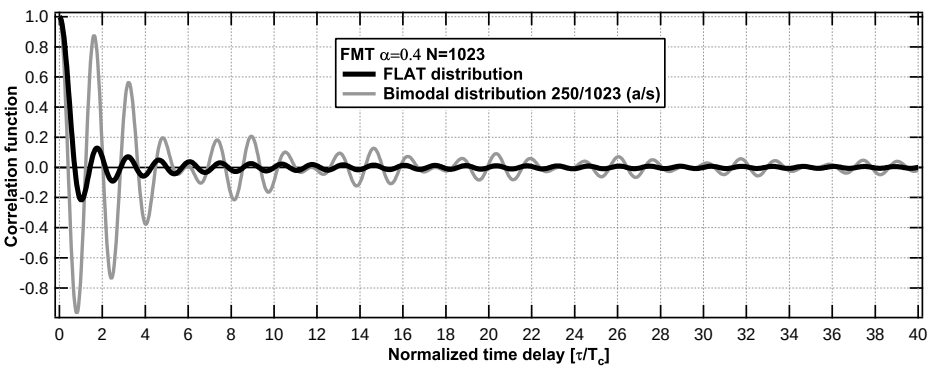

Figure 4.15: *Correlation function of the FMT schemes.*

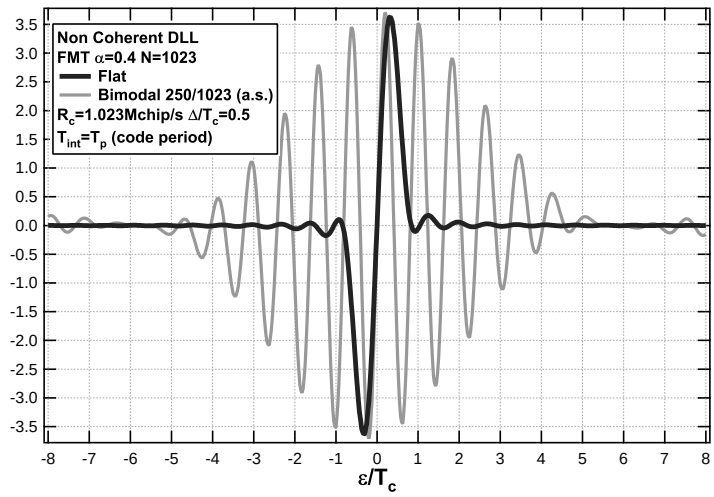

Figure 4.16: *S-curve function of the non coherent DDLL scheme. Simulation for Flat and Bimodal distribution on 250/1023 active subcarriers.*

The DDLL performance for the two FMT schemes are reported in Figures 4.16 and 4.17 in terms of average error characteristic (S-curve) and of RMSE, respectively. Following the characteristics of the correlation functions, the S-curve of the bimodal waveform has an high number of false-lock points and a narrower *operating range* than the flat one. Hence, it will need an high precision in the phase of acquisition with an higher complexity in the receiver to avoid the sidelobes. Figure 4.17 reports the RMSE and the jitter of the non coherent estimator, together with the relevant modified Cramér-Rao bound (MCRB) (4.9), as a reference. For medium-high C/N_0 values, the DDLL is unbiased and for both the schemes the RMSE lines match the theoretical bound, which in turn is inversely proportional to the Gabor bandwidth of the signal, higher for the bimodal distribution. Only in the (very) low C/N_0 region a squaring loss appears, due to the presence of nonlinear blocks in the circuit of estimation, but this can be further enhanced increasing the integration time to averaging the noise effect.

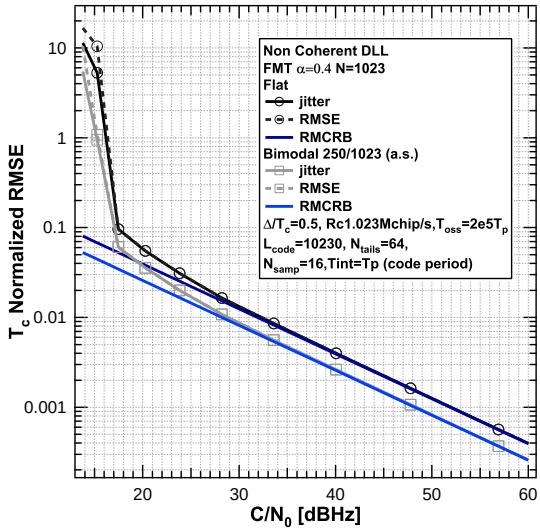

Figure 4.17: *RMSE for the proposed non coherent DDLL scheme. Simulation for Flat and Bimodal distribution on 250/1023 active subcarriers.*

FMT synthesis of Filtered QPSK and filtered BOC(1,1) spectra

As investigated in the Sect. 4.2.5, the MC signal represents an excellent example of spectral flexibility. Exploiting this characteristic, two examples of *spectral synthesis* are analyzed and tested. The limited bandwidth of the MC signal binds the selection of the signal to band limited waveforms, so the FMT structure is adopted to emulate filtered $QPSK(1)$ and filtered $BOC(1,1)$ spectra, but the method can be adopted for every pre-existing waveforms. The synthesis is performed by sampling the PSD of the "analog" signal on equally spaced subcarriers and using the values obtained to shape the power distribution within the FMT subcarriers. The higher is the number of the subcarriers, the better the "resolution" and the accuracy of the synthesis.

The synthesized spectra are depicted in the Fig.4.18. The signals result strictly filtered on a bandwidth of $BW = 6R_c^{(a)} = 6.138MHz$, with $R_c^{(a)} = 1.023Mchip/s$ the chip rate of the analog signals, showing very limited out-of-band (OOB) emission. The FMT synthesis chip rate depends on the bandwidth selected and it results $R_c^{(s)} = BW/(1+\alpha) = 4.384Mchip/s$ with $\alpha = 0.4$. In this analysis N=93 has been chosen. The integration time is chosen equal to a code period length and the equivalent noise

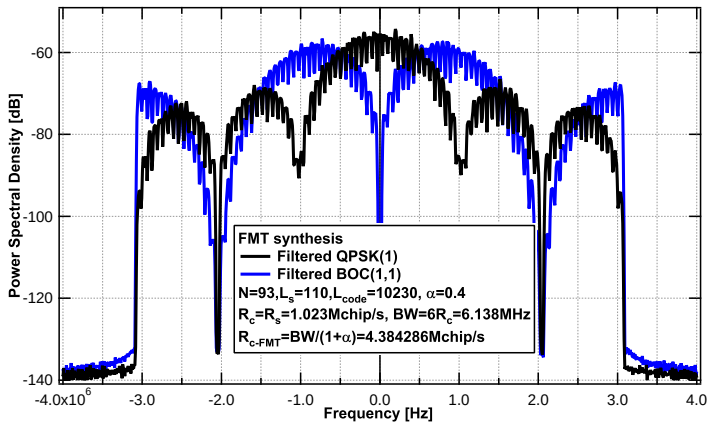

Figure 4.18: *Spectra of the FMT synthesis.*

bandwidth of the loop is assumed equal to 1 Hz. One Gold sequence with a length of 10230 chips is divided on 93 active subcarriers and on 110 symbol times. The delta correlator spacing is set equal to half chip and one sixth of chip, respectively for the QPSK and the BOC signal, normalized to the analog chip $T_c^{(a)}$. The performance of the two signals are depicted in Figures 4.19a-4.22, in terms of S-curve and RMSE, and every results are normalized to the analog chip rate $R_c^{(a)}$, which is the same for both the cases.

The S-curves reported match the standard shaping which could be obtained simulating the corresponding analog signals, except for the *residual* secondary false locks, due to the MC nature of the signal, around the multiple of the (MC) symbol time. As expected, the QPSK(1) S-curve has a larger operating range compared to the BOC one, considering also that a different delta spacing is adopted for the two waveforms, however the latter one shows an higher S-curve slope and consequently a lower error variance and faster tracking.

In the Fig.4.21 and Fig. 4.22 the RMSE and the jitter of the non coherent estimator are shown, together with the relevant modified Cramér-Rao bound (MCRB) (4.9), as a reference. In the case of QPSK(1), the upper root of CRB depending on the non-coherent DLL settings is also adopted [10] and it is obtained from the theoretical analog filtered spectral shaping, whereas the lower root of MCRB does not depend

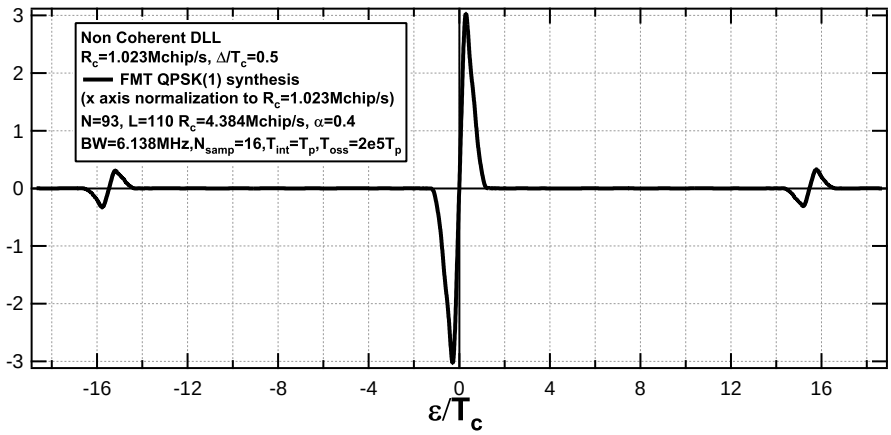

(a) S-curve function.

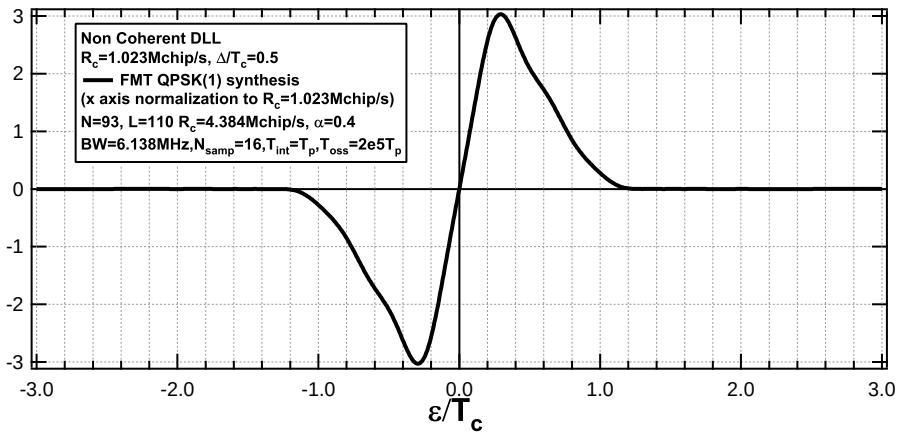

(b) Zoomed plot

Figure 4.19: *S-curve function for the proposed non coherent DDLL scheme. Simulation for the QPSK(1) SS-FMT synthesis.*

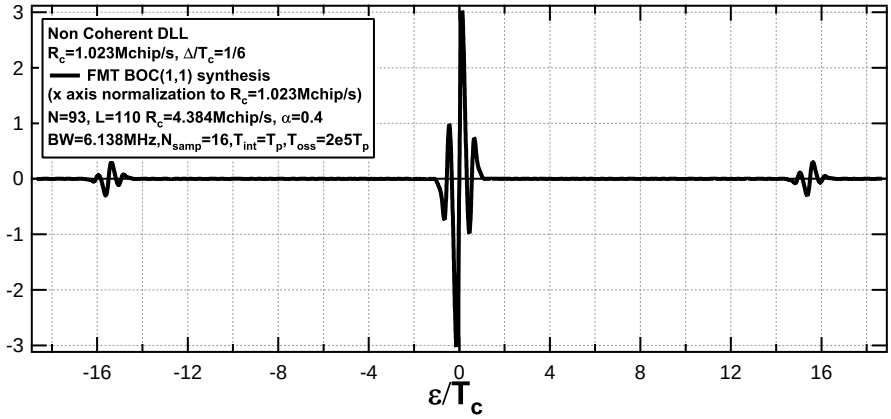

(a) S-curve function.

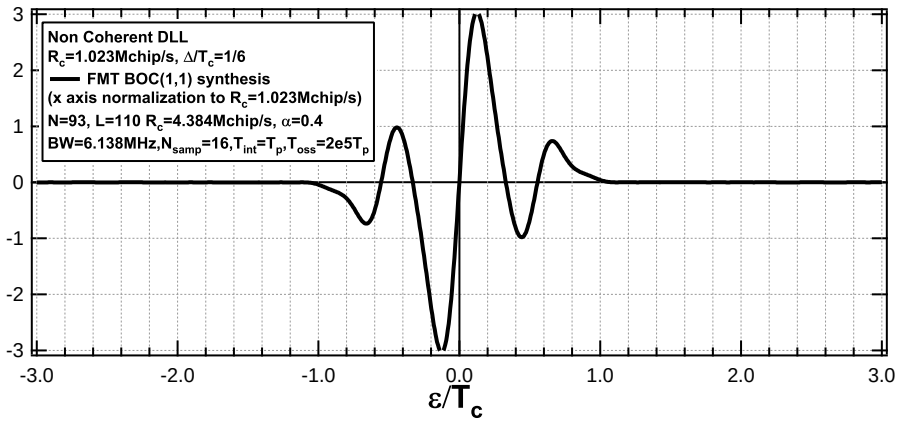

(b) Zoomed plot.

Figure 4.20: *S-curve function for the proposed non coherent DDLL scheme. Simulation for the BOC(1,1) SS-FMT synthesis.*

on the estimation algorithm but only on the signal and it is calculated with the (4.9). The estimation is unbiased for all the values of C/N_0, but a squaring loss is shown (theoretically and with simulation) at low C/N_0 values. The result in this sense can be improved, increasing the integration time here supposed equal to one code period. The RMSE curves perfectly match with the bound computed for the specific non coherent E-L DLL settings (red curve in top of the circles). The 4.2 dB distance from the ideal lower RMCRB for high C/N_0 are related to the selected delta space ($\Delta/T_c^{(a)} = 0.5$). In the comparison we can see that the FMT waveform obtain the same performance of the QPSK analog signal, proofing once again, that the TOA estimation performance depends only on the PSD itself, regardless of the modulation techniques and the signal processing adopted to implement it. In the case of BOC synthesis, the non coherent DLL performance matches the theoretical one (RMCRB) for high C/N_0 values for the value of the discriminator delta spacing adopted, whereas a squaring loss is anyway shown at low C/N_0, which can be improved increasing the integration time. Besides, as expected from the CRB theory, the BOC(1,1) waveform outperforms the QPSK(1) one in the AWGN channel, because even if they are designed to occupy the same bandwidth, the Gabor bandwidth in the first case is higher than the latter one.

As already discussed in the previous sections, the FMT schemes here reported can be supposed as part of a set of waveforms synthesized amidst which the transmitter and the receiver can choose the best one, according to the particular (interference, multipath) scenario. In fact, a flexible FMT system can be designed, maintaining all the systems parameters except for the power distribution, with a modulation technique adaptable to the changes of the channel, keeping the signal strictly bandlimited in the available bandwidth regardless of the frequency mask.

4.4.2 Performance in a two-ray Multipath channel

The performance analysis described so far is suitable for AWGN channels. However, multipath still remains the dominant factor in a GNSS error budget. The MP performance of a given signal/estimator combination is so analyzed by its MPEE plot [37], [38]. The MPEE plot reflects the performance of a two-ray multipath channel (line-of-sight + one reflected ray), by showing the bias induced by the non-line-of-sight path onto delay estimation. The bias is computed establishing a receiver configuration (TOA estimator, early-late spacing) as a function of the reflected path delay, and with

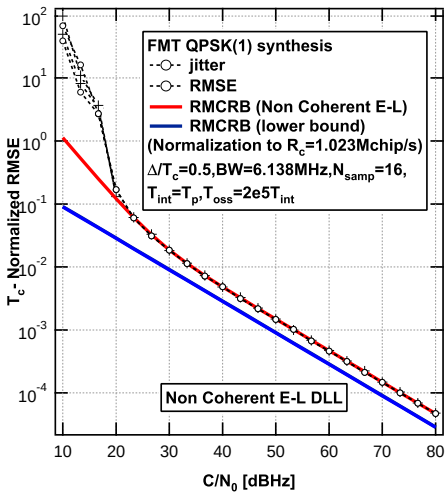

Figure 4.21: *RMSE for the proposed non coherent DDLL scheme. Simulation for the QPSK(1) FMT synthesis.*

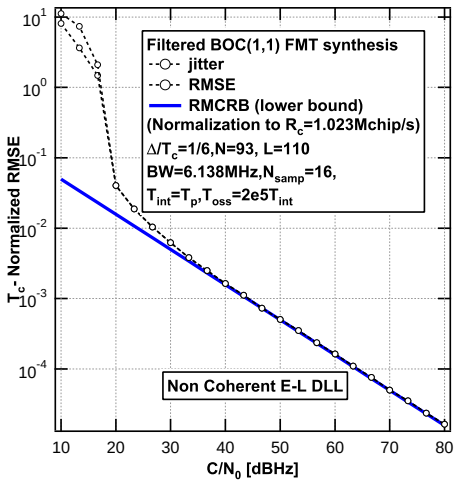

Figure 4.22: *RMSE for the proposed non coherent DDLL scheme. Simulation for the BOC(1,1) FMT synthesis.*

the MP (relative) amplitude kept constant.Figures 4.23 and 4.24 show the MPEE of the previous flat and bimodal schemes and SS-FMT synthesis. The curves are computed considering the non-coherent DDLL, with a different early-late spacing Δ for each waveform, following the previous section simulation parameters. The signal-to-multipath ratio (SMR) is equal to 3 dB, 6 dB and 10 dB, typical values for ranging systems. For each signal configurations, two lines are plotted, corresponding to the two worst cases of in-phase reflected signals, whilst the cases with intermediate phase shifts that lie in between are not considered. The figures report the bias error expressed in chip as a function of the delay of the specular ray expressed in chip as well.

For the flat and bimodal schemes, the MPEE curves show a different behavior. Even if smaller errors are shown in the first lobe of the MPEE when the Gabor bandwdth is higher, for the other values of the specular delay the flat distribution performance is better than the bimodal one. For the synthesized waveforms, an usual behavior reports the a BOC(1,1) bias error lower than the QPSK(1) one, for its higher Gabor bandwidth compared to the latter and also a narrower delta spacing adopted.

4.4.3 Summary of performance results

Different FMT waveforms are designed, spanning from a flat to a bimodal modulation scheme, synthesizing filtered standard GNSS SIS and showing potentialities of the multicarrier flexibility.

In the AWGN channel, the relative behavior of the proposed tracking scheme reveals independent of the selected signal. The DDLL behavior results irrespective of the MC parameters adopted and its performance is modeled on the theoretical limits. The estimator correlates the FMT signal replica without any frequency demodulation in baseband achieving the best theoretical performance.

The modulation schemes tested as example, like the bimodal one or the (synthesized) BOC(1,1) depicted, with an higher Gabor bandwidth compared to the flat waveform or the (synthesized) QPSK(1), respectively, reveal better performance in terms of tracking accuracy as expected.

In the MP channel, performance in terms of MPEE enhance, i.e. multipath resistance, enhances, with the increasing of the oscillating nature of the signal, obtained by shifting the power at the edges of the available bandwidth.

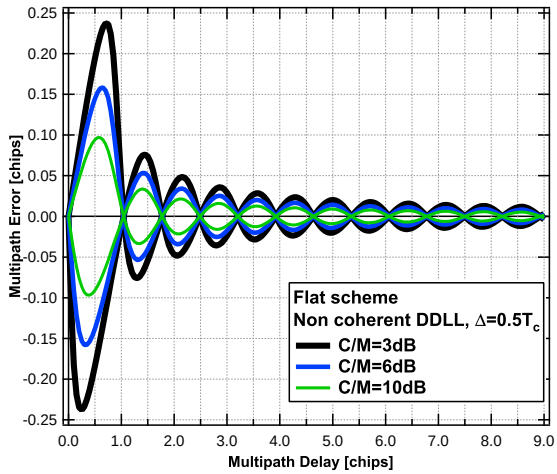

(a) Flat

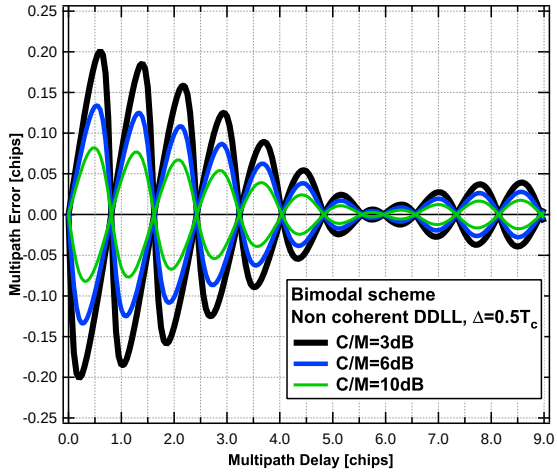

(b) Bimodal

Figure 4.23: *MPEE figures of flat and bimodal SS-FMT schemes.*

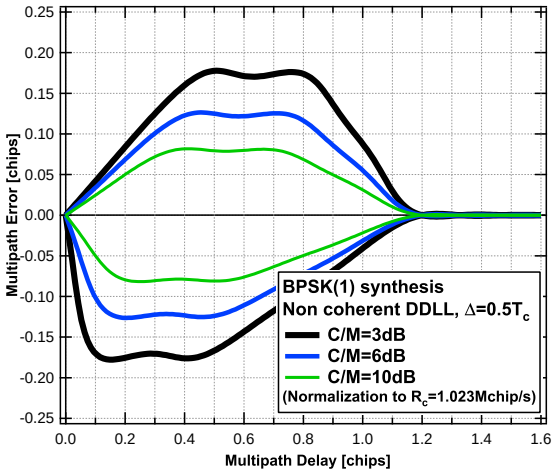

(a) QPSK(1)

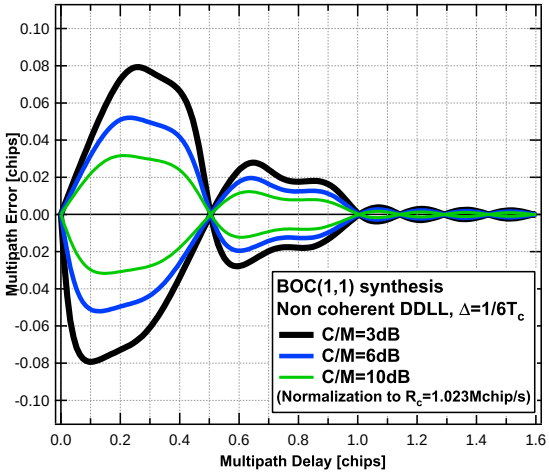

(b) BOC(1,1)

Figure 4.24: *MPEE figures of filtered QPSK(1) and filtered BOC(1,1) SS-FMT synthesis.*

Examining these results and also the spectral and correlation properties, maintaining the very low OOB emission, increasing the Gabor bandwidth allows for higher tracking performance and MP rejection, at the expense of an increase of autocorrelation sidelobes and receiver complexity to avoid the deleterious ambiguities.

In conclusion, after analyzing SS-FMT we have seen that they allow an excellent spectral flexibility, by simply adapting the design parameters to the scenario analyzed.

4.5 Conclusions

This chapter has shown main spread-spectrum multicarrier signal qualities and potentialities to be used as a possible ranging signal in future-generation positioning systems.

Let us outline the main conclusions from the sections above:

- The full waveform flexibility of a multicarrier signal represents the most important signal characteristic in a constrained design scenario. The signal can be adapted to the different system's requests, simply modifying some of the basic parameters of the signalling waveform.

- For the FMT case, the spectral efficiency is allowed by the use of strictly limited basic pulse, limiting the out-of-band emission and interference with pre-existing systems, shaping opportunely the power distribution within the subcarriers.

- Conventional multicarrier formats are geared towards spectrum-efficient data communications. In a GNSS system, the focus of SIS design is accurate time-delay estimation, that calls for a different spectral distribution of the signal power, namely, an high second-order moment. FMT signals meet the requirement above when shifting the power transmitted on the active subcarriers at the edges of the permitted bandwidth;

- A spectral signal synthesis can be easily performed, sampling the selected PSD and tuning with the same spectral shaping the power distribution coefficients.

- The DDLL algorithm mentioned in the chapter match to its TOA CRB in terms of AWGN RMSEE;

Increasing the second order moment of the spectrum, allow higher tracking performance and MP rejection, at the expense of an increase of autocorrelation sidelobes and receiver complexity. spread spectrum multicarrier (SS-MC) with ad-hoc settings of frequency pulse, of T_c and of power distribution could be suitable for forthcoming satellite positioning systems, thanks to their characteristics of spectral flexibility and negligible OOB emission, once requirements from system design are set. More work can and has to be done in terms of i) optimization of the FMT power spectral density in case of multipath, analyzing also the correspondent theoretical performance [20]; ii) mitigation of the MP impact, engaging an ad-hoc circuit based on the multicarrier nature of the signal, which jointly estimates the channel parameters and the signal time of arrival.

Chapter 5

Application of the MZZB to Standard and Innovative GNSS Signals

5.1 Introduction

"One-way signal Time-Of-Arrival (TOA)" estimation represents the basis of all current Global Navigation Satellite Systems (GNSSs). The accuracy of user position is directly related to the (pseudo-)ranges estimation performed by the receiver via TOA estimation. The mean square error (MSE) is often used to evaluate the performance of positioning algorithms and to compare different estimators. Their optimality can be also compared with theoretical lower bounds.

Commonly the well known Cramér-Rao bound (CRB) represents the first choice amidst all of the analytical tools to calculate the minimum MSE in parameter estimation for its ease of calculation. Unfortunately, it produces significant values only for high signal-to-noise ratio (SNR), since it does not usually consider (at least in its simplest and most popular version) any *a priori* information on the parameter to be estimated. Various theoretical bounds such as the *Bayesian* (Gaussian) CRB, (*Bayesian*) Bhattacharyya and Barankin bounds have been developed in literature [56], and can accomodate *a priori* information, but their analytical evaluation reveals very complicated. Moreover, the main requirements for application of CRB are a sufficiently smooth signal waveform [60] and possibly a differentiable parameter probability density function (pdf). In some cases of practical interest, both these

conditions are not satisfied - this is the reason of the abovementioned inaccuracy of the CRB in many practical cases, and especially as far at the standard GNSS Signal-In-Space are concerned. GPS, GLONASS, Galileo, and other GNSSs adopt Binary Phase Shift Keying (BPSK) and Binary Offset Carriers (BOC) modulations [9] with (theoretically) rectangular pulses, so that the CRB is not applicable.
Other bounds can be found in literature, which prove to be tighter than the CRB, but cannot in general be easily cast into a simple closed form expression. One of these is the Ziv-Zakai bound (ZZB) [11], [60] that stems out of detection theory and also considers possible parameter *a priori* information. The ZZB can be used without any constraints (signal shape, pdf of the parameter) and for any value of the SNR. For these reasons, it represents a very interesting MSE benchmark for any signal format. Regrettably, the received signal very often contains additional unknown and random parameters other than the time delay (e.g., carrier amplitude and phase, values of the ranging code chips, channel multipath etc.), defined in the previous sections *nuisance parameters*. Computing the ZZB in the presence of nuisance parameters is very hard. The aim of this section is to analyze the *modified* version of the bound, i.e. the *modified* ZZB (MZZB) [18–20], defined in the Sections 2.4 and 2.5.3, whose computation in the presence of nuisance parameters is much simpler. We use the MZZB here to evaluate the performance of TOA estimation during signal acquisition and tracking for standard GNSS SIS (BPSK, BOC) and for *innovative GNSS waveforms* designed with Multicarrier modulation. In particular, assuming the proper *a priori* information, we can evaluate for the different applications the minimum C/N_0 threshold that is needed to acquire or track the signal delay with an MSE lower than a fixed value. Numerical results are shown for the main GNSS standard signal formats: BPSK and (filtered) Binary Offset Carriers (BOC) modulations in Additive White Gaussian Noise (AWGN) channel. Finally, performance of Multicarrier signal is also analyzed, with different signaling waveform characteristics. Through the computation of the MZZB we can also clearly evaluate the impact of the shape of the signal autocorrelation function on the estimation performance.

5.2 Application of MZZB to standard SIS

For the sake of clarity let's recall here the final expressions of ZZB and MZZB for TOA estimation found in presence of the nuisance parameters $\mathbf{u}$, already defined and

theoretically deeply discussed in the Chapter 2. The *true* and *modified* ZZB result

$$ZZB\left(\tau\right)=\frac{1}{T_x}\int_0^{T_x}\Delta G\left[\left(T_x-\Delta\right)E_{\mathbf{u}}\left\{Q\left(\sqrt{\frac{d^2\left(\Delta|\mathbf{u}\right)}{2N_0}}\right)\right\}\right]d\Delta \tag{5.1}$$

and

$$MZZB(\tau)\triangleq\frac{1}{T_x}\int_0^{T_x}\Delta G\left[\left(T_x-\Delta\right)Q\left(\sqrt{\frac{E_{\mathbf{u}}\{d^2(\Delta|\mathbf{u})\}}{2N_0}}\right)\right]d\Delta \tag{5.2}$$

where $[0,T_x]$ is the uncertainty range of the delay, assumed with a uniform probability density function (pdf), chosen according to the TOA estimation stage. Assuming a realistic time of observation (T_{obs}), we can adopt the approximation in (2.49), so the ($\mathbf{u}$-conditioned) squared distance between the signal replicas, delayed by two trial delays which differ each other of a Δ value, becomes

$$d^2\left(\Delta|\mathbf{u}\right)=\frac{\int_0^{T_{obs}}\left|x\left(t|\mathbf{u}\right)-x\left(t-\Delta|\mathbf{u}\right)\right|^2dt}{2}=2E_{T_{obs}}(1-\rho_{T_{obs}}\left(\Delta|\mathbf{u}\right)) \tag{5.3}$$

with the (conditional) signal correlation function $\rho_{T_{obs}}\left(\Delta|\mathbf{u}\right)$ defined in (2.50) normalized to the signal energy $E_{T_{obs}}=P_xT_{obs}$, with P_x the transmitted signal power (which is usually also called C).

Let us consider now the performance of TOA estimation for BPSK and BOC signals in an Additive White Gaussian Noise (AWGN) channel. Hereafter we compute only the MZZB, due to the heavy computational cost of ZZB. We can show that the gap between the original and the modified versions of the ZZB is negligible whenever the size of the $\mathbf{u}$ vector gets large [19, 20].

The $BOC(f_s,f_c)$ modulations consist of superposing a square wave subcarrier of frequency $f_s{=}mf_g$ to the spreading code of a standard Spread-Spectrum BPSK (SS-BPSK) of rate $f_c{=}nf_g{=}1/T_c$, where m and n are two integers and $f_g{=}1.023MHz$. The chip time T_c is sliced in Ω half-cycle times $\frac{T_s}{2}$ of the square wave ($T_s{=}1/f_s$) and $\Omega{=}2\frac{f_s}{f_c}{=}2\frac{m}{n}$ is the modulation order.

The superposition (product) with the square wave leads to splitting and shifting the baseband SS-BPSK spectrum - for this reason BOC are also known as split-spectrum modulations. This allows for better performance in terms of tracking accuracy than the original BPSK owing to Gabor bandwidth enhancement, but at the cost of a worsening the correlation function. BOC waveforms are characterized by an autocorrelation function containing multiple peaks that lead to potential acquisition

and tracking ambiguities. To mitigate this problem, a number of techniques have been suggested in the literature, at the cost of an increased receiver complexity. One of the scopes of this section is to emphasize the capability of the MZZB bound to take into account these deleterious ambiguities [23, 24, 58, 59].

The $BOC(f_s, f_c)$ signal can be written as

$$x_{BOC}(t) = x_{BPSK}(t)\, sign\left[\sin(2\pi f_s t)\right] \tag{5.4}$$

with

$$x_{BPSK}(t) = \sqrt{2P_x}\sum_k c_k rect\left(\frac{t - kT_c - T_c/2}{T_c}\right) \tag{5.5}$$

where P_x is the signal power, c_k are the independent and identically distributed (i.i.d.) chips belonging to $\{\pm 1\}$. Signal (5.4) can be easily seen as a linear modulation

$$x_{BOC}(t) = \sqrt{2P_x}\sum_k c_k (-1)^{k\Omega} q\left(t - k\frac{\Omega T_s}{2}\right) \tag{5.6}$$

with the basic pulse

$$q(t) = \sum_{m=0}^{\Omega-1} (-1)^m \mu(t - mT_s/2) \tag{5.7}$$

composed of the sum of Ω rectangular pulses

$$\mu(t) = rect\left(\frac{t - T_s/4}{T_s/2}\right) \tag{5.8}$$

with amplitudes regulated by the factor $(-1)^{k\Omega}$. The distance needed in (5.1) and (5.2) can be computed starting from (5.6)-(5.8), evaluating the conditional squared distance (5.3), and carrying out the expectation on nuisance parameters $\mathbf{u}$ that in our case are the i.i.d. code chips $\mathbf{u} = \mathbf{c}$. The result after the expectation becomes

$$E_{\mathbf{c}}\{\rho_{BOC}(\Delta|\mathbf{c})\} = \tag{5.9}$$
$$R_{BOC}(\Delta) = \sum_{k=0}^{\Omega-1}\left(\frac{\Omega - k}{\Omega}\right)(-1)^k\left\{\Psi\left(\frac{2\Delta}{T_s} - k\right) + \Psi\left(\frac{2\Delta}{T_s} + k\right)\right\} - \Psi\left(\frac{2\Delta}{T_s}\right)$$

where

$$\Psi\left(\frac{2t}{T_s}\right) = \left(1 - \frac{2|t|}{T_s}\right) rect\left(\frac{t}{T_s}\right) \tag{5.10}$$

is the triangular function.

The final expression of the bound reported for clarity here, becomes

$$MZZB(\tau) = \frac{1}{T_x}\int_0^{T_x} \Delta\,(T_x - \Delta) Q\left(\sqrt{\frac{LE_c}{N_0}\,(1 - R_{BOC}(\Delta))}\right) d\Delta \tag{5.11}$$
$$= \frac{1}{T_x}\int_0^{T_x} \Delta\,(T_x - \Delta) Q\left(\sqrt{\frac{CT_{obs}}{N_0}\,(1 - R_{BOC}(\Delta))}\right) d\Delta$$

where the $E_c = C \cdot T_c$ is the signal energy per chip, L is the number of observed chips and C is the power of the received signal. Figure 5.1 shows the normalized autocorrelation functions of the theoretical BOC signals and of BPSK, with different chip rates, so that the 99% power bandwidth $B_{99\%}$ is the same for all signals. The BOC autocorrelation function runs out in a single chip time, with a number of secondary lobes, $\Omega - 1$ for each side, that have non negligible relative peaks compared to the main lobe at $\tau = 0$. If we assume an uncertainty on the delay greater or equal than a chip time, the estimation will be certainly impaired by the ambiguities caused by these secondary peaks. Fig.5.2 depicts the MZZB for these signals in terms of RMSE. The uncertainty on the delay for the MZZB computation is fixed to one chip time ($T_x = T_c$), different for each signal, so the integration in (5.11) on Δ consider the contributions of all of the correlation side lobes.

For (very) low C/N_0 (SNR), the rms error of any estimator tends to $T_c/\sqrt{12}$ i.e. the standard deviation of a uniform random variable τ in $[0, T_c]$. In this region, the optimum estimator actually uses the *a priori* information on τ, estimating the variable with its mean value, and neglecting received noise-corrupted data. For a larger C/N_0, the MZZB curves decrease proportionally to $(C/N_0)^{-2}$ and approach to each other regardless of the signal, due to the assumption on the same bandwidth and consequently a similar spectrum shaping. The boundary of the two regions is a threshold, and the higher the BOC modulation order, the higher the number of ambiguities in the correlation function and the higher the C/N_0 threshold to attain the "high-SNR" zone. The slope of -20dB/decade sounds strange if compared to the standard MCRB slope of -10dB/decade (for generic bandlimited signals) [17], due to the assumption of an infinite-bandwidth rectangular pulse in this theoretical example. In this case, as previously reported, the CRB can not be computed

In a more realistic scenario, *filtered* signals have to be considered. Maintaining the previous hypotheses on binary random chips, the only difference in the resulting

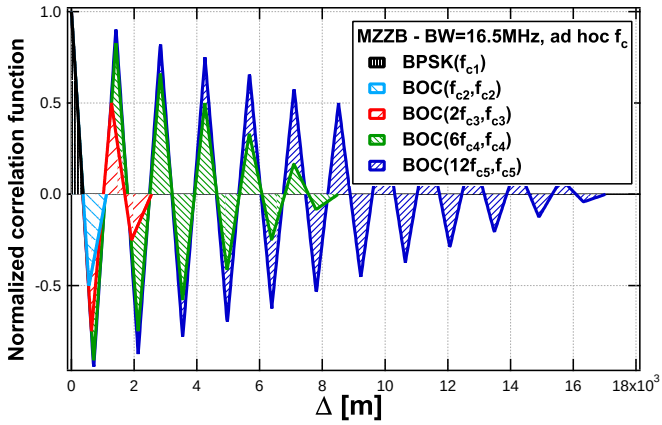

Figure 5.1: *Theoretical BOC correlation functions with fixed bandwidth and ad hoc chip rates.*

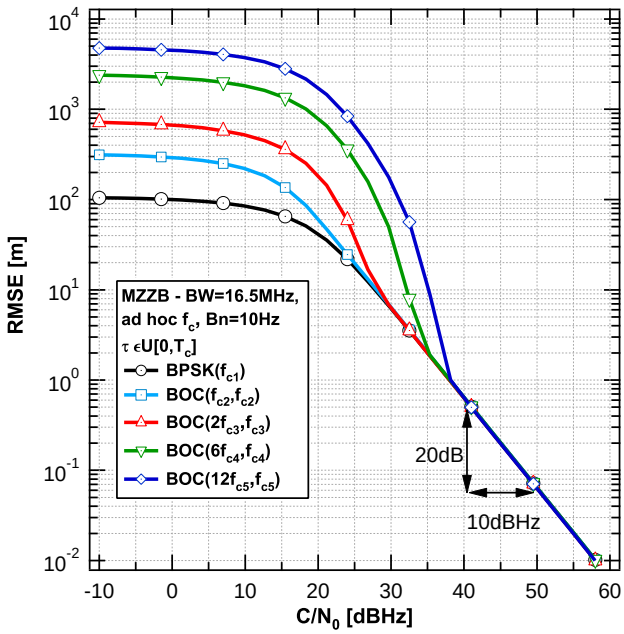

Figure 5.2: *Multi-peaks effect - theoretical BOC modulations.*

expression of the MZZB is the correlation function to be used in (5.11) which becomes

$$R^F_{BOC}(\Delta) = R_{BOC}(\Delta) \otimes h(\Delta) \otimes h(-\Delta) \tag{5.12}$$

where $h(t)$ is the impulse response of the filter, that we assume low-pass with a $-3dB$ bandwidth BW. In fig.5.3 we show the RMSE curves for the filtered BOC signals with $BW = B_{99\%}$. In this case the MCRB can be also computed as a reference, adopting the frequency domain version [2, 27] for filtered signals introduced in the Sect. 2.5.3. For low and medium C/N_0 values, as expected, the performance is similar to the ones previous seen (inside the bandwidth the spectra remain practically the same). In these C/N_0 regions the mismatch between the MZZB and the MCRB curves is due to the absence of a priori information for the latter. For high C/N_0, the MZZB curves decrease proportionally to $(C/N_0)^{-1}$ perfectly matching with MCRB, and also show a little improvement for larger values of Ω caused by the increase of the Gabor bandwidth.

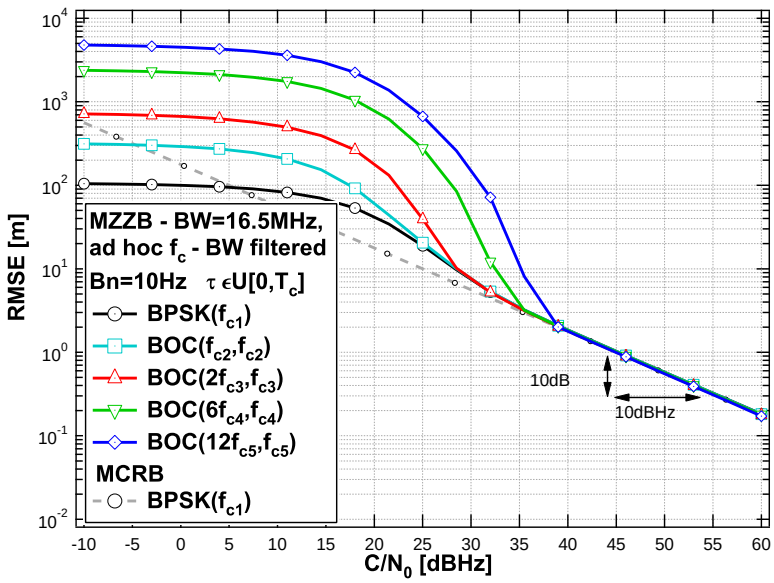

Figure 5.3: *Multi-peaks effect - filtered BOC modulations.*

5.3 Application of (M)ZZB to Multicarrier signals

In the time of writing Multicarrier (MC) modulations have attracted strong interests both for communication purposes and navigation and positioning ones. After the full analysis in the Chapter 4, the aim of this section is first to briefly test the matching between the ZZB and the MZZB considering very easy MC cases of study, hence to compute the theoretical performance for possible GNSS significant schemes. Recalling the definition of a multicarrier signal in Chapter 4, its equivalent base-band is

$$x_{SS-MC}(t) = \sqrt{2P_x} \sum_{k \in D_f} \sqrt{w_k} x_k(t) e^{j2\pi k f_k t} = \tag{5.13}$$

$$\sqrt{2P_x} \sum_{k \in D_f} \sqrt{w_k} \left[\sum_{n=-\infty}^{+\infty} \gamma_n^{(k)} g(t - nT_s) \right] e^{j2\pi(kf_{sc}+\Delta_f)t}$$

where the coefficient w_k identifies the fraction of total power transmitted on the k-th subcarrier centered in f_k with $\sum_{k \in D} w_k = 1$, D_f is the set of active subcarrier centers, $\gamma_n^{(k)}$ is the symbol/chip (or chip-data product $\gamma_n^{(k)} = d_n^{(k)} c_n^{(k)}$) on the k-th subcarrier, $P_x = C$ is the real total power, f_{sc} is the subcarrier frequency spacing, Δ_f is a frequency offset, T_s is the multicarrier symbol time, $T_s = NT_c$, with N the number of equally spaced subcarriers and T_c the chip time. In this section we show the computation of the the (M)ZZB for TOA estimation error for two MC waveforms, the Orthogonal Frequency Division Multiplexing (OFDM) and the Filtered Multitone (FMT) signals, respectively, in Additive White Gaussian Noise (AWGN) channel, but results found can be easily extended to any multicarrier signal.

For OFDM waveform the subcarrier spacing is $f_{sc} = 1/T_s$ and $g(t)$ is a rectangular pulse of duration T_s and unit amplitude, while for FMT $f_{sc} = \frac{1+\alpha}{T_s}$ using a Squared Root Raised Cosine (SRRC) pulse with the roll-off factor $\alpha = 0.2$. In that case, the Continuous Fourier Transform (CFT) of $g(t)$ is defined as $G(f) = T_s \sqrt{\frac{G_N(f)}{T_s}}$ with the Raised Cosine pulse $G_N(f) = CFT\{g_N(t)\}$ with $G_N(0) = T_s$ and a bandwidth equal to $\frac{1+\alpha}{T_s}$.

As we have seen with the (single carrier) BOC modulations analyzed in the previous Sect. 5.2, the ZZB and MZZB for the MC signals can be obtained from (5.1) and (5.2) once selected the uncertainty T_x and computed the (conditional) squared distance in (5.3). For the sake of simplicity, the a priori information on the parameter was selected equal to the symbol time T_s or the chip time $T_c = T_s/N$, assuming τ uniformly

distributed in $[0, T_s]$ or $[0, T_c]$, respectively, and identifying $\mathbf{u}$ with $\mathbf{c}$, which represents the vector of nuisance code chips.

The last step, after the squared distance is calculated, is the expectation on the vector $\mathbf{u}=\mathbf{c}$ made of independent and identically distributed (i.i.d.) chips belonging to $\{\pm 1\}$. The observed chips are assumed $N_c = (L+1)\cdot N$ for OFDM and $N_c = L\cdot N$ for FMT in the observation time $T_{obs} = L\cdot N\cdot T_c$.

The ZZB expression for OFDM and FMT are reported in the following (5.14) where the squared distances are respectively (5.15) and (5.16), assuming the observation time $T_{obs}{=}LT_s$ and the frequency offset $\Delta_f = 0$.

$$ZZB\left(\tau\right) = \frac{1}{T_x}\int_0^{T_x}\Delta G\left\{\left(T_x-\Delta\right)\frac{1}{2^{N_c}}\sum_{\nu=0}^{2^{N_c}-1}Q\left(\sqrt{\frac{d^2\left(\Delta\right)|\mathbf{c}^{\nu}}{2N_0}}\right)\right\}d\Delta \tag{5.14}$$

$$\frac{d^2_{OFDM}(\Delta)|\mathbf{c}^{\nu}}{2N_0} = \frac{LE_s}{N_0} - \frac{E_s}{NN_0}\sum_{n=0}^{L-1}\sum_{k,p\in D_f}\sqrt{w_k w_p}c_n^{(k)\nu}c_{n-1}^{(p)\nu}\frac{\Delta}{T_s}sinc\left(\frac{\Delta}{T_s}(k-p)\right)\cos\left(\pi\left(\frac{\Delta}{T_s}\right)(k+p)\right) \tag{5.15}$$

$$-\frac{E_s}{NN_0}\sum_{n=0}^{L-1}\sum_{k,p\in D_f}\sqrt{w_k w_p}c_n^{(k)\nu}c_n^{(p)\nu}\left(1-\frac{\Delta}{T_s}\right)sinc\left(\left(1-\frac{\Delta}{T_s}\right)(k-p)\right)\cos\left(\pi\left(1+\frac{\Delta}{T_s}\right)(k+p)\right)$$

$$\frac{d^2_{FMT}\left(\Delta\right)|\mathbf{c}^{\nu}}{2N_0} = \frac{LE_s}{N_0} - \frac{E_s}{NN_0}\sum_{n=0}^{L-1}\sum_{m=0}^{L-1}\sum_{k\in D_f}\sqrt{w_k}c_n^{(k)\nu}c_m^{(k)\nu}g_N\left(\frac{\Delta}{T_s}-(n-m)\right)\cos\left(2\pi k(1+\alpha)\frac{\Delta}{T_s}\right) \tag{5.16}$$

The MZZB expression for MC waveforms (5.13), after the expectation on the nuisance chips becomes

$$MZZB\left(\tau\right) = \frac{1}{T_x}\int_0^{T_x}\Delta G\left\{\left(T_x-\Delta\right)Q\left(\sqrt{\frac{LE_s}{N_0}\left(1-R_{MC}\left(\frac{\Delta}{T_s}\right)\right)}\right)\right\}d\Delta \tag{5.17}$$

where

$$R_{MC}\left(\frac{\tau}{T_s}\right) = \rho\left(\frac{\tau}{T_s}\right)\sum_{k\in D_f}w_k\cos\left(2\pi(kf_{sc}+\Delta_f)\tau\right) \tag{5.18}$$

is the real part of the normalized (theoretical) correlation function of the signal, f_{sc} is the subcarriers spacing, Δ_f is the frequency offset, with the (specific) normalized correlation pulses

$$\rho\left(\Delta/T_s\right) = \begin{cases} \left(1-|\Delta/T_s|\right), & \text{for } OFDM, \\ g_N\left(\Delta/T_s\right), & \text{for } FMT. \end{cases}$$

For OFDM, on every subcarrier, L+1 symbols fall under T_{obs} observation time. ZZB for FMT results approximated for low L (it can be considered exact only for high L). In this case, L represents both the number of intervals of symbol observed and the number of symbols for every subcarrier considered within T_{obs}. The approximation is due to the infinite FMT pulse duration, which makes the computation of the exact ZZB for low L difficult. As expected, the ZZB computation in (5.14) is feasible only for very low ("toy") values of N and L, since the expectation on all possible realizations of $\mathbf{c}$ ($2^{(L+1)\cdot N}$ for OFDM and $2^{L\cdot N}$ for FMT) is outside the $Q\left(\sqrt{\cdot}\right)$ function. The situation is different for the modified bound (5.17), in which the expectation is carried out inside the argument of $Q\left(\sqrt{\cdot}\right)$, so that the expression can be simplified using the known momenta of i.i.d. binary code chips in $\mathbf{c}$.

5.3.1 True and modified ZZB convergence

Exploiting the expressions reported in the previous section, lets assume, for a comparison of the true and modified versions of the bound, a flat power distribution within the N subcarriers ($w_k = 1/N$) and an asymmetric distribution of the subcarrier centers, with $D = \{0, 1, ...N-1\}$ and $\Delta_f = 0$. According to these settings, the correlation function in (5.18) becomes,

$$R_{MC}\left(\frac{\Delta}{T_s}\right) = \frac{\rho\left(\frac{\Delta}{T_s}\right)\cos(\pi\left(N-1\right)\Delta f_{sc})\sin(\pi N\Delta f_{sc})}{N\cdot\sin(\pi\Delta f_{sc})} \tag{5.19}$$

to substitute in the MZZB expression.

The set of curves in Fig. 5.4a-5.4b depicts a comparison between the ZZB and MZZB for some OFDM and FMT examples. To ensure low complexity of our computations, only small values of L and N were used, but the results could be extended for larger values. In Fig. 5.4a the OFDM signal has ($N = 3$) subcarriers and a common chip time T_c, whilst the observation time L is variable. Figure 5.4b shows the bounds for

FMT assuming that the number of observed chip $L \cdot N$, the chip time (and therefore the signal bandwidth) are constant.

Increasing L, i.e. the observation time for a fixed number of subcarriers N involves a rigid down shift of the curves in Fig.5.4a, as could be easily seen from (5.14)-(5.17) and [19].

For (very) low C/N_0 (SNR), the rms error of any estimator tends to $T_s/\sqrt{12}$ ($T_c/\sqrt{12}$), i.e. the standard deviation of a uniform random variable τ in $[0, T_s]$ ($[0, T_c]$). In this region, the estimator actually uses the *a priori* information on τ, estimating the variable with its mean value, and neglecting received noise-corrupted data. For a larger C/N_0, both the ZZB and the MZZB decrease proportionally to $(C/N_0)^{-1}$ and approach to each other regardless of the particular *a priori* information. The two regions are clearly divided by a sort of threshold, which depends on the signal settings (number of subcarriers N and power distribution) and the estimation time (T_{obs}).

As already mentioned, the ZZB, shown in marked curves, was computed, averaging on all the possible ranging chips sequences, only for low N and L values due to its heavy computational cost. Despite this, the differences between the two bounds is almost imperceptible (except for some cases with OFDM). The gap between the curves is due to low-probabity "bad" sequences of ranging chips, (e.g., c_n^k constant $\forall$ n and k) whose specific contribution are observable only in the ZZB whereas they are averaged in the MZZB.

For high values of the **u**-vector size (N_c), the MZZB is not only easier to compute, but it is a very good approximation of the true ZZB whenever the ranging codes in the ZZB look "random". When the N_c is in fact large, the chip sequences c^ν become statistically "typical" with high probability - the "atypical" sequences like all -1s or all 1s become very low probability, and the internal and external expectations of the function $Q\left(\sqrt{\cdot}\right)$ tend quickly to be the same. The case of study here reported can be obviously seen as a generalization of the single carrier case, in which $N = 1$ and the (M)ZZB matching enhances with increasing the number of random chips (nuisance parameters) L.

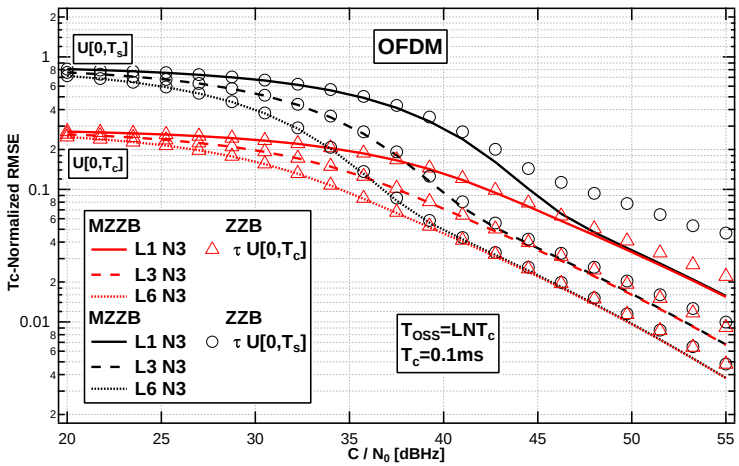

(a) OFDM - Fixed N and T_c

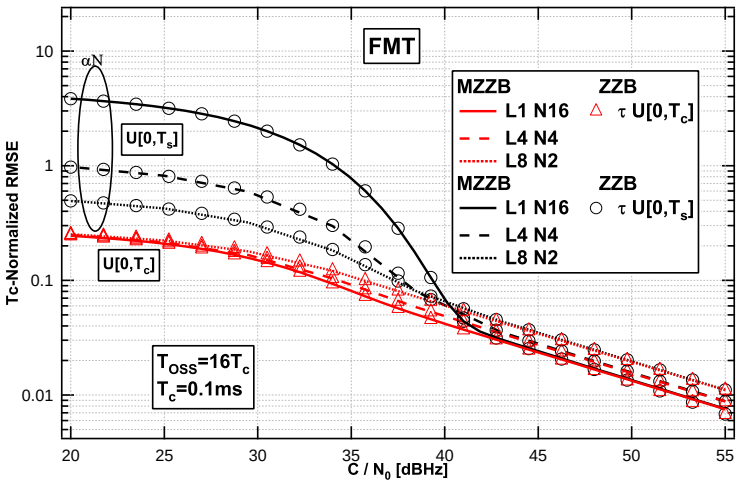

(b) FMT - Fixed T_{obs} and T_c

Figure 5.4: *(M)ZZB of MC in AWGN channel.*

5.3.2 MZZB for innovative GNSS waveforms

Once the (M)ZZB matching is proven, we can assume the equivalence between the bounds for a high number of nuisance parameters (chips) and we can compute here-

after only the modified bound. As seen in the Chapter 4, the multicarrier modulation allows a high degree of design thanks to the large set of constituent parameters. The full MC spectral flexibility and, in specific case of the FMT, also the strict limited bandwidth give to this waveform the chance to be welcomed in a GNSS scenario, solving a number of problems related to systems interference, compatibility and reconfigurability. In this section we analyze two (general) FMT profiles which could be significant for satellite navigation purposes. The schemes can be properly modified to match the particular systems requirements. The results depicted for these particular schemes can be generalized to any waveforms, generate by both single and multicarrier modulations. Fig.5.5 shows the PSD of the two FMT signals which occupy one single bandwidth and two separated bandwidths, labeled as *low-pass (LP)* and *Band-pass (BP)* scheme, respectively. The power distributions within the active subcarriers were selected to obtain different performance and analyze two different general cases, whereas the other parameters are the same for both the waveforms. The

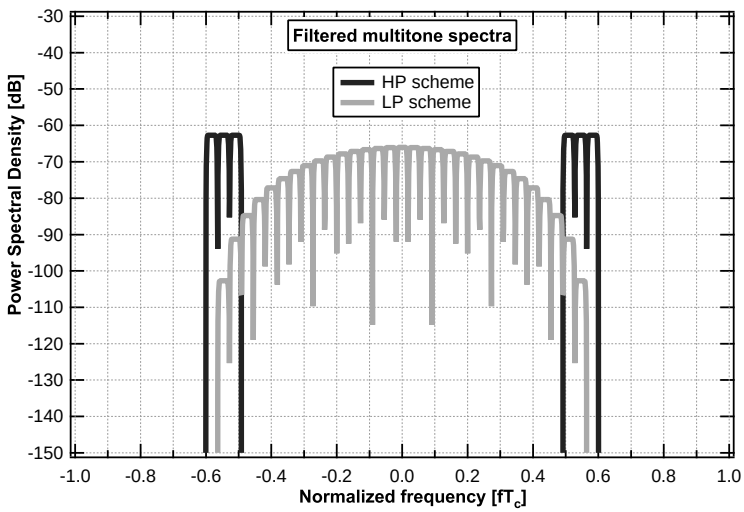

Figure 5.5: *Low-Pass/Band-Pass FMT schemes Power Spectral Density*

signal autocorrelation function of the two waveforms is depicted in Fig.5.6 with black solid lines, together with the SRRC correlation pulse (in red) and the array function in the background (in grey). Fig.5.6a shows the correlation of the LP signal. It has only

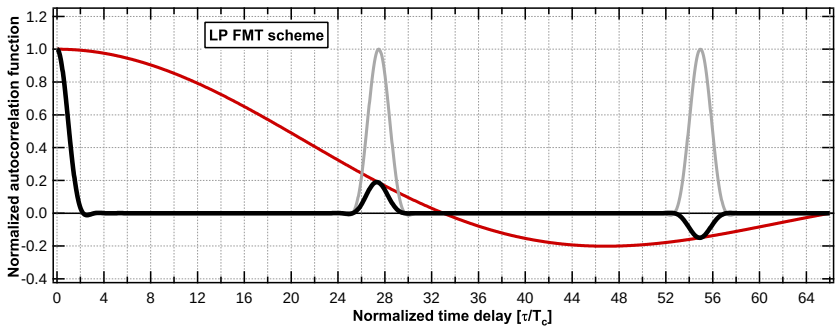

(a) Low-Pass FMT scheme

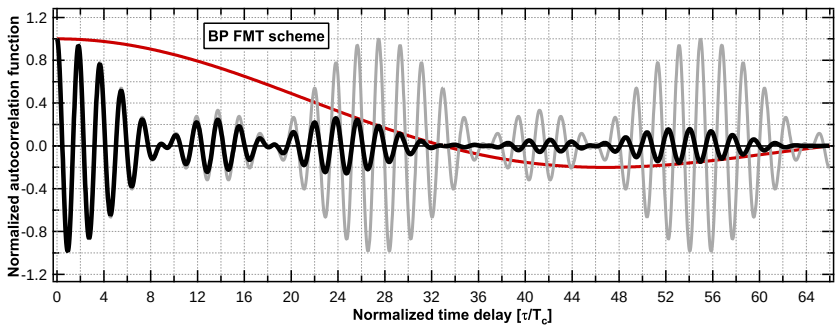

(b) High-Pass FMT scheme

Figure 5.6: *Low-Pass/Band-Pass FMT schemes Autocorrelation function*

one main lobe in the near delay region, and other (attenuated) replicas in multiple of the symbol time ($kT_s/(1+\alpha)$). In the other case the BP correlation appears very oscillating in Fig.5.6b with a number of side lobes, which are also periodic around the multiple of the symbol time. The oscillating nature of the correlation function, from one hand can be considered deleterious for the induced ambiguities in the detection of the mainlobe position for the acquisition of the signal. On the other hand, the TOA estimation accuracy depends on the second-order moment of the spectrum (Gabor bandwidth, GB), and in particular the higher the Gabor bandwidth and the lower the error, but the higher the sidelobes. The LP scheme occupies an effective bandwidth larger than the BP one, with good correlation properties, but conversely it reveals lower performance in terms of GB. As reported in the Sect. 2.5.3 the MSE dependence on the GB is evident for high T_x and SNR values in the MZZB approximation (2.53-2.54), where the CRB and the ZZB converge each other and proportionally decrease with the product between the SNR and the (squared) Gabor bandwidth, β_x^2, defined as

$$\beta_x^2 \triangleq \frac{\int_{-\infty}^{\infty} f^2 S_x(f)\, df}{\int_{-\infty}^{\infty} S_x(f)\, df}, \tag{5.20}$$

where $S_x(f)$ is the PSD of the complex signal.

Theoretical performance for low-pass and band-pass FMT schemes are depicted in the Fig.5.7-5.8. In the group of charts in Fig.5.7, the RMSE limit is calculated through the MZZB with respect to $E_{T_{obs}}/N_0$, where $E_{T_{obs}}$ is the signal energy in the time of observation. Additionally, in Fig.5.8 the charts depict the performance of the LP and BP signals, with respect to the uncertainty interval T_x. In both the groups of charts, the RMSE values are normalized to the respective signal Gabor bandwidth.

Analyzing the charts in Fig.5.7 we can observe a similar behavior described in the Sect. 5.2 and in the previous section for the BOC modulation. In both the cases of study analyzed (LP/BP waveforms) and for (very) low SNR, i.e. in the *a priori* information region, the (normalized) RMSE is proportional to the delay uncertainty T_x and tends to $T_x/\sqrt{12}$, i.e. the standard deviation of a uniform random variable distributed on $[0, T_x]$. In the region of high SNRs, the received data are fully informative and so the curves of RMSE converge to a unique line, which coincides with the CRB, inversely proportional to the signal Gabor bandwidth β_x and the SNR value. The

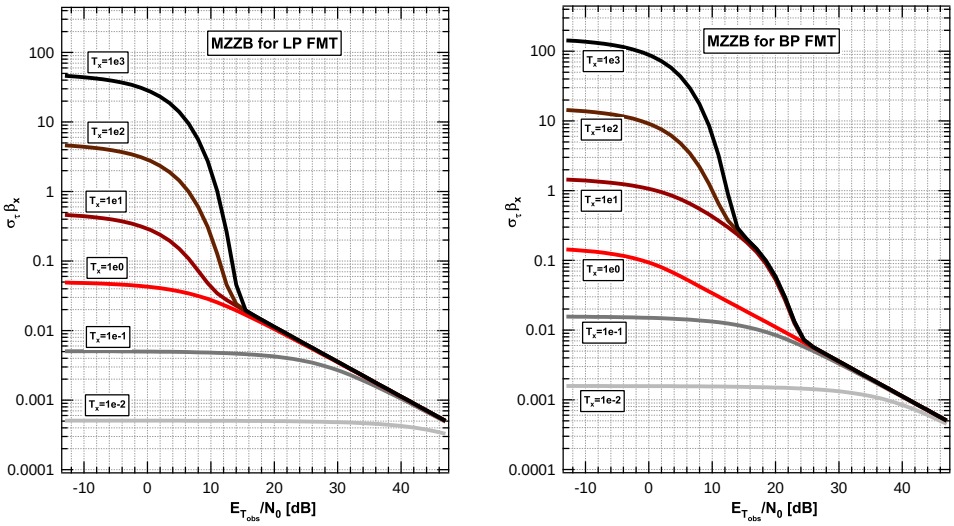

(a) Low-Pass FMT scheme **(b)** Band-Pass FMT scheme

Figure 5.7: *β_x-normalized RMSE vs $E_{T_{obs}}/N_0$*

MZZB takes into account the ambiguities, if there are, within the selected uncertainty region, especially for medium signal-to-noise ratios, where the profile of the bound depends on the respective autocorrelation function properties, and in particular, the larger and the higher the ambiguities (sidelobes) in the correlation function, the larger the number of *bulges* and the higher the deterioration of the performance. The charts in the figures 5.7a and 5.7b show the different behaviors of the two schemes, which directly depends on the oscillating nature of the BP correlation function conversely absent in the LP one, for a set of T_x values analyzed. Considering an uncertainty lower than a chip time, the LP/BP performance is similar, because their correlation function mainlobes are both greater than one chip time. The RMSE lines result constant in these cases for a wide range of low-medium SNR values, matching the CRB only for high SNR.

Figures 5.8a and 5.8b show the performance with respect the uncertainty range. For low SNR values, the RMSE is proportional to the T_x value, and in general all the curves are below the straight line $\sigma = T_x/\sqrt{12}$ reached when $E_{T_{obs}}/N_0 \to 0$ or/and for very low T_x values. For high T_x and high SNRs, the MZZB matches the CRB,

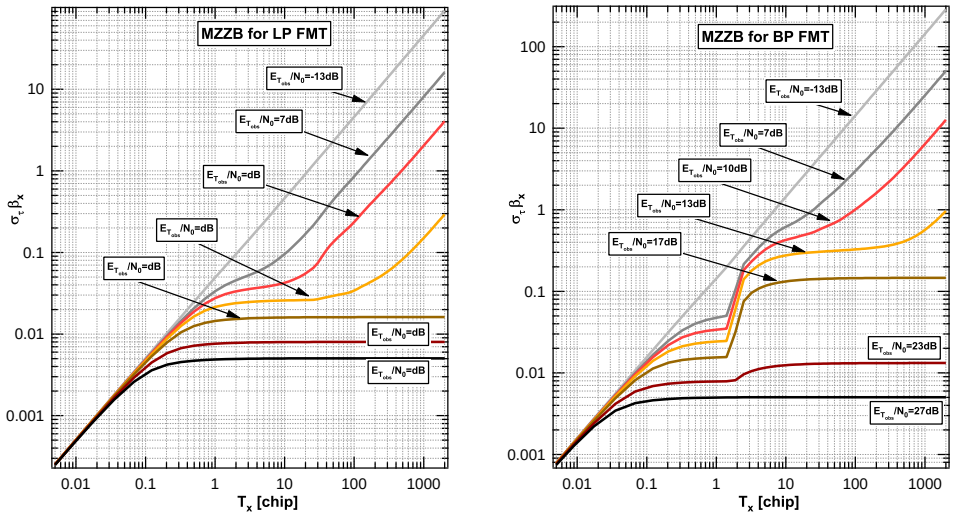

(a) Low-Pass FMT scheme **(b)** Band-Pass FMT scheme

Figure 5.8: *β_x-normalized RMSE vs T_x*

hence the lines result constant with respect the uncertainty. The main difference in comparing the charts of LP and BP schemes, due to the presence of different correlation ambiguities, is the evident gap in the BP performance experienced over a particular threshold value approximately equal to $T_x = ACW$, i.e. the autocorrelation function mainlobe width. The gap is less evident in the LP performance, for its (almost) ambiguity-free correlation function, except for the decreasing peaks in the multiple of $T_s/(1+\alpha)$.

After to have depicted the general theoretical performance, in the following sections we will focus on apply these curves to the TOA estimation.

5.4 Relating the bounds for signal acquisition and tracking

We have seen that the main "ingredients" of the MZZB are i) the signal correlation function (in the expression of the distance between the delayed replicas), and ii) the

"a priori" uncertainty on the parameter to be estimated. The correlation function is directly linked to the signal capability to be detected with different delays, and intuitively the lower the correlation values, the higher the distance and the lower the estimation error. Once we choose to analyze the theoretical performance of a certain signal, the main element that has to be properly chosen is the uncertainty on the unknown parameter, which depends on the particular stage of estimation and on the adopted estimator. By properly selecting the a-priori uncertainty, we can model the two different phases of initial acquisition (large uncertainty) and steady-state tracking (smaller uncertainty).

Let's start from TOA acquisition. We assume not to have any information on the delay, so in general the uncertainty adopted in this phase for the delay is equal to the full length of the ranging code, NT_c. Hence we consider the delay as a random variable uniformly distributed on a chip code period ($T_x = NT_c$). Once the uncertainty is fixed, the MZZB can be computed for the acquisition performance and the curve of RMSE can be plotted wrt the C/N_0 ratio, to find the theoretical operating range in which the optimum estimator can achieve a pre-set accuracy during this phase. We assume also that acquisition has successfully completed when the estimation error ε falls within a pre-set range r, $|\varepsilon| \leq [r/2]$. This defines an event whose probabilty is just what we call *probability of detection*: $P_d = \Pr\{|\varepsilon| \leq [r/2]\}$. Assuming that the error ε is a Gaussian random variable[1] $N(0, \sigma_0)$, then $P_d{=}1{-}2Q\left(\frac{[r/2]}{\sigma_0}\right)$. Inverting this relation, a maximum standard deviation threshold for the error can be found for the constrained probability of detection and error range r. From this standard deviation, a minimum $C/N_0^{Acq}(P_d, r)$ threshold can be found from the RMSE curve of the MZZB.

Of course, the MZZB does not depend on the acquisition algorithm that is adopted, but it only depends on the starting uncertainty interval, here fixed to NT_c. Usually, during signal acquisition the search of the coarse delay is done on a limited number of "cells" with a duration δT. The total uncertainty interval is partitioned into a certain number of cells, and the higher the number of cells, the more accurate the estimation. Once the signal is acquired, the (residual) error will be $|\varepsilon| \leq [\delta T/2]$ ($r = \delta T$). On the other hand, the higher the number of cells, the longer the acquisition time (in GNSS parlance, time to first fix). Usually, the cell time width is proportional

[1] This is true for instance for Maximum-Likelihood estimator on a large estimation window

to the *pull-in-range* (PIR) of the estimator used for the tracking of the signal, to ensure the tracking is initiated with a sufficiently small error. After acquisition is (successfully) accomplished, we have to update the uncertainty for the residual TOA to just the width of a time cell, and a new MZZB, that applies during tracking, has to be computed.

One possible definition of the pull-in-range is the linear, non-ambiguous region of the S-curve of the estimator, which depends on the correlation of the signal and on the estimator that is used. For this analysis we assume a conventional Early-Late estimator, whose pull-in-range is approximated by the early-late spacing d, which in turn is usually chosen equal to an half of the autocorrelation main lobe width (named ACW) of the tracked signal. To sum up, once the ACW is calculated from the signal autocorrelation function, we can evaluate the relevant performance during acquisition through the computation of the MZZB with full uncertainty (one code length) and with the needed residual error range given by $\delta T = PIR = d = \frac{ACW}{2}$. In particular, we can find the minimum (threshold) C/N_0 which makes sure that an optimum estimator performing on the bound will have with the prescribed probability a residual error inside the PIR of the tracking estimator $C/N_0^{Acq}(P_d, r)$. The RMSE curve of the bound will depend on the particular shaping of the autocorrelation function of the signal, and so the threshold C/N_0^{Acq} will depend on its characteristics.

Coming now to the bound for tracking performance, the ingredients are again the initial a priori uncertainty on the parameter (much narrower now), and the signal autocorrelation function. After coarse acquisition, the curves of MZZB for tracking are re-computed assuming the residual error as a uniform random variable on the time bin span $T_x = \delta T = \frac{ACW}{2}$. During the tracking phase, the error has to stay inside the PIR of the estimator, so an operating range can be found choosing the maximum error deviation threshold with the experimental rule $3\sigma_{DLL} \leq \frac{PIR}{2} = \frac{ACW}{4}$, reading from the MZZB curve the minimum C/N_0^{Tr} which ensures the constraint.

5.4.1 Case of Study - Galileo SIS Results

Once the methodology is clear, we analyzed the performance of BPSK and BOC Galileo SIS. The signal parameters that we considered are defined in the Open Service Signal-In-Space Interface Control Document Issue 1 (OS SIS ICD) of February 2010. In particular, we considered the specific ranging code chip rates, and the primary code

lengths ($T_x = NT_c$ for the acquisition uncertainty), the receiver bandwidths reported in the document and we computed the correlation CW ($T_x = \frac{ACW}{2}$ for the tracking uncertainty) from the theoretical signals. For the standard SIS, we reported the maximum standard deviations for the acquisition (for a set of probability of detection) and tracking with the respective minimum C/N_0 thresholds to ensure the constraints: $P_d = \Pr\{|\varepsilon| \leq [PIR/2]\}$ and $3\sigma_{DLL} \leq \frac{PIR}{2}$. Estimation performance will depend on the time of observation T_{obs} for the acquisition stage, or equivalently on the DLL filter equivalent noise bandwidth B_n for the tracking phase. We assume the equivalence $T_{obs} = 1/2B_n$ for the computation of the bounds, considering a B_n value of $10Hz$ and an time of observation (for the acquisition) of 0.05 s.

Figure 5.9 shows the curves of RMSE for acquisition and tracking. In addition, Tab. 5.1 summarizes our results and report the parameters adopted in the simulations. Regarding the acquisition performance, the minimum C/N_0^{Acq} threshold increases, as is natural, for increasing P_d, and ranges from a minimum of 28.30 dBHz (BPSK(5), $P_d = 0.99$) to a maximum of 29.65 dBHz (BOC(15,2.5), $P_d = 0.999$). As clearly can be seen in the (5.11), the MZZB linearly depends on the observation time and C/N_0 product, so the results for different values of T_obs (assumed here 0.05s) can be simply obtained by shifting the curves in Fig.5.9 and so the respective thresholds in Tab.5.1.

Once acquisition is over, fine estimation requires a *lower* C/N_0^{Tr} than the previous stage, thanks to its better a priori information. We see in the Tab. 5.1 that the required values range from 16.40 to 23.06 dBHz, i.e. more than 10 dBHz difference compared to the acquisition ones. The same remarks reported for the acquisition analysis remain valid also for the tracking one, in fact when a different DLL filter bandwidth is adopted the relative performance can be obtained by linearly shifting the curves in the Fig.5.9 and so the respective thresholds in Tab.5.1.

The σ values reported in the table are the maxima allowable for the minima C/N_0. Obviously better values can be achieved with higher C/N_0, following the curves computed in Fig.5.9.

Acquisition		**Uncertainty** NT_c		$P_d = 0.99$		$P_d = 0.995$		$P_d = 0.999$	
Modulation	**Chip Rate**	**Unc** $[T_c]$	**Unc [Km]**	σ **[m]**	C/N_0^{Acq}	σ **[m]**	C/N_0^{Acq}	σ **[m]**	C/N_0^{Acq}
BPSK(5)	5115000	5115	300	11.50	28.30	10.43	28.37	8.98	28.48
BPSK(10)	10230000	10230	300	5.75	28.76	5.22	28.83	4.49	28.94
BOC(1,1)	1023000	4092	1200	19.17	28.59	17,39	28.65	14.96	28.74
BOC(6,1)	1023000	4092	1200	2.50	29.64	2.27	29.70	1.95	29.89
BOC(15,10)	10230000	10230	300	1.15	29.20	1.04	29.25	0.90	29.34
BOC(15,2.5)	2557500	4092	480	1.0	29.52	0.91	29.57	0.781	29.65
BOC(10,5)	5115000	5115	300	1.64	29.13	1.49	29.19	1.28	29.28
Tracking			**AC mainlobe width**		**Uncertainty PIR**		σ		
Modulation	**Chip Rate**	BW**[MHz]**	**ACW** $[T_c]$	**ACW [m]**	**Unc** $[T_c]$	**Unc [m]**	σ $[T_c]$	σ **[m]**	C/N_0^{Tr}
BPSK(5)	5115000	40.92	2.0	117.30	1	58.65103	0.167	9.78	16.40
BPSK(10)	10230000	20.46	2.0	58.65	1	29.32551	0.167	4.89	17.27
BOC(1,1)	1023000	24.552	0.667	195.50	0.33	97.75	0.0556	16.29	16.40
BOC(6,1)	1023000	24.552	0.087	25.50	0.0435	12.75	0.00725	2.12	18.89
BOC(15,10)	10230000	51.15	0.4	11.73	0.2	5.87	0.0333	0.978	18.50
BOC(15,2.5)	2557500	24.552	0.087	10.2	0.0435	5.10	0.00725	0.85	23.06
BOC(10,5)	5115000	40.92	0.286	16.78	0.1429	8.379	0.0238	1.396	18.64

Table 5.1: *Acquisition and tracking parameters.*

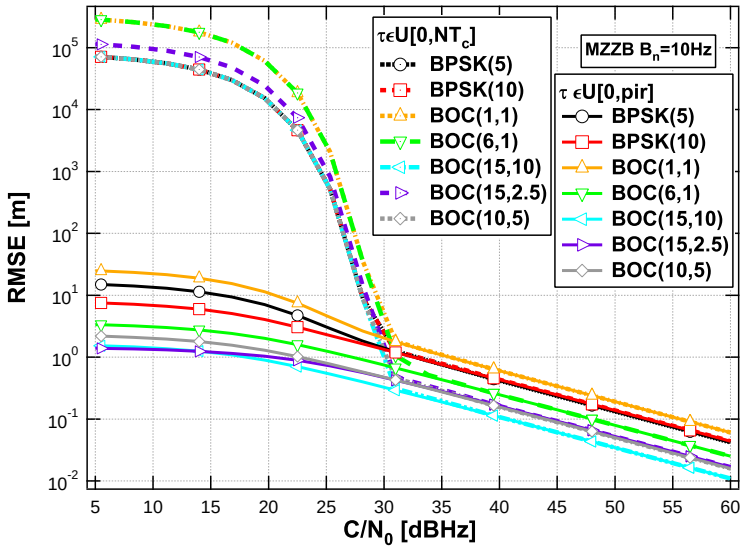

Figure 5.9: *Acquisition and tracking performance of Galileo GNSS.*

5.5 Conclusions

This chapter investigated a *modified* version of the Ziv-Zakai bound, the so-called MZZB, that makes it feasible to find the bound in the presence of nuisance parameters, such as the chips of a random ranging code. The MZZB was mainly applied to BPSK and BOC modulations, and also to some significant MC schemes, allowing to highlight the impact on time estimation of signal autocorrelation side lobes. The related performance loss was shown to be strictly related to the number and the amplitude of the lobes.

The MZZB proved also expedient to estimate the minimum C/N_0 thresholds that ensure safe acquisition of the Galileo SIS under a certain probability of detection, and to keep signal tracking.

Chapter 6

Conclusions and perspectives

In this thesis we have investigated the fundamental limits in time delay estimation (TDE) accuracy of SS signals making use of estimation theory and signal synchronization tools, referring to standard and innovative signalling waveforms.

The focus is addressed on positioning systems, such as the global navigation satellite system (GNSS), deriving some criteria to improve positioning accuracy in a white Gaussian noise scenario. As it is well known, positioning accuracy directly depends on the accuracy of TDE between satellite transmitted codes and local receiver replicas.

We have reviewed the ultimate limits in TDE, characterized by the Cramér-Rao lower bound (CRB) and the Ziv-Zakai lower bound (ZZB) fully investigating the AWGN scenario. These limits represent the performance benchmarks for any estimator, so the simple criterion to reach the ultimate accuracy of a GNSS system at transmitter side, is design the signal minimizing such bounds. Nevertheless, the minimization of the accuracy doesn't reflect into an optimization of the entire system, so in general a trade-off has to be found with other system's constraints.

Innovative SS modulation schemes properties and performance have been analyzed, adapting the signal characteristics to the requirements of the GNSS systems.

Let us outline the main conclusions from the development above:

- The review of TDE fundamentals limits has been further exploited; formulations of the CRB and of the ZZB have been focused, defining a *modified* version of the ZZB to lighten its heavy computation in presence of nuisance parameters. Alternative formulations of the bounds as a function of the spectral properties of a generic modulation format have been discussed;

- the adoption of the ZZB as benchmark for both acquisition and tracking stage

performance has been addressed, analyzing innovative and standard signalling waveforms, such as Galileo SIS. The results are independent from the estimation algorithm adopted and represent the ultimate performance achievable.

- SS-CPM modulation have been analyzed as ranging signals; this waveform demonstrated particularly expedient due to the properties of being intrinsically constant envelope and spectral efficient; a special subset of CPM, called here "Semi-integer MSK (SiMSK)" obtained by properly setting the modulation parameters, revealed easily adaptable to the requirements on emissions, ensuring a constant envelope by definition, while still allowing good tracking performance. Besides, an ad hoc encoding of the SS-SiMSK has allowed the transmission of a two rate services signal, which allows to be tracked with different TDE accuracy according to the bandwidth of the receiver. Some standard estimation algorithms for SS-SiMSK signals have been tested, adopting their linear approximation, which have shown performance close to the correspondent CRB;

- the high degree of freedom in the design of the multicarrier (MC) signal pushed to the analysis of this waveform as possible new ranging signal. We showed how MC waveform can be formatted to obtain maximum estimation accuracy or minimum interference simply by adaptively modifying the system's parameters, proposing the special case of Filtered Multitone (FMT) as possible candidate. The strictly bandlimited property and the full spectral flexibility possessed by the FMT have been exploited in some cases of study to adapt the system to channel conditions or in particular to emulate existing or innovative spectra. Finally a standard tracking algorithm is tested for some SS-FMT waveforms, showing performance close to the correspondent CRB;

The analysis and fundamental issues investigated in this thesis in terms of estimation error bounds can be reapplied without any loss to real systems. The proposed modulation schemes and correspondent estimators reach the theoretical performance in AWGN channel, showing ready for their use in future GNSS systems. For multicarrier signals, the theoretical analysis performed with the fundamental estimation error bounds and with a standard estimator represent the basis for future design of estimators, that may be further investigated to improve other characteristics of the system. Design and performance assessment of code-tracking algorithms for MC ranging signals is ongoing in multipath [20] and interference channel, exploiting

the signal spectral flexibility. Jointly to the design of innovative estimators, also theoretical bounds have to be investigated in these scenarios.

Bibliography

[1] (2004) Agreement on the promotion, provision and use of GALILEO and GPS satellite-based navigation systems and related applications. [Online]. Available: http://pnt.gov//public/docs/2004-US-EC-agreement.pdf

[2] T. Alberty, "Frequency domain interpretation of the Cramér-Rao bound for carrier and clock synchronization," *IEEE Trans. Commun.*, vol. 43, no. 2-3-4, Feb.-Apr. 1995.

[3] J. B. Anderson, T. Aulin, and C. E. Sundberg, *Digital Phase Modulation.* New York, NY: Plenum Press, 1986.

[4] F. Antreich and J. Nossek, "Minimization of the tracking error in a GNSS receiver," in *Proc. ESA Workshop on Satellite Navigation User Equipment Technologies (NAVITEC)*, Noordwijk, The Netherlands, Dec. 2006.

[5] *NAVSTAR GPS space segment/user segment L1C interfaces*, IS-GPS-800A, ARINC Research Corporation, El Segundo, CA, 2010.

[6] J. Ávila-Rodríguez, S. Wallner, B. Eissfeller, A. Schmitz-Peiffer, J. Floch, E. Colzi, and J. Gerner, "Study on a galileo signal and service plan for c-band," in *Proc. of the International Technical Meeting of the Institute of Navigation, (ION-GNSS)*, Savannah, GA, 2008.

[7] K. Bell, Y. Steinberg, Y. Ephraim, and H. Van Trees, "Extended ziv-zakai lower bound for vector parameter estimation," *Information Theory, IEEE Transactions on*, vol. 43, no. 2, pp. 624 – 637, mar 1997.

[8] S. Bellini and G. Tartara, "Bounds on error in signal parameter estimation," *Communications, IEEE Transactions on*, vol. 22, no. 3, pp. 340 – 342, mar 1974.

[9] J. W. Betz, "Binary offset carrier modulations for radionavigation," *J. Inst. Navigation*, vol. 48, no. 4, pp. 227–246, Winter 2001-2002.

[10] J. Betz and K. Kolodziejski, "Extended theory of earlylate code tracking for a bandlimited GPS receiver," *Journal of the Institute of Navigation (ION)*, May 2000.

[11] D. Chazan, M. Zakai, and J. Ziv, "Improved lower bounds on signal parameter estimation," *IEEE Trans. Inform. Theory*, vol. IT-21, pp. 90–93, Jan. 1975.

[12] G. Cherubini, E. Eleftheriou, and S. Olcer, "Filtered multitone modulation for high-speed digital subscriber lines," *IEEE J. Select. Areas Comm.*, vol. 20, no. 5, June 2002.

[13] A. J. R. M. Coenen and D. J. R. V. Nee, "Novel fast GPS/GLONASS code-acquisition technique using low update rate FFT," *IEE Electronics Lett.*, vol. 28, no. 9, pp. 863–865, Apr. 1992.

[14] E. Colzi, G. Lopez-Risueno, J. Samson, P. Angeletti, M. Crisci, R. D. Gaudenzi, J.-L. Gerner, F. Zanier, and M. Luise, "Assessment of the feasibility of GNSS in C-band," in *Proc. Int. Commun. Satellite Systems Conf. (ICSSC)*, San Diego, CA, June 2008.

[15] T. M. Cover and J. A. Thomas, *Elements of Information Theory.* New York, NY: Wiley, 1991.

[16] H. Cramér, *Mathematical methods of statistics.* New York, NY: Princeton Univ. Press, 1946.

[17] A. N. D'Andrea, U. Mengali, and R. Reggiannini, "The modified Cramér-Rao bound and its application to synchronization problems," *IEEE Trans. Commun.*, vol. 42, no. 2-4, pp. 1391–1399, Feb.-Apr. 1994.

[18] A. Emad and N. C. Beaulieu, "Lower Bounds to the Performance of Bit Synchronization for Bandwidth Efficient Pulse-Shaping," *IEEE Trans. Commun.*, vol. 58, no. 10, Oct. 2010.

[19] A. Emmanuele and M. Luise, "Fundamental limits in signal time-of-arrival estimation with application to next-generation satellite positioning," in *Proc. 52nd International Symposium ELMAR-2010.*

[20] ——, "Fundamental Limits in Signal Time-of-Arrival Estimation in AWGN and Multipath scenarios with Application to Next-Generation GNSS," in *Proc. 5th ESA Workshop on Satellite Navigation Technologies*, Noordwijk, NL, Dec. 2010.

[21] A. Emmanuele, M. Luise, J.-H. Won, D. Fontanella, M. Paonni, B. Eissfeller, F. Zanier, and G. Lopez-Risueno, "Evaluation of Filtered Multitone (FMT) Technology for Future Satellite Navigation Use," in *Proc. of the 24th International Technical Meeting of the Satellite Division of the Institute of Navigation, (ION-GNSS)*, Savannah, GA, 2011.

[22] A. Emmanuele, M. Luise, F. Zanier, and M. Crisci, "Filtered Multitone (FMT) modulation for GNSS applications," in *Proc. European Workshop on GNSS Signals and Signal Processing (GNSS Signals)*, Toulouse, France, Dec 2011.

[23] ——, "Ziv-Zakai bound for Time-Of-Arrival Estimation of GNSS Signal-In-Space," in *Proc. European Workshop on GNSS Signals and Signal Processing (GNSS Signals)*, Toulouse, France, Dec 2011.

[24] ——, "Modified Ziv-Zakai bound for Time-Of-Arrival Estimation of GNSS Signal-In-Space," in *Proc. IEEE Int. Conference on Acoustics, Speech and Signal Processing (ICASSP)*, Kyoto, Japan, Mar. 2012.

[25] (2008) The ESA website. [Online]. Available: http://www.esa.int/

[26] *Galileo open service, Signal in space interface control document*, OS-SIS-ICD, d. 1, European Space Agency / European GNSS Supervisory Authority, Brussels, Belgium, 2008.

[27] F. Zanier and M. Luise, "Fundamental issues in time-delay estimation of multicarrier signals with applications to next-generation gnss," in *Proc. of IEEE 10th International Workshop on Signal Processing for Space Communications (SPSC)*, Rhodes, Greece, Oct. 2008.

[28] F. Zanier, G. Bacci, M. Luise, "Non-binary spread spectrum signals with good delay-tracking features for satellite positioning," in *Proc. Int. Waveform Diversity and Design Conference (WDD)*, Pisa, Italy, June 2007.

[29] F. P. Fontán, M. Vázquez-Castro, C. E. Cabado, J. P. García, and E. Kubista, "Statistical modeling of the LMS channel," *IEEE Trans. Veh. Technol.*, vol. 50, no. 6, pp. 1549–1567, Nov. 2001.

[30] G. M. Polischuk and S. G. Revnivykh, "Status and development of GLONASS," in *Acta Astronautica, Proceedings of the Plenary Events*, vol. 54, no. 1-120, World Space Congress 2002, June 2004, pp. 949–955.

[31] D. Gabor, "Theory of communication," *J.IEE*, vol. 93, no. 26, pp. 429–457, Nov. 1943.

[32] R. D. Gaudenzi and M. Luise, "Decision-directed coherent delay-lock tracking loops for DS-spread-spectrum signals," *IEEE Trans. Commun.*, vol. 39, no. 5, pp. 758–765, May 1991.

[33] G.Bacci and M.Luise, "A new set of spreading sequences that improves time-delay estimation in satellite positioning," *Proc. 15th IST Mobile and Wireless Communications Summit*, pp. 1–10, Jun. 2006.

[34] F. Giannetti, M.Luise, and R. Reggiannini, "Chip timing recovery in digital modems for continuous-phase cdma radio communications," *IEEE Trans. Commun.*, vol. COM-43, no. 2/3/4, pp. 762–766, Feb-March-April 1995.

[35] L. Giugno and M. Luise, "Optimum pulse shaping for delay estimation in satellite positioning," in *Proc. European Signal Processing Conference (EUSIPCO)*, Antalya, Turkey, Sept. 2005.

[36] G.W. Hein, M. Irsigler, J.Á. Ávila-Rodríguez, S. Wallner, T. Pany, B. Eissfeller and P. Hartl , "Envisioning a future gnss system of systems - part 3," *Inside GNSS*, pp. 64–73, June 2007.

[37] G. W. Hein, J. Ávila-Rodríguez, S. Wallner, A. R. Pratt, J. Owen, J. Issler, J. W. Betz, C. J. Hegarty, S. Lenahan, J. J. Rushanan, A. L. Kraay, and T. A. Stansell, "MBOC: The new optimized spreading modulation recommended for GALILEO L1 OS and GPS L1C," in *Proc. IEEE Positioning, Location and Navigation Symposium (PLANS)*, San Diego, CA, Apr. 2006.

[38] M. Irsigler, J. Ávila-Rodríguez, and G. Hein, "Criteria for GNSS multipath performance assessment," in *Proc. Int. Technical Meeting Sat. Division Inst. of Navigation (ION GNSS)*, Long Beach, CA, Sept. 2005.

[39] A. Jones, T. Wilkinson, and S. Barton, "Block coding scheme for reduction of peak to mean envelope power ratio of multicarrier transmission schemes," *Electronics Letters*, vol. 30, no. 25, pp. 2098 –2099, dec 1994.

[40] K. Pollpeter, "To be more precise: The Beidou satellite navigation and positioning system," *China Brief*, vol. VII, no.10, May 2007. Available at: http://www.jamestown.org/terrorism/news/uploads/cb_007_010.pdf.

[41] E. D. Kaplan and C. J. Hegarty, *Understanding GPS principles and applications.* Norwood, MA: Artech House, 2006.

[42] S. M. Kay, *Fundamentals of statistical signal processing: Estimation theory.* Englewood Cliffs, NJ: Prentice-Hall, 1993.

[43] P. Laurent, "Exact and approximate construction of digital phase modulations by superposition of amplitude modulated pulses (amp)," *IEEE Trans. Commun.*, vol. COM-34, no. 2, pp. 150–160, Feb. 1986.

[44] M. Lixia, M. Murroni, and V. Popescu, "Papr reduction in multicarrier modulations using genetic algorithms," in *Optimization of Electrical and Electronic Equipment (OPTIM), 2010 12th International Conference on*, may 2010, pp. 938 –942.

[45] M. Luise and U. Mengali, "A new interpretation of the average matched filter for msk-type receivers," *IEEE Trans. Commun.*, vol. COM-39, pp. 14–16, Jan. 1991.

[46] U. Mengali and A. N. D'Andrea, *Synchronization Techniques for Digital Receivers.* New York: Plenum Press, 1997.

[47] M. Moeneclaey, "On the true and the modified Cramér-Rao bounds for the estimation of a scalar parameter in the presence of nuisance parameters," *IEEE Trans. Commun.*, vol. 46, no. 11, pp. 1536–1544, Nov. 1998.

[48] F. D. Nunes and J. M. N. Leitao, "A new fast code/frequency acquisition algorithm for GPS C/A signals," in *Proc. IEEE Veh. Techn. Conf.*, Lake Buena Vista, FA, Oct. 2003.

[49] S. Pace, G. Frost, I. Lachow, D. Frelinger, D. Fossum, D. K. Wassem, and M. Pinto, *The Global Positioning System Assessing National Policies.* Santa Monica, CA: RAND Corporation, 1995. [Online]. Available: http://www.rand.org/publications/MR/MR614/

[50] C. Park and T. S. Rappaport, "Short-range wireless communications for next-generation networks: UWB, 60 GHz millimeter-wave WPAN, and ZigBee," *IEEE Wireless Commun.*, vol. 14, no. 4, pp. 70–78, Aug. 2007.

[51] B. W. Parkinson and J. J. Spilker, *Global Positioning System: Theory and Applications.* Washington, DC: Amer. Inst. of Aeronautics, 1996, vol. 1.

[52] R.C.Dixon, *Spread Spectrum Systems with Commercial Applications.* New York: Wiley Interscience, 1994.

[53] A. Schmitz-Peiffer, L. Stopfkuchen, F. Soualle, J.-J. Floch, R. King, A. Fernandez, R. Jorgensen, B. Eissfeller, J. Ávila-Rodríguez, S. Wallner, J.-H. Won, T. Pany, M. Anghileri, B. Lankl, T. Schler, and E. Colzi, "Assessment of the use of C-Band for GNSS within the european GNSS evolution programme," in *Proc. of the International Technical Meeting of the Institute of Navigation, (ION-GNSS)*, Savannah, GA, 2008.

[54] L. P. Seidman, "Performance limitations and error calculations for parameter estimation," *Proc. IEEE*, vol. 58, no. 5, pp. 644–652, May 1970.

[55] S.G.Revnivykh, "GLONASS status and modernization," in *6th Meeting of International Committee on Global Navigation Satellite Systems (ICG)*, Tokyo, Japan, Sept. 2011. Available at: http://www.unoosa.org/pdf/icg/2011/icg-6/3.pdf.

[56] H. L. V. Trees, *Detection, Estimation and Modulation Theory.* New York, NY: Wiley, 1968.

[57] M. Vergara, F. Andreich, M. Meurer, and G. Seco-Grados, "Spreading code design for a MC-CDMA based GNSS pilot signal," in *Proc. 5th ESA Workshop on Satellite Navigation Technologies*, Noordwijk, NL, Dec. 2010.

[58] E. Weinstein and A. Weiss, "Fundamental limitations in passive time delay estimation. part II: Wide-band systems," *IEEE Trans. Acoust., Speech, Signal Processing*, vol. ASSP-32.

[59] A. Weiss and E. Weinstein, "Fundamental limitations in passive time delay estimation. part I: Narrow-band systems," *IEEE Trans. Acoust., Speech, Signal Processing*, vol. ASSP-31.

[60] S. White and N. C. Beaulieu, "On the application of the Cramér-Rao and detection theory bounds to mean square error of symbol timing recovery," *IEEE Trans. Commun.*, vol. 40, no. 10, pp. 1635–1643, Oct. 1992.

[61] J.-H. Won, D. Fontanella, M. Paonni, B. Eissfeller, A. Emmanuele, M. Luise, A. Garcia-Pea, O. Julien, C. Macabiau, F. Zanier, and G. Lopez-Risueno, "Receiver Architecture for Multicarrier-based GNSS Signals," in *Proc. European Workshop on GNSS Signals and Signal Processing (GNSS Signals)*, Toulouse, France, Dec 2011.

[62] F. Zanier, G. Bacci, and M. Luise, "Nonbinary bandlimited signature waveforms for spread spectrum signals with application to satellite positioning," in *Proc. ESA Workshop on Satellite Navigation User Equipment Technologies (NAVITEC)*, Noordwijk, The Netherlands, Dec. 2006.

[63] F. Zanier and M. Luise, "A new look into the issue of the CramÉr-Rao bound for delay estimation of digitally modulated signals," in *Proc. IEEE Int. Conference on Acoustics, Speech and Signal Processing (ICASSP)*, Taipei, Taiwan, April 2009.